University of Hull
Department of Engineering

Footfall Energy Harvesting

Footfall Energy Harvesting Conversion Mechanisms

Thesis submitted for the Degree of

Doctor of Philosophy in the University of Hull

Farouk Balouchi

December 2013

Abstract

Ubiquitous computing and pervasive networks are prevailing to impact almost every part of our daily lives. Convergence of technologies has allowed electronic devices to become untethered. Cutting of the power-cord and communications link has provided many benefits, mobility and convenience being the most advantageous, however, an important but lagging technology in this vision is the power source. The trend in power density of batteries has not tracked the advancements in electronic systems development. This has provided opportunity for a bridging technology which uses a more integrated approach with the power source to emerge, where a device has an onboard self sustaining energy supply. This approach promises to close the gap between the increased miniaturisation of electronics systems and the physically constrained battery technology by tapping into the ambient energy available in the surrounding location of an application. Energy harvesting allows some of the costly maintenance and environmentally damaging issues of battery powered systems to be reduced.

This work considers the characteristics and energy requirements of wireless sensor and actuator networks. It outlines a range of sources from which the energy can be extracted and then considers the conversion methods which could be employed in such schemes. This research looks at the methods and techniques for harvesting/scavenging energy from ambient sources, in particular from the motion of human traffic on raised flooring and stairwells for the purpose of powering wireless sensor and actuator networks. Mechanisms for the conversion of mechanical energy to electrical energy are evaluated for their benefits in footfall harvesting, from which, two conversion mechanisms are chosen for prototyping.

The thesis presents two stair-mounted generator designs. Conversion that extends the intermittent pulses of energy in footfall is shown to be the beneficial. A flyback generator is

designed which converts the linear motion of footfall to rotational torque is presented. Secondly, a cantilever design which converts the linear motion to vibration is shown. Both designs are mathematically modelled and the behaviour validated with experimental results & analysis. Power, energy and efficiency characteristics for both mechanisms are compared. Cost of manufacture and reliability are also discussed.

Acknowledgments

During the course of completing this research I have been fortunate to have had the support and encouragement of many people. Here, I would like to acknowledge and thank those people who have helped me reach the end of this journey.

First of all, I'd like to thank my supervisor Dr Jim Gilbert for his tireless support throughout the course of this research, without his patience and guidance I could never have hoped to have accomplished this gargantuan undertaking - I will forever be in your debt!

In the manufacture of the prototypes I have been very fortunate to have been assisted by many people in the Engineering Department. For all their assistance, I would like to thank Chris Ingleby, Russ Kenyon, Dave Joyce, Nick Waites and Simon Cowell. In their own way, they were all instrumental in providing me the support to get the job done.

I am ever grateful to my family for all their support. I would like to thank my mother who has shown me the strength and character of a single mother raising three children alone and on the welfare system. I would like to thank my wife for all her support through the good & bad, my children without whom I would never have had the courage and ambition to take this on in the first place. I would like to thank my sister and brother for their encouragement and unwavering confidence and my uncle for being there for me, in many ways like the father I lost as a young boy.

Lastly, I'd like to thank my friends for their support and understanding. Most of all, I'd like to thank them for keeping grounded.

Table of Contents

Table of Figures

Chapter 1 – Introduction

This research looks at the methods and techniques involved in harvesting/scavenging energy from ambient sources; in particular, from the motion of human traffic on raised flooring and stairwells for the purpose of powering wireless sensor and actuator networks. Mechanisms for the conversion of kinetic energy to electrical energy are the focus of this research with the view to integrating these mechanisms into under floor footfall generators for collective human energy harvesting.

The advent of ubiquitous computing is beginning to impact almost every part of our daily lives. An important but lagging technology in this vision is the power source for the sensor networks. The energy density and miniaturisation of batteries has not tracked the advances in electronics, where more transistors are placed on a silicon board. This allowed a newer more integrated approach to prevail, where a device will have an onboard self sustaining energy supply. This approach promises revolutionise mobile and wireless technology by eliminating the regular maintenance of sensor networks and disposal of spent power supplies.

Energy harvesting has become a wide and varied field of research; this report, for completeness, provides a background to energy harvesting and so attempts to provide a broad picture of energy harvesting and the markets it services, thereby giving a well informed and focused direction to future work in this field. It is important to note that the recent surge in interest in energy harvesting has been driven by the search for battery-free techniques for powering wireless sensor networks. Therefore, it is essential to include this technology and its power requirements for a complete understanding of the scope of the research.

Energy harvesting is the conversion of ambient energy to useable, or defined more clearly, mWatts to Watts of electrical power. Some of the more common power sources available for energy harvesting are: solar, wind, vibration, human, inductive, thermal, radioactive and others. Particular attention will be focused on the power available from human motion, which can be considered as low frequency high amplitude vibration. The conversion methods employed for transforming these sources of energy into useable electrical energy are; electromagnetic, piezoelectric, electrostatic, thermoelectric photoelectric electrochemical. These conversion methods, also known as transduction methods, will be investigated so as to enable an informed and considered selection in terms of efficiency and suitability. Self powered or self sustaining electronics is a term used for devices that scavenge or harvest their energy from ambient sources within the locality of the device. These devices convert the ambient energy into useable electrical power. Wireless sensor networks are promising to be one of the major enabling technologies in many areas of research and commercialisation for examples discussed in subsection 2.1.1 of chapter 2. Currently all emerging wireless technologies, with the exception of a very small minority, are designed to operate on batteries which have a limited lifespan, hence limiting the device and its application.

Much research has been conducted to enable sensor networks to be a part of our environment [1], [2] without particularly being invasive or obtrusive to our everyday activities; the idea is to make sensors ubiquitous to our everyday life, and to allow this type of sensory activity to be non invasive and non obtrusive. The sensor nodes are required to be: firstly almost invisible, secondly and more importantly, self-sustaining. The power supply of the sensor node is one of the major obstacles in the way of a ubiquitous vision for sensor networks. Batteries are a finite energy source requiring maintenance, and where primary batteries are used, replacement necessitates proper disposal, all adding to the cost and inconvenience of

maintaining a sensor network, especially one with many nodes. Enabling a device to harvest its own energy is the logical solution to a self-sustaining sensor network.

An area of academic research and commercialisation which has seen some attention in recent times is Footfall Energy Harvesting (footfall harvesting). This is the conversion of kinetic energy in footfall to useable electrical energy. Footfall harvesting has been researched for many applications, particularly for bodyworn systems where the motion of footfall can be harvested to power electronic devices. This study investigates a closely related concept to bodyworn systems, where footfall is used to power off-body electronic devices using footfall harvesting mechanisms in sprung flooring and stairwells. Some early stage commercial products [3][4][5][6] have been developed in this space but very little academic literature can be found on the subject.

The objective in designing an energy harvesting system is to extract the maximum possible power from pedestrians without having a significant negative impact on those pedestrians at a reasonable cost of manufacture, installation and maintenance. The aim has been to identify those parameters which are important to the design of a footfall energy harvesting device and to determine appropriate values for those parameters in particular application scenarios.
Existing technologies which may be applicable to footfall energy harvesting have been examined. There are relatively few examples of energy harvesting systems designed to be installed in a floor/stair locations. A larger number of devices have been developed for in-shoe use and for capturing energy from vehicular traffic. Devices will be classified according to the underlying energy conversion technology and the mechanisms used for coupling input energy into the conversion device.

1.1. Scope and Research Focus

For the purpose of this work only human movement is considered for the energy source; furthermore, only electromagnetic conversion is used and two types of generators are designed:

1. Rotational electromagnetic – flyback conversion
2. Linear electromagnetic – vibrational cantilever

Both the prototype mechanisms are fitted to a purpose built staircase and are fully functional and demonstratable. The prototype devices are envisaged to be placed in high footfall areas where crowds are funnelled into confined spaces; such as bridges, underground tunnels, pavements, stairwells.

The focus of the research and the underlying question for the work has been to establish how much energy can be extracted from human footfall and where is the best location for such devices to be installed to capture this energy. More specifically, to design and develop prototypes for the extraction of energy in locations of footfall and vehicular traffic.

1.2. Thesis Layout

The thesis is presented with a background chapter introducing energy harvesting in **chapter** 2; typical applications of wireless sensor networks are discussed and a special focus on the power requirements of these devices is presented. Energy reservoirs, sources and conversion methods are also discussed in this chapter. **Chapter 3** introduces the design requirements for footfall harvesting. Parameters affecting the available energy in footfall harvesting are investigated and scenarios where these devices would see most footfall are explored. Available technologies and a comparison of these existing technologies are investigated. Concept selection criteria along with concept generation are presented. Finally, a discussion

on the selected concepts for prototyping is presented. **Chapter** 4 explores the ground force reaction (GRF) of pedestrians on a level and raised flooring. A system for instrumentation and measurement of GRF is presented along with results and recommendation for the design in footfall scenarios. **Chapter 5** presents the first of the two prototype mechanisms: the flyback converter. A mathematical model is developed and validated with experimental results. Optimisation using the model is presented looking at power, energy and efficiency of the system. **Chapter 6** presents the second of the two mechanisms: the vibrating cantilever. Mathematical modelling of physical parameters, validation with experimental results and optimisation are presented. **Chapter 7** presents a comparison of the two energy conversion mechanisms. Complexity and reliability of the mechanisms is presented and a breakdown of the volume costs associated with manufacture for both mechanisms is examined. Also, some indications of power generation for footfall, road and rail use are presented. Finally, the design process and optimisation strategies for further development are presented. Finally **Chapter 8** presents the thesis conclusions and a discussion on further development.

2. Chapter 2 – Background

This chapter explores the broader applications of energy harvesting technology, particularly for the most popular application of wireless sensor networks (WSN) and thereby provides the context for the energy harvesting technology, discussed later. It will be shown that WSN themselves have diverse applications and are well suited for energy harvesting technology.

The chapter will also explore the energy reservoirs, energy sources and the conversion methods available for energy harvesting. The chapter is concluded with a section on available technologies for footfall harvesting.

2.1. Sensor networks and their energy requirements

Wireless sensor networks came about as a result of a shift from wired to wireless links for communication in sensor networks. This enabling factor, discussed in the sections 2.1.2 to 2.1.4, coupled with low power, low data rate and low cost make WSN an attractive solution for many monitoring and data gathering applications. The development of energy efficient WSNs is the cornerstone of pervasive/ubiquitous computing. Pervasive computing has some possible negative environmental impacts, particularly in physical waste and energy consumption [7]. A number of areas of applications of WSNs are described in the following section.

2.1.1. Typical applications

A large number of potential applications of sensor networks have been reported ranging from early research investigations to commercial systems [8]. A review of a broad range of applications is given in [9] as the basis for the proposal of a design space model.

Environmental monitoring

A widely considered area for the application of sensor networks is in environmental monitoring. Measurement of glacier dynamics using nodes capable of measuring location, temperature, pressure and orientation at points inside the glacier over a period of several years was described in [10]. Marshall et al. [11] used nodes on the sea bed to monitor pressure, temperature, conductivity, current, and turbidity. These were connected to buoys on the surface to allow radio communication through self organising ad-hoc wireless networks. The ARGO project [12] uses a sensor network to observe the temperature, salinity, and current profile of the upper ocean. Nodes are attached to free-drifting carriers which cyclically sink to a depth of 2000m and then resurface to allow communication with a satellite. WSNs have been considered for precision agriculture applications such as monitoring grape growing conditions [13]. Here nodes with temperature, soil moisture, light, and humidity sensors are deployed on a 20m grid across a vineyard to provide information to guide the adaptation of water/fertilizer/pesticide supply to the needs of individual plants and to optimise harvesting.

Animal tracking and control

Tracking and controlling the movements of domestic and wild animals presents interesting challenges in WSNs. The breeding behaviour of birds was considered by [14] using sensor nodes installed inside burrows. Clusters of nodes, each capable of measuring humidity, pressure, temperature, and ambient light level, along with infrared sensors to detect the presence of the birds, form local networks and each cluster has a node fitted with a long-range directional antenna to pass cluster data to a base station. Nodes fitted to wild animals (e.g., wild horses, zebras, and lions) capable of roaming over a very large area was considered in [15]. Each node logs the animal's behaviour and environment and passes data

to any other node which comes within range. At regular intervals, a mobile base station (e.g., a car or a plane) moves through the observation area and collects the recorded data from the animals it passes. In the case of [16] the WSN is used both to monitor behaviour and to control it. In this case, the positions of cattle are monitored and 'virtual fences' created by using an acoustic stimulus to discourage an animal from crossing a defined line. The network of nodes are connected to a base station so that feeding behaviour can be monitored and virtual fences adjusted to improve usage of the feedstock.

Safety, security and military applications

WSNs have been developed to assist rescue teams in saving people buried in avalanches [17]. By monitoring heart rate, respiration activity, orientation and blood oxygen level it is possible to automate the prioritization of victims and to guide rescuers to their location. Tracking of military vehicles using networks of nodes deployed by unmanned aerial vehicle (UAV) was considered by [18]. Data collected from the nodes by a UAV was used to identify the path and velocity of ground vehicles. Anti-tank landmines capable of monitoring for signs of tampering have been formed into networks so that, if an individual mine is disabled, a neighbouring device is able to take its place using a rocket thrusters to affect the necessary movement [19]. Combining data from a network of acoustic sensors in order to determine the location of a sniper and the direction of the bullet, based on the time of flight of muzzle blast was considered by [20]. Monitoring of buildings and emergency response personal has been considered by Yang [21] with the aim of improving safety in dealing with fires and other life threatening situations in the built environment.

Health

Health applications for wireless sensor networks provide patient monitoring; drug administration; tracking of patients at home [22][23][24], and doctors [25] in hospitals. Body

sensor networks [26] are used in the medical sector; implanted medical devices with integrated wireless technology are used for therapeutic and diagnostic applications. Physicians can use this technology to monitor device performance and patient response without the need for invasive surgery. Drug manufactures are also interested in this technology to reduce their costs when introducing a new drug. The patients can be monitored wirelessly and data about the patient's internal chemistry can be analysed for abnormal reaction and side effects, over a secure link. Yang [26] undertook a thorough analysis of the wireless technologies available and concluded that the Institute of Electrical and Electronics Engineers (IEEE) 802.15.4wireless standard with provisions for body sensor networks (BSN) in the Zigbee application layer was the most appropriate for the body sensor networks. An analysis of the performance of medical sensor body area networking [27] also endorsed the advantage of using IEEE 802.15.4 and Zigbee for medical sensor technologies.

Built environment

Monitoring of the internal environmental conditions and adaptation of heating, lighting etc in response to human occupancy and activity is a major potential application for sensor networks, whether based on wireless communications or on wired connections. In [28] a WSN was developed to monitor power consumption in large and dispersed office buildings with the aim of detecting locations or devices that are consuming a lot of electrical power.

2.1.2. Power requirements

The power consumed by a network node can be split between the various functions it has to perform. A number of authors have described the structure of a general sensor network node [29]. The key elements are illustrated in Figure 2-1. It should be noted that not all of these elements will be present in all types of nodes. The power requirement of each element depends on the particular application and so it is difficult to generalise about which parts of

the node consume the most power. For instance, it is commonly the case that actuators, if present, consume a large proportion of the total power. In addition, consumption depends on the operating mode of a device such as whether it utilises sleep mode to reduce consumption and how frequently it transmits and receives data. [30] considered the split of power consumption in a typical node and concluded that communication functions consumed a large proportion of total power. The same paper outlined the design issues regarding the development of a highly energy efficient system architecture for embedded wireless sensor network; beginning with device technology and progressing to the application layer.

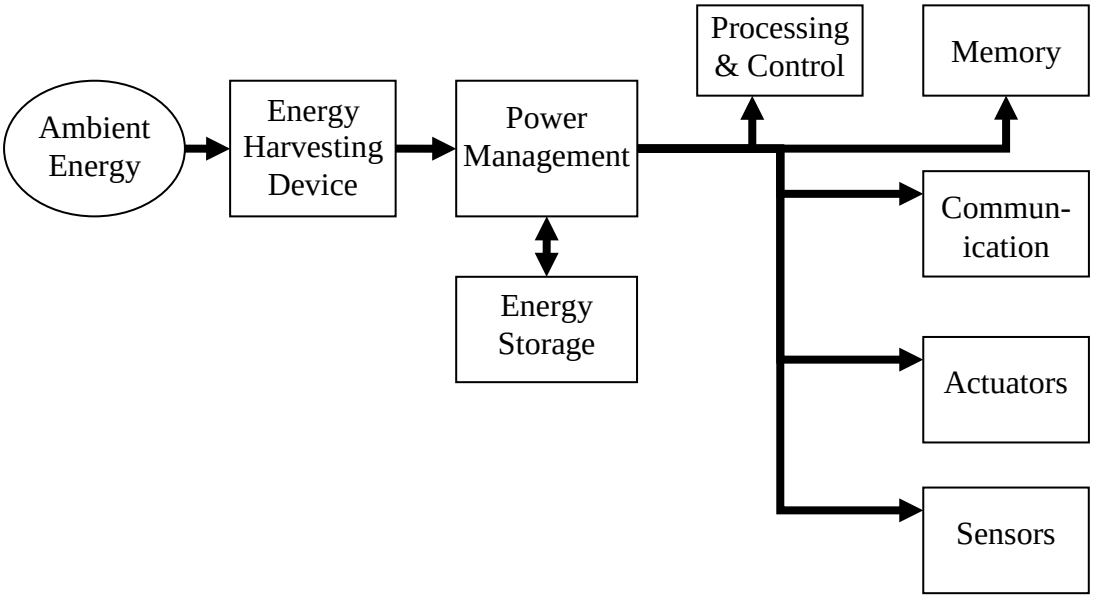

Figure 2-1 A Generic Sensor Network Node with Energy Harvesting Device

2.1.3. Processing

The choice of processor is a major factor in determining the size and power consumption of the node. The processing unit is responsible for managing data acquisition, handling communication protocols, scheduling and preparing data packets for transmission once it has gathered, filtered and synchronised the data from the sensors. The consumption and

performance of the processor depend on the architecture, technology and clock speed utilised. A number of chip producers are offering low cost, low power processors for sensor networks with power consumption in the region of 12 picoJoules/instruction (pJ/instruction) [29].

2.1.4. Communications

There are a wide range of wireless communication standards available for network communications with the choice of standards being determined by factors such as inter-node distance, data rate, power requirements, flexibility of network structure, the time required to establish communications and the cost of implementation. The most widely considered standards are grouped within the IEEE 802.11 standard for Wireless Local Area Networks (WLANs) and the IEEE 802.15 standard for Wireless Personal Area Networks (WPANs).

Specific communication protocols frequently considered for WSN applications include Bluetooth and its low end variant Wibree and Zigbee. There are a number of other systems developed for specific application areas such as Z-wave [32], designed for home automation and control and the propriety communication standard developed by EnOcean [33] for devices such as energy harvesting light switches.

In many sensor network applications it is not necessary for nodes to be constantly active and communicating. It is often possible for nodes to enter a sleep mode for a significant proportion of time and wake up either at fixed time intervals or in response to some external event. Key considerations in this context are the time required for a node to wake up and re-establish communications and the ability to synchronise the waking of multiple nodes in a network. From low power sleep mode a Zigbee node can join an existing network in about 3ms whereas a Bluetooth node can take up to 3-10 seconds to join a network [34].

Examples of the power consumption of a selection of commercial sensor network nodes are given in Table 2-1 for a range of operating conditions. The average values given in Table 2-1 are based on an operating regime of communication Receiving & Transmission (Rx & Tx) for 1% of the time, processing for 10% of the time and sleeping for the remaining time.

	Crossbow micaZ [35]	Intel IMote2 [36]	Jennic JN5139 [37]
Radio standard	802.15.4/Zigbee	802.15.4	802.15.4/Zigbee
Typical range	100m (outdoor) 30m (indoor)	30m	1km
Data rate	250kbps	250kbps	250kbps
Sleep mode (deep sleep)	15µA	390µA	2.8µA (1.6µA)
Processor only	8mA active mode	31-	2.7+0.325/MHz mA
Rx	19.7mA	44mA	34mA
Tx	17.4mA (+0dbm)	44mA	34mA (+3dBm)
Supply Voltage (min)	2.7V	3.2V	2.7V
Average	2.8mW	12mW	3mW

Table 2-1 Summary of power consumption of commercial sensor network nodes

[1] consumption depends on clock speed selected between 13-104MHz

2.2. Energy reservoirs

In essence an energy harvesting device is a low power energy source with an unbounded energy supply, but the intermittent nature of some sources limits their use. A low power device could tap into this intermittent source provided it adheres to some strict operating conditions. This may become impractical as sensor networks have some inherent power hungry functions as seen in Table 2-1. Functions such as data transmission, cause sudden current drain which energy harvesters may not be able to support. Therefore a more practical approach would be to store the intermittent converted energy in storage-units such as passive

components like super capacitors, inductors and rechargeable batteries for use when the need arises.

In [38][39][40] energy reservoirs are introduced to classify energy storage elements such as rechargeable batteries used in personal digital assistants (PDAs), categorised as macroscale and more exotic storage are described as microscale batteries, ultracapitors, microfuel cells, micro heat engines and radioactive power sources. Sources for energy scavenging are defined differently to those for energy reservoirs. Reservoirs have characteristic energy density, and how much power they can provide is dependent on the lifetime over which they operate.

2.2.1. Battery theory

Batteries store electrical energy chemically; energy is released through a chemical reaction within the battery. The reaction transfers electrons from its anode to its cathode across an electrolyte material [45]. Charging the battery has the opposite effect by restoring the electrical energy back into the chemical bonds. It is widely understood that the main type of energy to power portable and low power electronics today is in the form electrochemical energy stored in a battery.

Battery capacity (C) is related to expected discharge duration, for example if a source is rated at 200 milliamps, charging a 200mAh battery will take one hour; or alternatively, charging a 100 mAh battery will take half the time according to H=C/I. Where C is the battery capacity, I is the current drawn from the battery and H is the amount of time, in hours, a battery can operate under the specified conditions. It should be noted for completeness that a battery actually requires a least 1.5*C to completely replenish [46] and typically 40% to 70% of usable capacity is achieved [49].

2.2.2. Rechargeable batteries

Conventional battery chemistries, such as nickel-zink (NiZn), nickel metal hybrid (NiMH) and nickel cadmium (NiCd) have high energy densities and good discharge rates but also suffer from short life cycles and memory effects [45]. Lithium ion (Li-ion) based battery technology has virtually eliminated these shortfalls with higher energy density and discharge rates, higher cell voltage, longer cycle life and almost no memory effects. A gradual movement in battery technology to the more recent NiZn, NiMH, and NiCd which exhibit high energy densities but with short cycle life and memory effects. Lithium ion batteries have become the choice for portable electronics with their high energy density, long cycle life and no memory effects. More recent advances in thin film lithium ion battery technology which less than 15μm thickness promises to allow the integration of lithium-ion batteries into a micro-system and still deliver relatively high power levels [50]. Commercial thin-film lithium-ion products are now available which exhibit similar performance capabilities as supercapaciters and which claim to be well suited to energy harvesting needs [51]. The cell provides a potential of 4.0Volts with a capacity of 0.7 mAh, it measures 1 in x 1in x 0.0043 in. The chemistry is Lithium phosphorus oxynitride (LiPON) and the cathode is lithium cobalt Oxide ( ) with proprietary material. A disadvantage of lithium-ion based chemistries is their susceptibility to damage if the cell voltage increases over 4.2 Volts, or decreases below 2.7 Volts. The battery can significantly degrade or even explode. To extend the life of lithium-ion cells it is essential to manage the charging and discharging process [45].

2.3. Energy sources for harvesting

In order for a sensor network to operate it requires electrical power and given that it is frequently desirable to install nodes in inaccessible locations, it can be difficult to provide a sufficiently large store of energy for long term operation. Although the performance of non-

renewable energy sources, such as batteries and fuel cells, has improved over the years [47], this improvement is fairly gradual compared with other areas of electronics [48] and cannot satisfy all of the simultaneous demands for long life, low volume, low weight and limited environmental impact.

There are a great many sources of energy and conversion devices which have been considered for energy harvesting [39], [42] and in order to compare different approaches, it is useful to consider the criteria for comparison. Clearly, a key consideration is whether the energy harvesting device can provide the level of power required by the sensor node but it is also important that the electrical power be at a suitable voltage and current level since conversion between voltage levels implies some dissipation of energy and, in general, the greater the ratio between input and output voltage, the greater the power losses.

In order to achieve a desired power level, some conversion devices can be appropriately scaled. Thus, for instance, if a Photovoltaic (PV) cell is considered then an increase in power demand can be accommodated by an increase in cell area. However, other sources/converters cannot be so readily scaled. For instance energy derived from human activity cannot generally be scaled up without either increasing the effect on the person concerned or increasing the number of people involved. While it may be possible to scale up a conversion device, many applications of sensor networks require nodes which are small and light weight. Thus an important consideration is the power density (in either W/ or W/kg) which can be achieved. In assessing power density, the volume and weight of associated energy storage may also be important.

A number of authors have proposed classification systems to categorise energy sources suitable for harvesting which, while broadly similar, do exhibit some differences. In [8] sources are grouped as human and environmental with kinetic and thermal considered as sub classes. Buren [44] uses a similar classification of thermal energy, radiant energy and mechanical energy sources when considering wearable micro-generators. This classification will be adopted here although mechanical source will be subdivided between those which are continuously present over long periods, such as air flow, those which involve vibration and those which involve short periods of energy availability such as footfall during walking.

2.3.1. Electromagnetic radiation

Electromagnetic waves carry energy that can be converted to electrical power through the use of photovoltaic cells. Useful energy in terms of harvestable energy can be found from the radio wave region to the gamma region of the electromagnetic spectrum. For solar cells the predominant regions of interest is from the ultraviolet (UV), visible (wavelength λ in 400nm to 700nm) and infrared region. Radio wave will be considered separately.

The efficiency of the conversion into electrical energy is dependent on which region of the spectrum is used, in general the higher the frequency (shorter the wavelength λ) of the travelling electromagnetic wave, the higher the energy in photons that are available to the converter.

Light is a significant source of energy, but it is highly dependent on the application and how much exposure the device is subjected too. On a sunny day the incident light on the surface of the earth has a power density of around 100mW/ [38], with efficiencies of 15%-20% for

single silicon solar cells [52] it is reasonable to forecast a power output of 15mW/-20mW/ for this type of solar cell.

Ambient light levels in indoor environments are significantly lower than those found outdoors, common office lighting provides about 100µW/ [39]. Thin film amorphous silicon or cadmium telluride cells offer better efficiencies indoors, because their spectral response more closely matches that of artificial lighting indoors; these cells still only offer 10% efficiency, corresponding to a power output of 10µW/.

2.3.2. Thermal

Conversion of energy derived from thermal gradients is the basis for much large scale power generation (e.g. steam turbines) but such technologies are not generally scalable to the level required for sensor network nodes. At this smaller scale, solid state devices are more attractive. Although the voltage and power levels associated with an individual thermocouple is very low, arrays of multiple thermocouples may be used in order to increase the voltage and power level. Further discussion on the conversion methods is provided in section 2.4 on thermal conversion methods.

2.3.3. Mechanical Energy Sources

Sources of mechanical energy may usefully be grouped as those dependant on motion which is essentially constant over extended periods of time, such as air flow used in a turbine, those dependant on intermittent motion, such as human footfall and those where the motion is cyclic, as in vibration sources. These different types of sources will be considered separately.

Steady State Mechanical sources

Sources of ambient energy which are essentially steady state are based around fluid flow, as in wind and air currents and water flow either in natural channels or through pipes, or around continuous motion of an object such as a rotating shaft. Fluid flow based sources of energy are widespread and used on the macro scale for electrical power generation as in wind turbines and hydroelectric plant but have also been considered for smaller scale harvesting applications. Starner [53], considered the potential for energy harvesting from blood flow and breathing in human subjects and determined that significant power was available but that these might not be acceptable to subjects.

Intermittent Mechanical sources

Energy is available from motion which may be cyclic in nature but in which the energy is only available for a short part of the cycle. Examples of this type include energy available from vehicles passing over an energy harvesting device [75] and intermittent human activity such as walking or typing where, for instance, footfall occurs over a period of milliseconds during a gait cycle of around one second. Harvesting of energy from these intermittent sources was also considered by Starner [53] who concluded that available energy ranged from around 7mW from finger motion during typing to 67W for lower limb movement. This paper also considered the effect that extracting this energy would have on the subject and concluded that inconvenience to the subject could only be avoided if significantly lower power levels were extracted. A particularly attractive source of energy in this context is foot fall or heel strike since normal walking involves dissipation of significant energy in the shoe and walking surface and so the user might be unaware if some of this energy were converted to electrical energy. It may readily be calculated that a subject weighing 60kg must apply a force of at least 588N through the foot during walking (The peak force is typically 25%

above body weight during walking and up to 2.75 - 3 times body weight during running [80]). If this is accompanied by a 10mm deflection of the floor or shoe, then the available energy is 5.88J and assuming two steps per second, an available power of 5.88W per foot. Similar calculations may be carried out for the case of vehicles passing over a deflection device and, given the far greater weight, a significantly greater energy level is found (for example a single 40 Ton vehicle causing a 10mm deflection could provide 4kJ), although clearly the frequency of vehicle passage will affect the average power level achievable.

Vibration

Vibration energy is available in most built environments. The energy that can be extracted from a vibration source depends on the amplitude of the vibration and its frequency. It also depends on the extent to which the presence of an energy harvesting device affects the vibration. This, in turn, depends on the mass of the harvesting device relative to that of the vibrating mass. Vibration sources vary considerably in amplitude and dominant frequency. Roundy [116] presents results for the measurement of a number vibration sources which indicate that the amplitude and frequency varies from $12ms^{-2}$ at 200Hz for a car engine compartment to $0.2ms^{-2}$ at 100Hz for the floor in an office building with the majority of sources measured having a fundamental frequency in the range 60-200Hz. Vibration present in most environments is not made up of a single frequency but is typically made up of a number of fundamental frequencies and their harmonics. As will be seen in the next section, the energy which can be extracted from a vibration source depends on the frequency and amplitude and, since the majority of vibration based conversion devices have a relatively narrow range of operating frequencies, it is important that the nature of the source be understood. It is difficult to establish a strong relationship between the amplitude and fundamental frequency of ambient sources because of the limited frequency range typically found. However if a harvesting device is tuned to a frequency above about 200Hz, it may be

necessary to use harmonics rather than the fundamental frequency of the source. The amplitude of these harmonics tends to be of significantly lower amplitude than the fundamental. Essentially these harmonics decay at an exponential rate from the fundamental and therefore any energy harvesting is considerably reduced.

2.4. Energy Conversion Methods

The effectiveness of an energy harvesting system depends on both the available energy and on the efficiency with which that energy can be converted to useable electrical energy. A broad range of conversion devices is available, each with its own advantages and disadvantages, as will be discussed in the following section.

2.4.1. Electromagnetic radiation

As noted in section 2.3, electromagnetic radiation sources may be grouped according to the part of the electromagnetic spectrum in which they reside. Radiation around the visible light part of the spectrum contains abundant energy in many environments and this energy may be conveniently converted to electrical energy. Conversion efficiencies of around 15-20% are readily achievable in commercial devices. Conversion of ambient radio frequency (RF) signals to useful electrical energy is far more challenging due to the broadband, low intensity nature of the signals typically present. Systems have been reported which are capable of harvesting sufficient energy for simple electronic circuits but these must generally be positioned close to the source of RF power. The limitations of such systems are outlined in [55].

2.4.2. Thermal

Conversion of energy derived from thermal gradients is the basis for much large scale power generation (e.g. steam turbines) but such technologies are not generally scalable to the level required for sensor network nodes. At this smaller scale, solid state devices are more attractive. Although the voltage and power levels associated with an individual thermocouple is very low, arrays of multiple thermocouples may be used in order to increase the voltage and power level. Stordeur and Stark [56] combined 2,250 thermocouples in a generator capable of producing 20μW for a temperature difference of 20K. A commercial device based on similar technology provides 100μW from a 10K temperature difference in a 9.3mm diameter device 1.4mm thick [57].

2.4.3. Steady State Mechanical

Conversion of steady state sources of mechanical energy, such as air or water flow, has been investigated by several researchers. [58] describes a device suitable for fitting to a domestic water tap capable of extracting energy from the water flow using a turbine. A miniature turbine designed for use in air flow is described in [59]. This device used a 13mm diameter, 1mm thick turbine disk and was capable of producing 1mW of electrical power. A larger device designed for use in heating, ventilating, and air-conditioning (HVAC) ducts is described in [60]. A turbine with a diameter of approximately 10cm was shown to produce around 27mW for an air flow rate of 1000 feet per minute, which is within the range found in a HVAC duct but greater than that found in most other environments.

2.4.4. Vibration

Vibrations are an abundant source of energy available all around us. This energy can be tapped into to power microelectronic devices. Vibration based energy harvesting devices are generally based around mass, spring, damper systems of the type illustrated in Figure 2-2.

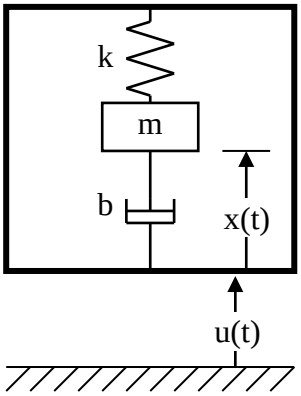

Figure 2-2 Generic vibration to electricity model

The kinetic energy of the vibrating mass can be converted to electrical power based on linear system modelling. A generic vibration to electricity conversion model was proposed by [38] based on the model shown in Figure 2-2 and described by Equation 2-1.

$$m\ddot{x}(t)+b\dot{x}(t)+kx(t)=-m\ddot{u}(t) \qquad \textbf{Equation 2-1}$$

The system is composed of a seismic mass, *m*, and a spring of stiffness *k*. The seismic mass is suspended within the device at a position $x(t)$ relative to the base of the device. The entire device moves relative to the inertial frame with the motion position at time *t* described by $u(t)$. Losses within the system and energy harvested from the system are represented by the damper. The characteristics of this damping element depend on the type of energy conversion utilized; typically the damping coefficient comprises the electrically induced damping coefficient and the mechanical damping coefficient. It is useful to know that the power converted to the electrical system is equal to the power removed from the mechanical system by the electrically induced damping coefficient. The electrically induced force is $b_e\dot{x}$ and power is the product of force F and velocity $\dot{x}$ provided both are constants.

Electromagnetic

Electromagnetic conversion of input energy, whether it is of cyclic or intermittent nature, is based on the generation of voltage resulting from the relative movement between a magnet and a coil. The voltage generated in a coil made up of *N* turns of side length *l* moving through a magnetic field with flux density *B* at a velocity $\dot{x}(t)$ is $v(t) = NlB\dot{x}(t)$. Assuming that $\dot{x}(t)$ varies sinusoidally with frequency ω and that the coil has resistance and inductance and is connected to a resistive load then the load current is $i = v/(R_L + R_c + j\omega L_c)$ and since the resulting force is $F = BilN$, the effective damping in equation Equation 2-1 becomes:

$$b = \frac{(NlB)^2}{R_L + R_c + j\omega L_c}$$

Because of the reactive behaviour of the inductance, there is a phase shift in the damping but it is generally assumed that the inductance is insignificant at the vibration frequency [70].

$$P_e = \frac{mA^2}{16\omega_n \xi_m}\left(1 - \frac{R_c}{R_L}\right) \qquad \textbf{Equation 2-2}$$

It can then be shown that the maximum electrical power delivered to a matched load when tuned to the frequency of the vibration source is as shown in [70],[71],[72].

Intermittent mechanical conversion

As noted when discussing energy sources in section 2.3, there are a number of sources of mechanical energy which are repetitive but are non-sinusoidal. For instance footfall occurs at

an approximately fixed frequency but is characterised as a series of impacts rather than a continuous sinusoidal variation. Conversion systems suitable for this type of energy source are significantly different from those used for vibrational sources. Given that these sources typically deliver power over a small part of the overall period, the challenge here is to devise mechanically robust devices able to convert the energy in an efficient manner without being large or heavy. The majority of studies reported in the literature have been aimed at capturing energy from footfall, since this is one of the most promising sources in human energy harvesting, although other researchers have investigated energy harvesting from moving traffic [75].

Piezoelectric Conversion

Starner and Paradiso [55] considered a number of shoe insert energy harvesting devices. They predicted that an insert constructed from 40 plies of Polyvinylidene fluoride (PVDF) positioned to extract energy from the flexing of a shoe sole should be capable of generating 5W when deflected by 5cm by a 52kg user. The device constructed was smaller than that used as the basis for these predictions and possessed fewer PVDF layer. The measured peak power from this device was 15mW with an average over the entire gait of 1.3mW. A second device, based on a Lead zirconate titanate (PZT) unimorph, was developed to capture energy from heel strike. This was found to deliver a peak power of 60mW and an average of 1.8mW. A further development of this device used two unimorphs arranged back-to-back and achieved an average power of 8.4mW. It was noted that this represented an efficiency of mechanical to electrical energy of only around 1%.

The efficiency of piezoelectric conversion is improved if the device is operated at its resonant frequency and so consideration has been given to methods to convert the low frequency footfall energy pulses to higher frequencies matched to piezo resonance. Antaki [68] used a passive hydraulic pulse amplifier to effect this frequency conversion and obtained average

power of up to 700mW during walking while Hagood [69] used an active valve to chop the hydraulic flow at the resonant frequency of a PZT resonator.

Electro-Active Polymers (EAP) Conversion

A number of polymeric materials exhibit significant strain when subjected to electric field and similarly are capable of generating electrical power when strained. Appropriate polymers are capable of undergoing significant strain, give efficient conversion between mechanical and electrical energy and have low density. A heel strike device based on EAPs has been demonstrated which is capable of developing 0.8J/step, indicating a power of around 2W at normal walking speed if fitted to both feet [148], [149]. The voltages generated by EAPs are generally high and so efficient conversion of these high voltages to more usable levels remains problematic. The durability of the materials has also been a matter for concern [148].

Electromagnetic Conversion

Given the design and material constraints imposed on electrical machines, they typically posses a limited range of speeds at which they operate efficiently. The majority of machines are most efficient when operated at high speeds and low force/torque. Thus there is an inherent mismatch with most intermittent sources of mechanical energy which have relatively high force but low average speed. One method for improving this matching is through the use of gears [87] but this introduces significant inefficiency and increasing the gear ratio used typically increases the losses.

One approach to ameliorate the problems associated with the high impact forces found in footfall and similar intermittent energy sources is to attempt to store the energy so that the conversion between mechanical and electrical energy can be performed over a longer period, thus making use of physically smaller devices. Mechanical energy may be stored in springs,

moving masses or in fluid flow or a fluid pressure vessel. Kymissis [65] demonstrated a system composed of gears, a spring and flywheel used to drive a generator which was able to produce an average of 250mW from a 3cm deflection of the heel during normal walking. It was noted that this device was obtrusive for the user.

A mechanism developed by Gilbert, based on mechanical analogues of electrical switched mode power supplies [88], has been used as an energy harvesting shoe heel insert. In this device energy supplied during compression is stored in a spring and when the heel lifts off the stored energy is transferred through a set of gears and a freewheel device to a flywheel and generator. Since the impact energy is only transferred to the spring, it is not necessary to use such large and robust gears as would be required for direct conversion during the heel strike impact. The device, shown in

Figure 2-3, has dimensions 50 x 65 x 30 mm and allows a deflection of 14mm. When driving a matched load of 70Ω it is capable of producing an output energy of 90mJ from a mechanical input energy of 450mJ at a peak voltage of approximately 7V. Thus for a speed of 1.1 steps/s, this represents an average power of 100mW.

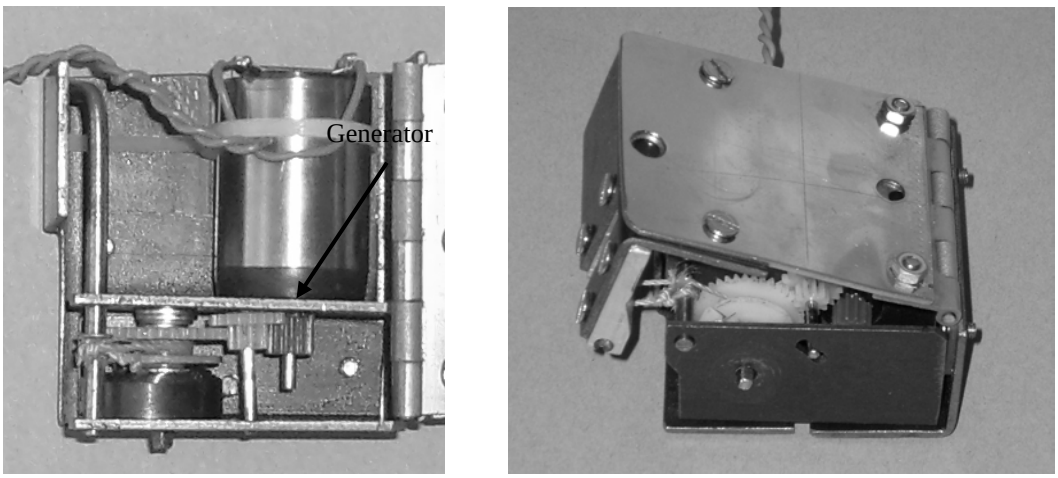

Figure 2-3 Energy harvesting shoe insert Error! Reference source not found.

The lower voltages typically derived from electromagnetic generators are more compatible with most electronic circuits than the high voltages of around 150V typically derived from

piezo converters [89]. While these high voltages can be reduced to more appropriate voltages for electronic circuits, this conversion process introduces further losses.

Piezoelectric conversion

The piezoelectric effect causes the generation of an electric charge when the material is put under stress. These materials also have the opposite effect that when a charge is applied to it, the materials experience a deformation. Therefore piezoelectric materials allow the generation of electricity and mechanical energy and vice versa. This property could be used to harvest energy from the environment.

The constitutive equations for a piezoelectric material are given in Equation 2-3 and Equation 2-4 [39]:

$$\delta = \sigma / Y + dE \qquad \textbf{Equation 2-3}$$

$$D = \varepsilon E + d\sigma \qquad \textbf{Equation 2-4}$$

Where δ is the mechanical strain, σ is the mechanical stress, Y is the modulus of elasticity, d is the piezoelectric strain coefficient, E is the electric field, D is the electrical displacement (charge density) and ε is the dielectric constant of the piezoelectric material.

The efficiency of a resonant generator clamped to a substrate and cyclically compressed at its resonant frequency is shown in equation Equation 2-5 [73]:

$$\eta = \frac{\frac{k^2}{2\left(1-k^2\right)}}{\frac{1}{Q}+\frac{k^2}{2\left(1-k^2\right)}}$$ **Equation 2-5**

Where η is the efficiency of the piezoelectric generator, *k*, describes the efficiency with which energy is converted between mechanical and electrical forms, Q is the quality factor of the resonator. As Q becomes larger, the efficiency tends towards unity but for typically achievable Q factors, the efficiency increases significantly for higher values of k.

Electrostatic conversion

Electrostatic conversion is based on the formation of a parallel plate capacitor onto which a charge is introduced from an external power source. Once the external source is disconnected then varying the capacitor configuration (plate overlap area or plate separation) causes the voltage and/or charge on the capacitor to vary. The varying voltage or charge may be extracted to provide electrical energy to a load.

For a parallel plate capacitor with plate area, *A* and plate separation, *d* the capacitance is approximately:

$$C = \varepsilon \frac{A}{d} = \frac{Q}{V}$$ **Equation 2-6**

where ε is the dielectric constant of the insulating material between the plates, *Q* and *V* are the charge and the voltage on the capacitor respectively. The energy stored on the capacitor is

$$E = \tfrac{1}{2} QV$$ **Equation 2-7**

If the charge is held constant then, combining Equation 2-6 and Equation 2-7, the energy becomes:

$$E = \frac{Q^2 d}{2\varepsilon A}$$ **Equation 2-8**

while if the voltage is constrained the energy becomes

$$E = \frac{\varepsilon A V^2}{2d}$$ **Equation 2-9**

Attempts to change the stored energy by moving the capacitor plates causes a reaction force. This reaction force depends on whether the gap or the overlap area of the capacitor is varied and on whether the voltage or the charge are constrained. For instance, if the separation of a parallel plate capacitor is changed and the charge constrained then since force is the rate of change in energy with distance, the force can be found from Equation 2-8 as:

$$F = \frac{Q^2}{2\varepsilon A}$$

while if the voltage is constrained, Equation 2-9 gives:

$$F = \frac{\varepsilon A V^2}{2d^2}$$

Thus in the first case, the reaction force is constant while in the second it is proportional to $1/d^2$. These differences will affect the response of the resonant spring mass system, particularly if the forces are larger than other sources of damping.

Photovoltaic

The design of a solar cell is generally the same and most basic solar cells are single layer solar cell. The designs involve connecting an n-type semiconductor to a p-type semiconductor. Photons (light) with energy equal to or greater than the band gap are absorbed and a concentration gradient is formed with free electrons on the n-doped side than the p-doped side. As a result diffusion of current is created as holes diffuse from the p-side into the n-side and electrons diffuse from the n-side to the p-side and electrical power generated from light photons [74].

Thermal

Temperature gradients are a natural source of energy available in many places which can be harnessed to provide power to sensor and actuator networks. The maximum efficiency of power conversion from a temperature difference is equal to the Carnot efficiency [39]. The equation is given in Equation 2-10 below,

$$\eta = \frac{T_{high} - T_{low}}{T_{low}} \qquad \textbf{Equation 2-10}$$

The amount of heat flow or power is given by equation Equation 2-11

$$q' = k\frac{\Delta T}{L} \qquad \textbf{Equation 2-11}$$

Where T is Temperature, k is the thermal conduction of the material and L is the length of the material through which the heat is flowing.

2.5. Available technologies for footfall harvesting

This section will summarise existing technologies which may be applicable to footfall energy harvesting. It is based on information published in the academic literature, trade and popular press, internet resources, patent searches and direct contact with selected researchers.

There are relatively few examples of energy harvesting systems designed to be installed in a floor/stair locations. A larger number of devices have been developed for in-shoe use and for capturing energy from vehicular traffic and the suitability of these devices for underfloor energy capture will be considered. Devices will be classified according to the underlying energy conversion technology and the mechanisms used for coupling input energy into the conversion device.

2.5.1. Piezo

Piezo electric materials exhibit the characteristic that they generate a voltage when stressed and undergo shape change when a voltage is applied. There are many naturally occurring and man-made piezo electric materials with the efficiency of mechanical-to-electrical energy conversion being a key consideration in the material choice. There are two main materials which have been widely considered for energy harvesting applications. PZT is a brittle ceramic with a high conversion efficiency. Because of its brittleness and stiffness, it is most suited to vibration based energy harvesting but has also been used in impact based systems. When used in direct compression, it has a resonant frequency of several kilohertz while if used in a bending mode the resonant frequency drops to around 100Hz.

PVDF is a polymeric material available as flexible sheets and is more robust than PZT but has a much lower conversion efficiency. Because of its lower stiffness and greater damping, PVDF is not suited to vibration based conversion but is more suited to impact based converters such as those used in footfall devices.

2.5.2. Piezoelectric Footfall Devices

The majority of floor mounted footfall energy harvesters are based around piezo conversion. The systems described in the literature are outlined below.

Japanese Railways and Keio University have developed a ticket gate electricity generation system which relies on a series of piezo elements embedded in the floor under the ticket gates (see Figure 2-4). A power generation mat using piezoelectric elements was tested in Tokyo station of Japan Railways east (JR-east) company in 2006 and 2008. Passengers generate electrical power by passing over the power generation mats through SUICA (RFID) gates. The system includes the power generation circuit and the super capacitor circuit to store the generated electric power. A total of 90 of piezo power generation mat were laid down in Tokyo station for a test period of two months on staircases and in front of busy shopping areas. The device is reported to generate 1mJ per step from a single generator but it is also stated that the expected output of the complete system would be 500kJ generated per day and 766kJ generated on a peak day [90] [91], [92]. These figures correspond to an average of 5.8W over 24 hours of an average day or 8.9W on a peak day. Pedestrian traffic levels and power usage are likely to vary significantly throughout the day so it seems reasonable to speculate that during peak times the power generation is probably 5-10 times higher than the average. The authors claim that the system generates sufficient power to operate the RFID ticket gate. The figures published imply a total footfall of 500 million per day. Even allowing

for the capture of energy from 100 steps per person, this still implies 5 million pedestrians passing over the system each day. This level of power generation thus appears improbable.

Figure 2-4 Energy Harvesting Ticket gate and staircase, Tokyo [90], [91]

A similar system, entitled POWERleap uses energy generated as people walk across it to light up the nighttime pavement [92]. The system uses 2-inch by 1-inch PZT plates with a brass reinforcement shim covered in nickel electrodes for low current leakage (see Figure 2-5). When these plates are bent the voltage (22V peak) and current (24μA) is induced and stimulates momentary electrical energy impulses used to light the LED's inside each tile. These current and voltage levels imply a peak power of 0.5mW but it is not clear how long this power is sustained for. It is likely that this occurs only over a very short portion of the gait cycle and so the average power is likely to be at least an order of magnitude lower than this. The system appears to have been developed as a proof of concept rather than being optimized for maximum power output.

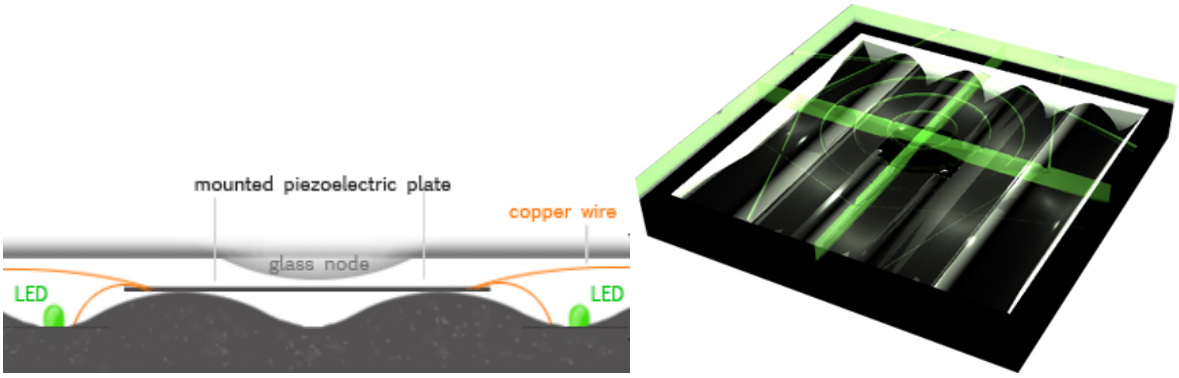

Figure 2-5 POWERleap tile structure [92]

2.5.3. Electro Active Polymers (EAP)

A number of polymeric materials exhibit significant strain when subjected to electric field and similarly are capable of generating electrical power when strained. Appropriate polymers are capable of undergoing significant strain, give efficient conversion between mechanical and electrical energy and have low density. A heel strike device based on EAPs has been demonstrated which is capable of developing 0.8J/step, indicating a power of around 2W at normal walking speed if fitted to both feet [95], [96]. The voltages generated by EAPs are generally high and so efficient conversion of these high voltages to more usable levels remains problematic. In addition, they need a high voltage applied to the polymer in order to initiate generation. The durability of the materials has also been a matter for concern [95]. The use of EAPs as mechanical to electrical converters is covered by several patents (eg [97] filed by SRI International) but their application to energy harvesting is not specifically covered in the claims.

2.5.4. Electromagnetic Conversion

Electromagnetic conversion of mechanical to electrical energy is well established in the utility generation sphere and machines capable of very high efficiency conversion are readily available. However, the source of energy in this case is the human body which is

characterized by motion which involves high force amplitude at low frequencies, inherently mismatched to rotary generators requiring high speeds with low force or torque to operate at their maximum efficiencies. In addition, footfall motion is essentially a linear translation while most electrical machines operate most effectively with rotational motion. It is thus desirable to convert from translation to rotation and from low speed to high speed motion. Gearing is the most obvious (and most widely used) method of achieving this conversion but because of the high impact forces involved in footfall, direct gearing requires large gears capable of transmitting these loads. These in turn tend to exhibit relatively high levels of friction and hence low efficiency. A number of developments from this basic concept have been considered using freewheel and flywheel mechanisms to increase the duration over which energy conversion is performed. In addition, springs have been used as energy storage elements to allow manipulation of the energy transfer process.

Electromechanical Shoe Inserts

Several research projects have considered mechanisms designed to convert the short intermittent pulse of a human gait to useable electrical energy. The idea of embedding a rotary generator into the heel of a boot has been around since the 1920's and has reappeared in different guises for different applications [81], [82], [83], [84]. The MIT team headed by Paradiso produced a system which generates peak powers of around 1W and an average power of 250mW with a deflection of 30mm [85], implying an efficiency of around 1.5%. This was improved upon by Hayashida [86] who integrated a generator into the sole of a sport shoe. However, as the mechanism transferred the heel impact via a geared mechanism the wear on the device was substantial and some concerns were noted as possible issues which needed to be improving upon. A shoe generator was developed by Gilbert based mechanical analogues of electrical switched mode power supplies [88], [108]. This used a spring to store energy during the heel strike which was then released via a lightweight gear

mechanism and freewheel to a generator. The use of spring storage reduced the size of the gears required and hence the level of friction. The device, which was embedded in the sole of a boot, delivered 90mJ from a mechanical input energy of 450mJ at a peak voltage of 7V, representing an efficiency of around 20%. The performance of the device was limited by the requirement to fit within a boot heel – a restriction which would not necessarily be present in an under-floor system.

Footfall device

A London nightclub has installed an energy harvesting dance floor in which the movements of the dancers causes deflection of the floor which is coupled to an electromagnetic generator. The resulting charge is stored on batteries and used to power parts of the club. Although no values for generated power are given Sustainable Dance Clubs has ambitions to reduce energy consumption by 30% with other sustainable products like low power LED lighting, with surplus power used for water management systems etc [3], [4], [5]. The company has, in 2012, developed a new prototype that is reported to produce 5 Joules per step from an available 8-9 Joules of energy [164].

Harvesting power from the movement of people in heavily congested areas like train station and music concerts was also investigated by two MIT architectural graduates [108] who envisaged that a responsive sub-flooring system made up of blocks that depress slightly under the force of human steps would be installed beneath the main lobby of a railway station. The slippage of the blocks against one another as people walked would generate power through the principle of the dynamo. This was developed as a concept but does not appear to have been taken to the prototype stage.

Although not a footfall device, the student's test case, displayed at the Venice Biennale and in a train station in Torino, Italy, was a prototype stool that exploits the passive act of sitting to generate power. The weight of the body on the seat causes a flywheel to spin, which powers a dynamo that, in turn, lights four LEDs

2.5.5. Non Footfall Electromechanical Devices

Notable recent advances in energy harvesting from human movement has come in the form of a knee generator which can harvest energy form the natural walking motion with minimal user effort. Donelan et. al [88] devised a method of extracting energy from the human gait which uses the principle of regenerative braking, where energy normally dissipated during the swing phase of walkers gait is used to generate power. The device is capable of generating 5 watts of electricity per leg and is claimed to have minimal effect on the user. Bionic power is producing biomechanical energy harvesters for military and medical applications, based on this research. An energy harvesting backpack designed for military applications has also been developed by Rome [89] which converts vertical movement of carried loads to electricity. The device, integrated into a backpack, is capable of delivering 7.4 W of electrical power.

2.5.6. Traffic tap systems

The conversation of kinetic energy from vehicles has been an area of interest for some time. A patent filed in 1981 [102] considers the movement of vehicles over a pivoted ramp and through a geared system, the energy is transferred via a shaft to a generator. In [103] another inclined ramp assembly is used to transfer the energy from the passage of a vehicle to a flywheel through a roller assembly and thence convert the rotary motion of the flywheel into electrical energy via a generator.

Recently commercial traffic tap systems which convert the passing of vehicles over a ramp to electrical power have been developed [105]. It is envisaged that traffic tap systems located at busy junctions could power traffic lights and other road management systems. Also the same organization (Hughes Research Ltd) describe a multi-ramp system located on slip roads, where traffic naturally slows as vehicles come off the highway, thereby using the concept of regenerative braking to capture the energy of slowing vehicles. In this system, energy would be extracted from the vehicle as it passes over each successive ramp.

2.5.7. Hydraulic Coupled Systems

The conversion between low speed foot motion and the high speed motion required for efficient electromagnetic conversion can be achieved using hydraulic and pneumatic systems as an alternative to gears and similar mechanisms. Hydraulic systems, although potentially much more problematic with regards leaks and maintenance, are an attractive solutions to harvesting energy from off-body human motion. McLeish and Marsh [98] demonstrated a hydraulic pump system in the heel of a user's shoe for the purpose of powering artificial implants. The system had a deflection of approximately 10mm and, according to a paper [6] referencing the original work, recovered on average 5W of power from the users gait. Although quite intrusive for on-body application, this could lend itself quite easily to an off-body system as proposed by this work.

Hydraulic shoe-sole generators incorporating separate fluid reservoirs in the sole and heel are presented in patents [100], [101]. These reservoirs are coupled via turbines so that fluid flows from heel to sole during heelstrike and back to the heel when the sole is compressed. Using appropriate valves, the fluid causes the turbine to rotate in the same direction during both phases of the fluid motion. The turbine is coupled to an electromagnetic generator. The devices described in the two patents [100], [101] appear to be very similar but they were filed

by different inventors at approximately the same time and both appear to have been granted without reference to each other. Details of the power generated using these devices are not given but the concept does have some attraction for energy harvesting systems fitted under sprung flooring and staircases.

As noted above, fluidic systems have potential disadvantages in terms of leaks but they also potentially benefit from lower cost and lower precision components than, for instance, mechanical gearboxes. They are generally expected to give lower efficiency but may be easier to scale for multiple inputs than mechanical systems.

2.5.8. Pneumatic

As with hydraulic systems, pneumatic systems have similar drawbacks but could provide unobtrusive solutions to the proposed designs. Marsden and Montgomery [99] conducted quite useful surveys into extracting useable electrical energy from heel strike. Although carrying out useful work with regards to the forces available in the human gait they concluded that a pneumatic system was not suitable for energy extraction from heel strike for powering artificial implants and recommended rotary mechanical systems because of the efficiencies these systems provide.

2.5.9. Comparison of technologies

In this section we seek to compare the advantages and disadvantages of the broad categories of energy harvesting devices considered. Within each broad category, we have considered the most appropriate of the systems described in the literature and patents. The summary data is presented in Table 2-2.

Technology	Sub category	Power output for single pedestrian	Likely cost	Scalability for multiple inputs
Piezo	PZT [106]	8.4mW	Moderate	Difficult
	PVDF [106]	1.3mW	High	Difficult
EAP [95]		1W	Not known	Not known
Electro-mechanical	Gear coupling [164]	5W	High	No
	Gear/flywheel/ spring coupling	90mW	Moderate	Moderate
	Hydraulic coupling [100][101]	Not known – efficiency probably low	Low	Easy

Table 2-2 Summary of available technologies

2.5.10. Conclusions

There are relatively few underfloor systems designed to generate electrical energy from human footfall and those which are described in the literature indicate relatively poor power output, expect for the device designed by Sustainable Dance Floors. As discussed and referenced in this chapter, there are however a large number of other technologies, designed for other energy harvesting applications which may be adapted to the proposed scenario. Based on the literature, it appears that electromagnetic conversion presents the most promising technology for high efficiency energy harvesting. The most appropriate means of coupling the footfall motion to the electromagnetic generator depends on the details of the application scenario and upon factors such as the relative importance of efficiency, cost and scalability.

3. Chapter 3 – Design for Footfall Harvesting

In this chapter parameters affecting the available energy in footfall harvesting are investigated and scenarios where these devices would see most footfall are explored. Concept selection criteria along with a range of concepts generated, are presented in appendix A. Finally, a discussion on the selected concepts for prototyping is discussed.

3.1. Application Scenarios and Operating Parameters

The objective in designing an energy harvesting system is to extract the maximum possible power from pedestrians without having a significant negative impact on those pedestrians at a reasonable cost of manufacture, installation and maintenance. The aim of this section is to identify those parameters which are important to the design of a footfall energy harvesting device and to determine appropriate values for those parameters in particular application scenarios.

3.1.1. Parameters Affecting Available Energy in Footfall Energy Harvesting

Based on fundamental physical considerations, it is possible to determine the amount of energy which could potentially be extracted from footfall. Energy is transferred by a combination of applied force and a resultant displacement. If the applied force is a constant, F, and the resultant displacement is d, then the energy, E, this represents is:

$$E = F.d$$

In the more general case where the reaction force varies with displacement, x, according to $F(x)$ then the energy becomes

$$E = \int_0^d F(x)\, dx$$

Graphically, this is the area under the curve of force against distance, as illustrated in Figure 3-1.

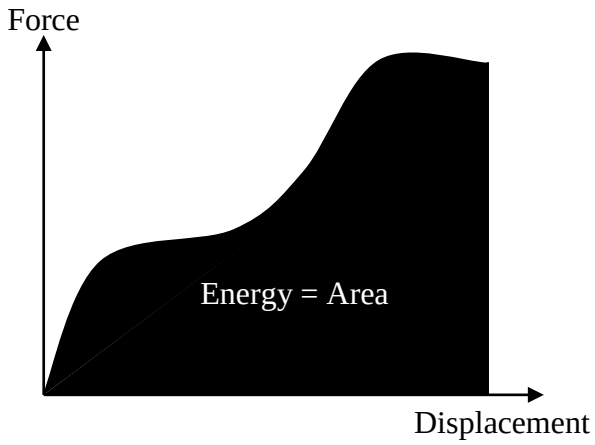

Figure 3-1 Energy as a function of force and displacement

Two types of situation likely to be found in practice are the constant force, *F*, described above where $E = F.d$ and the situation where the force is generated by a spring (with spring constant, k) where the force is proportional to displacement ($F = k.x$) where the energy is $E = \frac{1}{2}k.d^2$. Given that the available force is limited then the maximum energy is obtained for the constant force case ($E = F.d$).

If footfall occurs at a frequency, *f*, then the average power is $P = E.f$. If it is possible to capture energy from multiple people simultaneously then the average power becomes $P = n.E.f$, where n is the number of simultaneous footfalls. For the constant force case, this becomes

$$P = n.F.d.f$$ **Equation 3-1**

In order to maximise the generated power, each term in Equation 3-1 must be maximised. These values are limited by the nature of the pedestrian population, the effect that energy harvesting has on those pedestrians and constrains imposed by the application environment. These four parameters will be considered in turn.

3.1.2. Displacement

The maximum displacement which a surface can undergo when stepped upon without causing an undesirable reaction from the pedestrian is not clearly defined and will probably depend on the environment. For a level surface, a step of 15mm or more is considered a trip hazard and it seems reasonable to take this as a limit in other situations. In many situations, the displacement experienced will depend on the weight of the pedestrian so that a light pedestrian will experience a smaller deflection than a heavy one. For energy harvesting purposes, it is desirable to maintain a displacement near to the acceptable maximum, irrespective of the pedestrian's weight.

3.1.3. Ground Reaction force

The force exerted on a walking surface depends on the weight of the person and upon their gait. In normal walking on a level surface, the vertical ground reaction force (GRF) has a maximum typically 25% above body weight while during running, this increases to 2.75-3 times body weight. The GRF varies through the gait cycle [79]. There is a rapid initial impulse as the heel hits the ground, then the full foot comes into contact with the ground. The force then increases again as the foot lifts off. The profile during jogging and running shows a similar overall profile but the magnitude at different phases is altered.

The GRF during climbing and descending of stairs does not appear to be documented in the scientific literature but it seems reasonable to assume that the forces involved are likely to be significantly greater, particularly during climbing, than for level walking. A study be to measure these forces in a typical stair case, will be discussed in Chapter 4.

3.1.4. Footfall frequency

The rate of footfall depends on the gait and physiology of the pedestrian but for normal level walking, the footfall frequency is between 2 and 2.2Hz. Given the small range of frequencies and the relatively small impact that this would have on power generation, a frequency of 2Hz will be assumed for subsequent considerations.

3.1.5. Number of pedestrians

As noted above, the potential for power generation increases in proportion to the number of pedestrians simultaneously walking on an energy harvesting device. However, the device must be capable of extracting energy from each of these individuals separately if the benefit is to be gained. Certain energy harvesting device concepts are better suited to this multiple input scenario than others. The ability to capture energy from multiple pedestrians depends on whether they can be constrained to remain on the harvesting device. This in turn depends on where and how the device is deployed.

3.2. Application Scenarios

Given the above considerations, it is possible to identify a number of scenarios in which it is reasonable to expect energy harvesting to be most effective. The ideal location will have a large number of pedestrians constrained within a small area and constantly in motion. Locations which satisfy the above requirements include:

- Staircase in a transport interchange such as a tube station. In this case a large number of pedestrians are funnelled into the staircase and are generally constantly in motion.

It is expected that the ground reaction forces present will be significantly higher than during level walking.

- Entrance to a large, busy building such as a shop. Here pedestrians are constrained by the width of the doors and it would be possible to capture energy from several pedestrians simultaneously if the energy harvesting device covered a region around the entrance.

Based on the above considerations, these two scenarios outlined above will be considered and the operating parameters listed in Table 3-1 will be assumed.

Parameter	Scenario 1 Tube staircase	Scenario 2 Building entrance
Average Ground Reaction Force	120N	80N
Available Harvesting area	1 step 1.2m wide	Level floor 5mx5m
Maximum Allowable Deflection	15mm	15mm
Footfall	2 steps per second	5 pedestrians entering area simultaneously. Maximum of 15 pedestrians within harvesting area at any time

Table 3-1 Proposed design parameters

3.3. Concept Selection Criteria

As part of the design process several concepts were generated and can be seen in **Appendix A.** The following criteria were used to identify and determine the most appropriate concepts to develop to the prototype stage. Each of the concepts generated were assigned a value between 0 and 10 indicating the extent to which the concept is expected to fulfil the corresponding criterion. These values were based on engineering judgement, experience, published data and, in some cases, preliminary experiments. The relative weightings of these criteria depended on the application scenario in Table 3-1 and were applied in the two scenarios identified in section 3.2.

- **Anticipated power output.** This is an estimate of the power level which it is anticipated it will be possible to generate from a single pedestrian of average weight and gait walking over the harvesting device. A high output power level corresponds to a high value for this criterion
- **Cost of implementation.** At this stage, this is based on estimates of the cost of major bought in materials and components plus an assessment of likely complexity of manufacture. A high cost of implementation corresponds to a low value for this criterion
- **Reliability and maintenance.** This is based on a judgement of the likely need for maintenance and the likelihood that components in the system may fail in service. A high maintenance requirement corresponds to a low value for this criterion
- **Voltage/current level generated.** For most of the applications envisaged, it is desirable to provide a voltage in the range 5-24V. It is possible to convert from higher and lower voltage levels to this desired range but this implies additional

inefficiencies. The greater the voltage increase/decrease required the greater the inefficiency involved, reflected in a low value for this criterion.

- **Ability to accommodate range of ground reaction force (GRF).** The energy available for conversion depends on the force applied by the pedestrian to the floor/stair and this depends on the weight of the pedestrian and the gait adopted. For adult pedestrians, the GRF varies by a factor of around 5 from a light adult walking to a large adult running. The average energy generated depends on the ability of the mechanism to convert this range of GRFs efficiently into electrical energy. A mechanism which can efficiently convert this range of GRFs will receive a high value for this criterion
- **Ease of expansion to multiple pedestrians.** The other criteria assume a single harvesting element and a single pedestrian but it may be possible to expand the device to harvest energy over a wider area and from multiple pedestrians. In general, it is desirable to take energy from several inputs and combine them in a single generator or similar since the generator element is frequently the most expensive element of the system. Thus scalability may reduce the overall cost per unit output power. A high value of this criterion indicates that such an extension would be relatively straightforward.
- **Installation space requirement.** Different technologies require different amounts of space, particularly depth below floor level for installation. This criterion aims to capture this difference with a high value corresponding to a small installation space requirement.
- **Technical risk.** This criterion aims to reflect the degree of uncertainty associated with each concept. Some concepts are more fully developed and understood than others and so possess lower technical risk. A high value of this criterion corresponds to low

risk. The relative importance of these criteria have been assigned a weighing for each scenario as detailed in Table 3-1.

Using these weightings, the 15 concepts described in appendix. As can be seen the final three concepts were considered for prototyping and only two were used in the final presentation of the results. A turbine design using compressed fluid was prototyped, however due to time limits and resources was not fully developed and will not be considered further. The two devices selected for further research were the electromagnetic converter: a rotational flyback convertor and a linear vibrational cantilever converter. These will be described more fully in Chapter 5 & 6.

4. Chapter 4 – Ground Reaction Force Measurement System

In this chapter typical population demographics are more closely examined and strategies on how to best extract the maximum energy from the widest section of the population considered. This allows systems to be developed based on the demographies in a particular location, assisted by information available about age, weight and footfall frequency. The chapter also describes a ground reaction force GRF measurement system that measures applied force with location detection to aid the design of footfall harvesting systems.

The maximum displacement which a surface can undergo when stepped upon without causing an undesirable response from the pedestrian is not clearly defined and will depend on the environment. For a level surface, a step of 15mm or more is considered a trip hazard and it seems reasonable to take this as a limit in other situations. In many situations, the displacement experienced will depend on the weight of the pedestrian so that a light pedestrian will experience a smaller deflection than a heavy one. For energy harvesting purposes, it is desirable to maintain a displacement near to the acceptable maximum since this will maximise the energy available for harvesting.

The force exerted on a walking surface depends on the weight of the person and upon their gait. In normal walking on a level surface, the vertical GRF has a maximum typically 25% above body weight while during running this increases to 2 or 3 times body weight [160]. The GRF varies through the gait cycle [161]. There is rapid initial impulse as the heel hits the ground, then the full foot comes into contact with the ground. The force then increases again

as the toe pushes off. The profile during jogging and running shows similar overall profile but the magnitude at different phases is altered.

The GRF during climbing and descending of stairs does not appear to be documented in the scientific literature but it seems reasonable to assume that the forces involved are likely to be significantly greater, particularly during climbing, that for level walking. The GRF depends on the pedestrian weight as well as on their gait. The distribution of body weight among the population depends on gender, age ethnicity etc. Data on the distribution of bodyweight amoung US adults is shown in Figure 4-1. The mean weight for females in this in this sample is 74kg while for males it is 86kg. It may also be seen that there is a significant proportion of the population with a body weight above 100kg. These figures are intended to represent the overall population and this distribution may not be reflected in a particular location. For instance, in some locations there may be a large proportion of children who would have significantly lower bodyweight. However, in the absence of specific information to the contrary, the distribution in Figure 4-1 will be assumed.

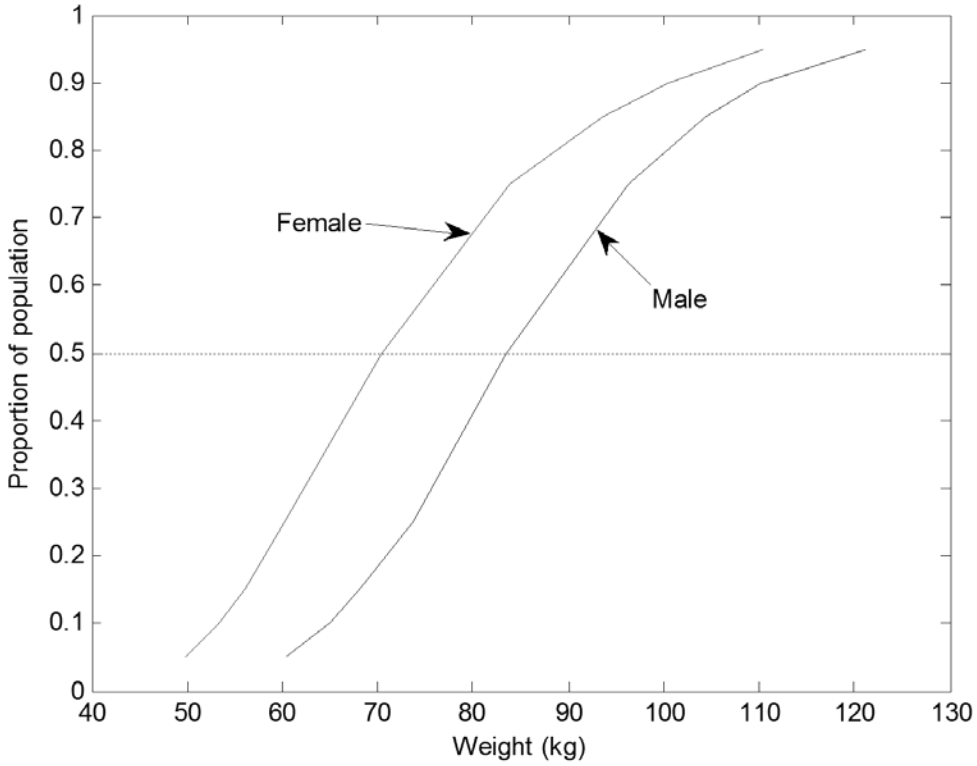

Figure 4-1 Distribution of average body weights among US adults [162]

Given the potential for installing an energy harvesting device in a staircase, but the limited understanding of GRF's in such situations, it is considered worthwhile to conduct experiments for GRF in a suitable location. Such a location proved problematic due to data gather issues and so a staircase was manufactured to conduct such trials in a laboratory based environment.

4.1. Ground Reaction Force Measurement System

The system shown in Figure 4-3 was designed to obtain the GRF on a single tread of a purpose built staircase. The manufacture of staircase was given to specialist company, however, some alteration to the actuating steps were carried out by the departments engineering workshops from designs developed by the author and a member of the

Engineering Innovation Institute, Mr Russell Kenyon. The system consists of four strain gauge load cells, arranged at the four corners of a step. Each button load cells can be used to measure forces in the range 0-4kN, more than sufficient for any body weight. The design of the GRF system and its footfall location detection is achieved by placing the load cells at the four corners of the step as seen in Figure 4-2. Signal conditioning of the load cells was achieved by using instrumentation amplifiers, as shown in Figure 4-2. Once past the amplifiers, the signals were discredited using a data acquisition card and then stored and analysed on MATLAB.

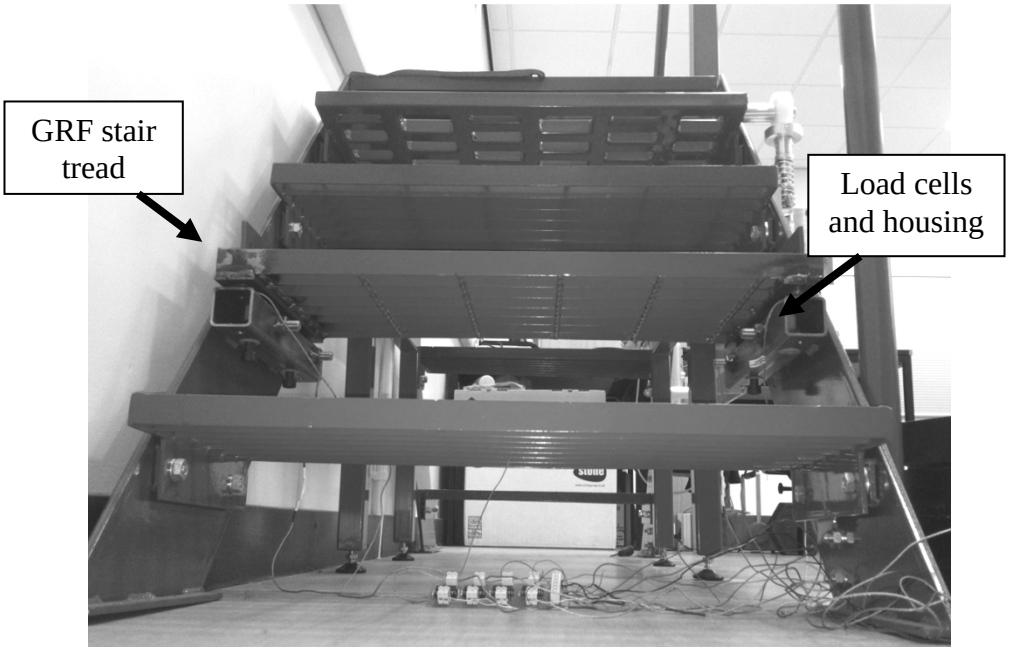

Figure 4-2 GRF test rig and load cell location

An image of the GRF system can be seen Figure 4-2, which shows that the second step from ground was fitted with four load cells attached at the corners of the step.

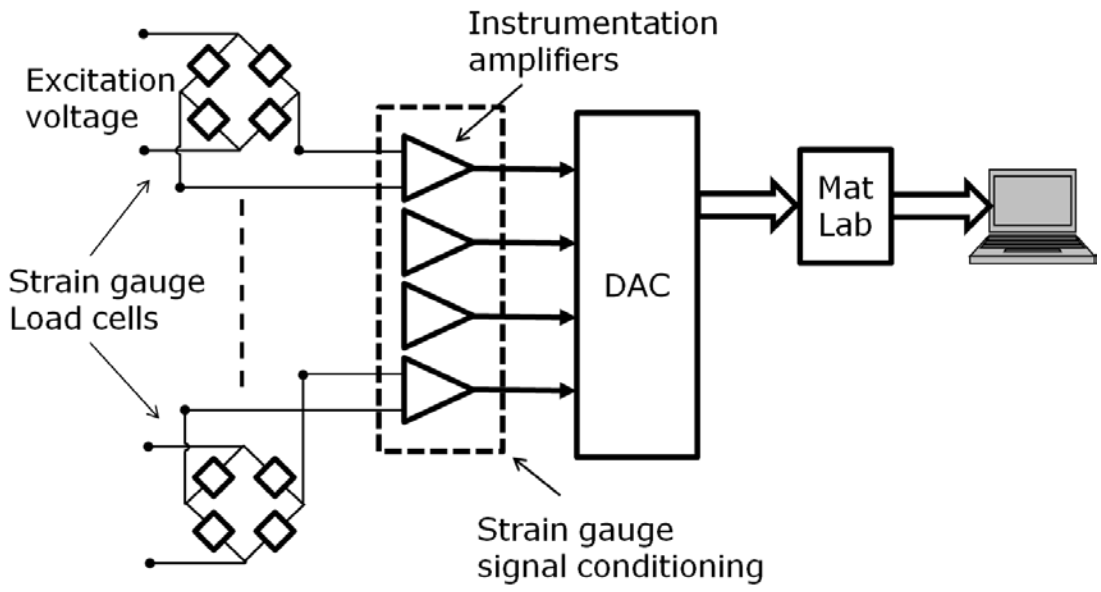

Figure 4-3 Ground reaction and force displacement measurement system

The dimensions of the stair case tread are illustrated in Figure 4-4. It can be seen that the tread has a width running along the x-axis of 600 mm and a depth of 300 mm running along the y-axis. Four load cells are fixed at the four corners shown in the illustration. The signals from the load cells are arranged so that the centre of the tread is the origin and represents zero geometrically when the sum of all the forces is zero numerically.

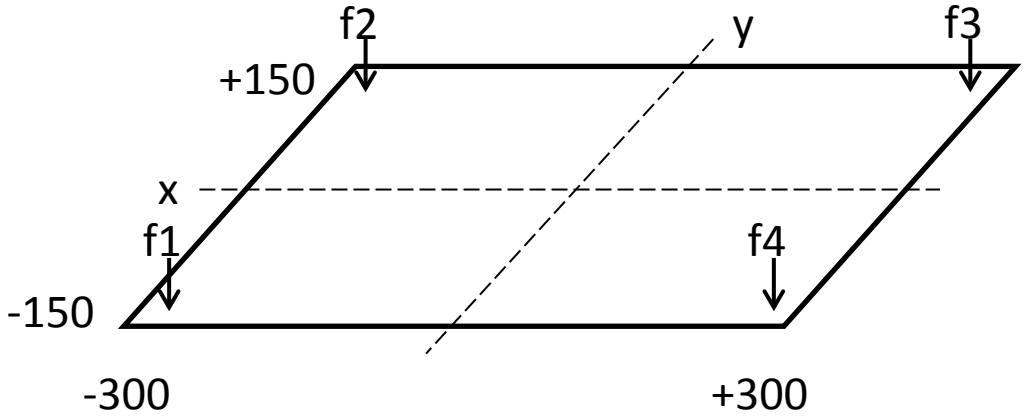

Figure 4-4 Staircase tread coordinates and sensor location

4.2. Experimental Results

With a configuration of load cells and dimensions shown in Figure 4-4, the x-positions of applied force can be calculated using the equation:

$$x_{postion} = Stair\_width * \left(\frac{(f3 + f4) - (f1 + f2)}{2(f1 + f2 + f3 + f4)} \right) \quad \textbf{Equation 4-1}$$

Using the same configuration and dimensions as discussed for the x-position, the y-position is calculated using the equation:

$$y_{postion} = Stair\_depth * \left(\frac{(f2 + f3) - (f1 + f4)}{2(f1 + f2 + f3 + f4)} \right) \quad \textbf{Equation 4-2}$$

Using this measurement system, the GRF profile for two subjects (see Table 4-1) climbing & descending stairs at different speeds were performed. Figure 4-5 shows a typical result made up of five signals measured over time. This represents a person climbing up the staircase and shows that a single footstep takes just over 0.25 seconds. Signal T, shown in bold, is the total force overtime and is the sum of all four forces combined, which peaks at just under 1.4kN. This is a significantly increased force compared with the actual weight of subject 1, shown in Table 4-1 should be easier.

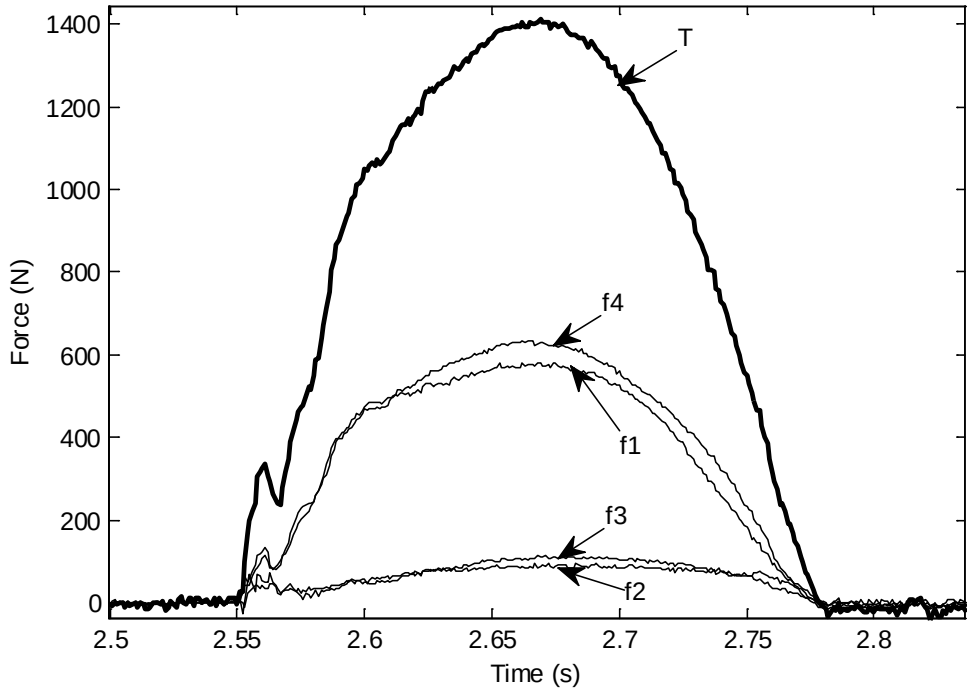

Figure 4-5 Total and individual force signals over time

In addition to the total GRF, it was valuable to have an understanding of where on the step the force is applied. Using a MATLAB script based on the equations Equation 4-1and Equation 4-2 it is possible to determine the x-y positions and force applied over time. Figure 4-6 shows the x-y position, along with force applied for subject 1 running up the stairs. To allow the force to be seen alongside the x-y position, the force is shown x10 smaller and can be seen to be 1.4kN.

It can be seen that the x-axis remains around zero, as expected, since the footfall occurs midway across the step. The y-axis location is -100 to -300mm, describing most of the contact period, indicating that the force is applied at the front edge of the stair tread.

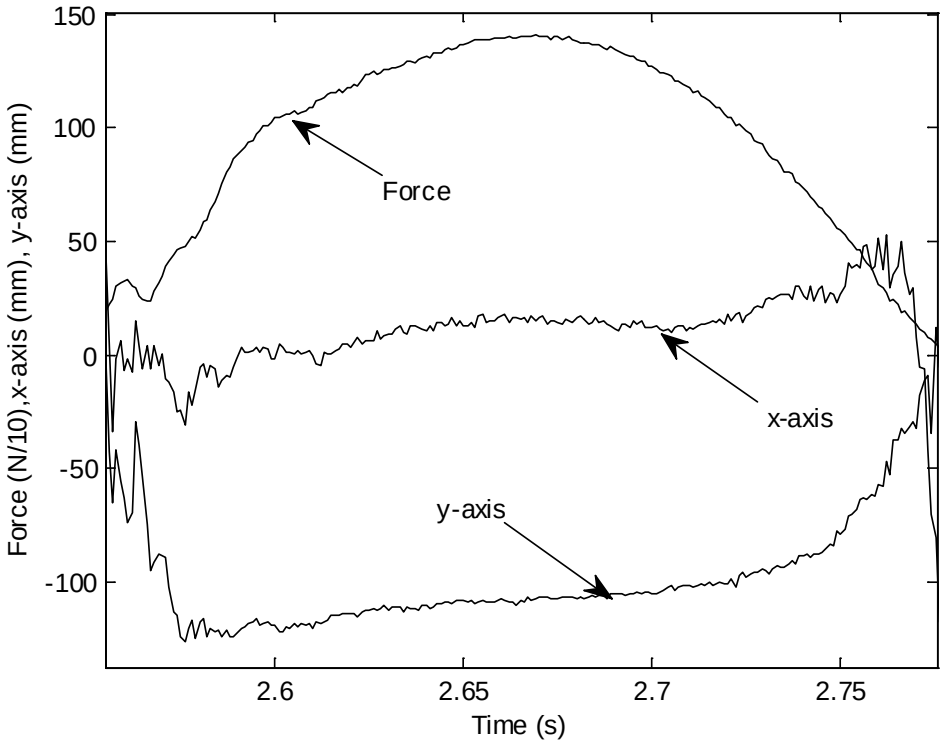

Figure 4-6 Force and x-y coordinates over time for pedestrian travelling up the staircase

Figure 4-7 shows a simple illustration of where and when the footfall occurs, along with some indication of how much force is applied and when. It can be seen that while running up the staircase the foot is placed centrally for a short period of time and the force applied during that time is indicated by the oval shape 1. The shape also represents the amount of force and the number is representative of when in time this occurred. It can be seen that the majority of the force is represented by the second shape for when the full force of footfall occurs during the test subjects running action. It can be seen that when running up the stairs the majority of force is applied at the front end of the stair tread.

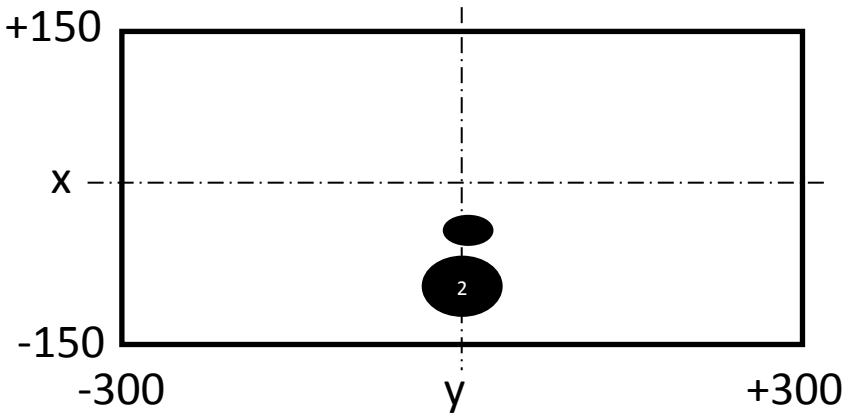

Figure 4-7 Footfall location and applied force for test subject running up staircase

Figure 4-8 shows a similar example, except in this figure, the test subject is walking down the staircase. It can be seen that the force applied is above 1.5kN and the peak force occurs when the x-axis is at around -130mm and y-axis is at around -100mm.

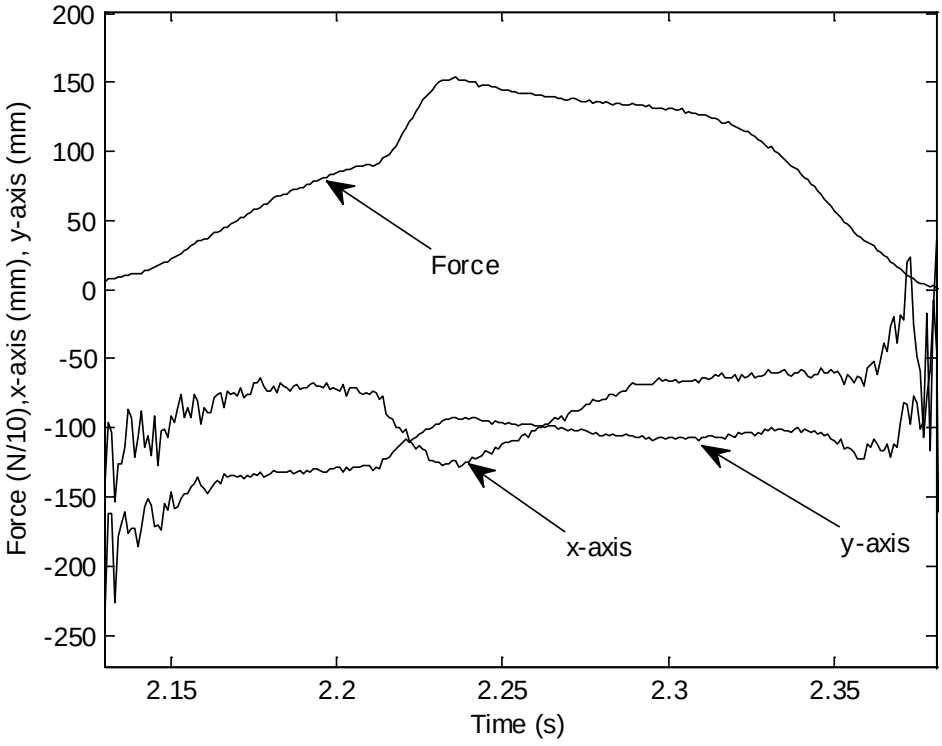

Figure 4-8 Force and x-y coordinates over time for pedestrian walking down the staircase

Figure 4-9 shows that the positions Figure 4-8 are again at the end of the stair tread but this time the majority of the force is first applied to the front of the step and then the some force is applied further inwards at some time after the first force is applied.

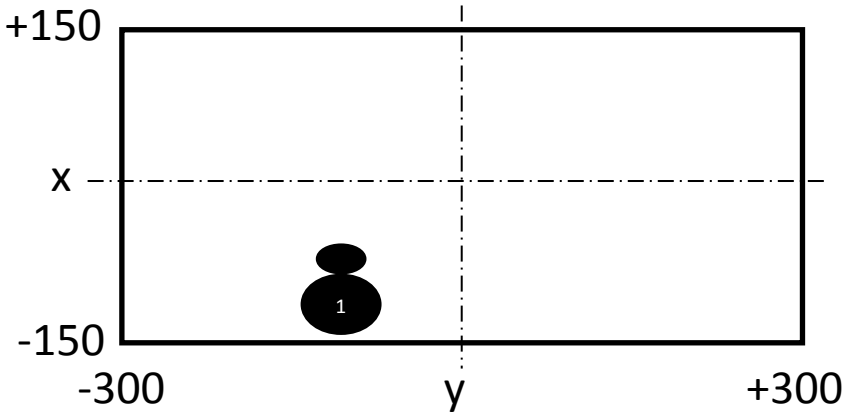

Figure 4-9 Footfall location and applied force for test subject running down staircase

Two test subjects were assessed to determine some key characteristics of gait and force applied during climbing and descending on the staircase. Table 4-1 lists the subject by age, weight, gender and also type of climbing and descending that was recorded. It can be seen that running up & down the stairs exerts over twice the body weight and walking up & down steps exerts forces approximately 25% above body weight as expected from level surface walking.

Subject	Age	Weight (kg)	Gender	Direction	Max Force (N) (f1+f2+f3+f4)	Max(f1+f4) (N)
1	47	75	Male	Walk up	810	680
				Walk down	880	800
				Run up	1400	1200
				Run down	1520	1220

2	37	83	Male	Run up	1380	1120
				Run down	1815	1300

Table 4-1 Test subjects showing bio-data and step action with force output

The purpose of the illustrations in Figure 4-7 and Figure 4-9 has been to show that, firstly, there is more energy obtained from climbing and descending staircases than which is available from a level floor and secondly that the maximum force exerted is at the front of the staircase tread.

4.3. Conclusions

It has been seen that the forces available when walking up and down stairs are much more than those seen for level walking. These forces can exceed 2-3 times body weight and would suggest that coupling a harvesting mechanism within a stair would see a greater amount of energy transferred to a mechanism and so providing a better source of potential energy.

5. Chapter 5 – Flyback Converter

In this chapter the first of the two harvesting mechanisms is presented. As discussed in chapter 3, harvesting electrical energy from normal human activity has a number attractions in fields such as sensor networks. The flyback converter extracts energy from human activity, without it becoming uncomfortable or inconvenient for the person involved. In order to achieve this efficient conversion, a novel mechanism has been developed which is capable of being used either in footwear or under a floor, which allows footfall energy to be efficiently coupled into an electromagnetic generator. In this section the structure of the mechanism is described, the optimisation of the system parameters, based on a dynamic model is discussed and experimental results for an under-stair system are presented.

5.1. Structure of the Flyback Mechanism

The Flyback mechanism is composed of a 'striker' mechanism which is coupled to the tread of a step on a purpose built staircase and so undergoes a vertical displacement when a pedestrian causes the step to be depressed. Attached to the input stage, the striker presses against the pivot arm causing it to rotate and twist the torsional spring attached to it. Once the striker approaches the end of its travel the pivot arm is released so that the spring may return to its starting position. The spring is coupled, via a sprag clutch (one-way clutch) to a flywheel and generator in such a way that when being wound up there is no torque transfer but when the spring unwinds, it drives the flywheel and generator. In addition, the sprag clutch allows the flywheel to continue to rotate once the spring stops unwinding. Thus the spring and flywheel are able to convert the short pulse of input energy into an extended pulse of energy applied to the generator. This prolonging of the pulse, and the associated reduction in peak power, allows smaller mechanical elements and generator to be used, typically with lower energy losses. The input stage operates independently of the output stage and multiple

inputs to the striking mechanism increases the velocity of the flywheel generator, producing more power from the generator. Although a stair tread is used to show the application, the system can equally be used in a sprung floor system.

5.2. Phases of Operation

The behaviour of the system during a single cycle may be split into four phases as described below and as illustrated in Figure 5-1. The evolution of the key variables illustrated in Figure 5-2.

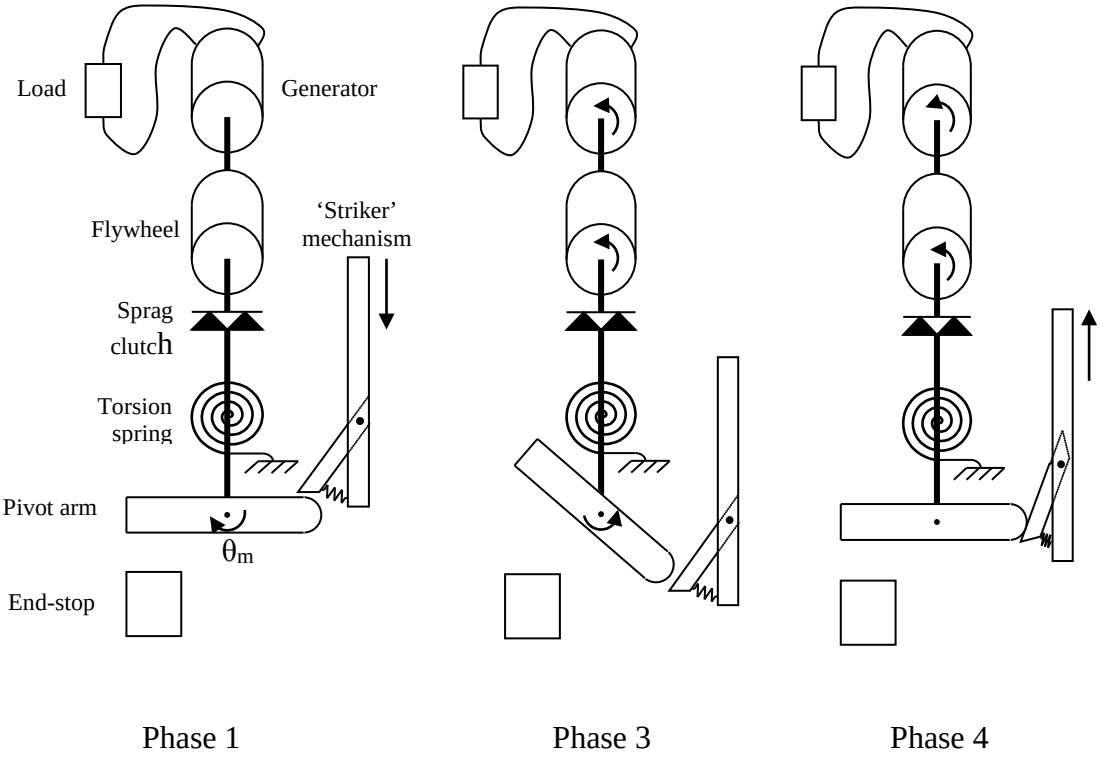

Figure 5-1 Structure and operating sequence of converter mechanism

It can be noticed that phase 2 is not illustrated in Figure 5-1. Illustratively, the images would be identical to that of phase 3. Phase 2 is described in the following discussion.

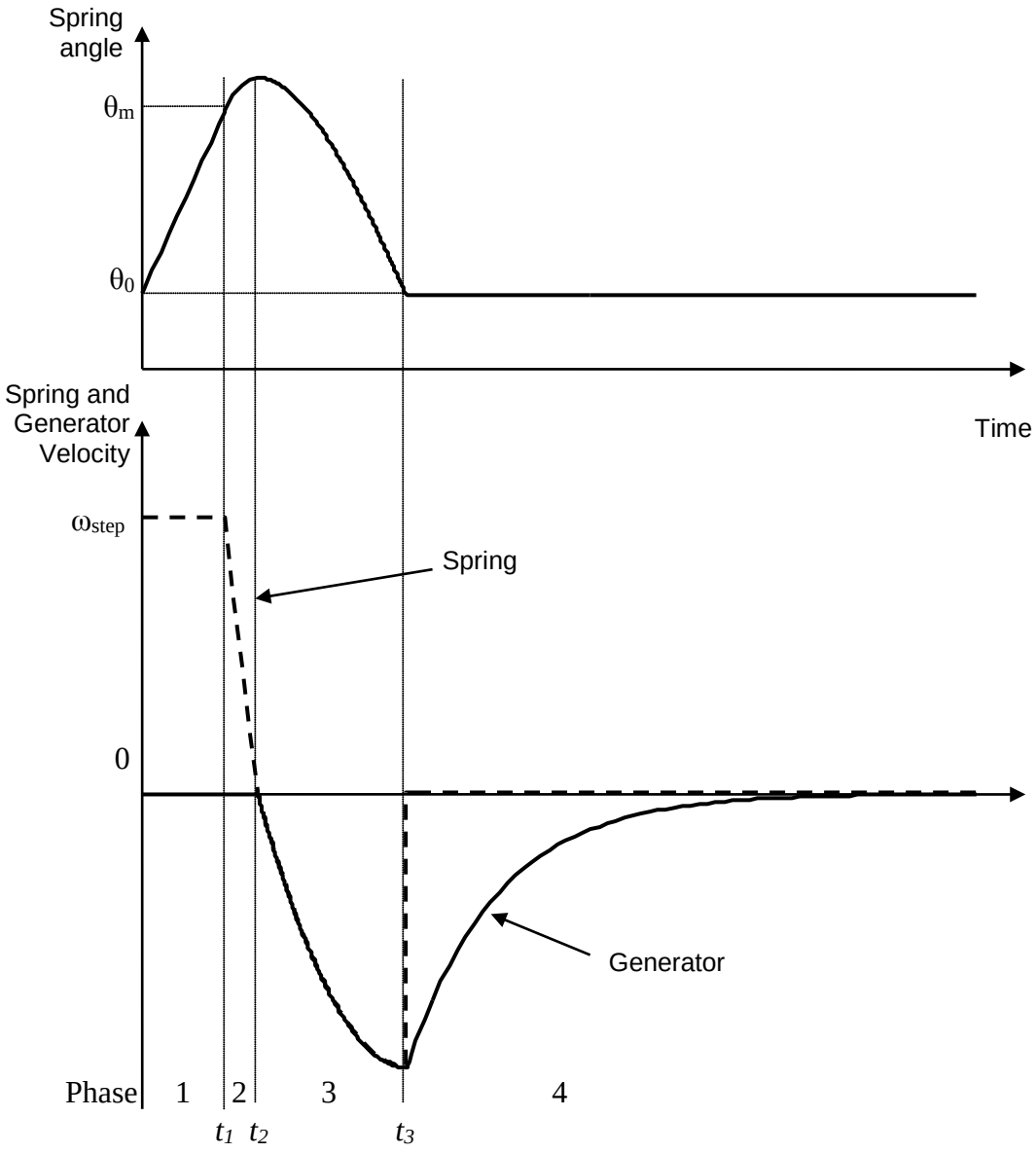

Figure 5-2 Evolution of variables during energy conversion cycle showing 4 phases of operation

1. **Spring windup during footfall.** It is assumed for illustration purposes that the foot compresses the step at a constant velocity. Thus the spring winds at a constant rate from an initial angle of . up to a maximum angle . Once the angle . is reached the spring is released and phase 2 begins. In the subsequent analysis, it will be assumed that the angles . and . are small and are symmetrically arranged around the horizontal

position so that the effective radius is constant and the torque applied to the spring is proportional to the applied force.

2. **Spring unwind to zero velocity.** Once released from the striker mechanism, the spring is free to accelerate. The effective inertia of the spring and associated parts accelerates under the influence of the spring torque and friction associated with the spring. During this phase the sprag clutch freewheels. Once the spring velocity passes through zero the sprag clutch engages and phase 3 begins.
3. **Spring drives generator.** Once the sprag clutch engages, the spring drives the flywheel and generator, causing them to accelerate. Note that during this phase, the spring is accelerating both its own inertia and that of the flywheel/generator and so the acceleration is lower than in Phase 2. The spring will drive the flywheel/generator until the spring end stop is reached (at the angle). This causes the mechanism to move to Phase 4.
4. **Rundown of flywheel.** Once the spring reaches its end stop, the spring velocity drops rapidly to zero but the flywheel continues to spin, driving the generator. The flywheel decelerates under the influence of friction and the reflected torque from the generator.

At some stage, the foot will be lifted from the step and the input mechanism reset. This is not shown in Figure 5-2.

This mechanism has several advantages over more conventional gearing mechanisms. During footfall the applied force is only used to twist the spring and accelerate the striker mechanism. These parts may be designed to have minimal inertia and hence the dynamic forces during impact are not significant compared to the spring forces. The sprag clutch

decouples the input and output side of the mechanism so that they may be designed separately, allowing greater freedom in the choice of parameters.

5.3. Mathematical model

In order to optimise the parameters of the mechanism, it is necessary to develop a model of its performance. The model for each phase of operation will be developed in turn. A number of assumptions will be made in order to develop the model. It will be assumed that the spring operates in a linear manner (obeys Hooke's law). It will be assumed that the friction affecting the spring, flywheel and generator may be modelled as being composed of a viscous element and a coulombic element. Stiction will be neglected since the mechanism may be designed so that the actuating torques are sufficient to overcome stiction torques. The friction of the freewheeling sprag clutch will be combined with the coulombic and viscous elements of the spring and flywheel.

Phase 1 - Spring windup during footfall (*0*<*t*<). In Figure 5-2 it is shown that the footfall occurs at a constant velocity however, the precise velocity profile is unimportant in terms of the subsequent behaviour. What is important is the spring velocity at the point where the input mechanism releases the spring. For the subsequent phases of the behaviour, it will be assumed that this velocity is . Since the spring is already under torsion at the beginning of phase 1, it has a stored energy of

$$E_0 = \frac{1}{2} k_s \theta_0^2$$

where is the spring constant and is the initial rotation of the spring.

At the end of phase 1 the total energy is made up of the spring potential energy and the spring inertia's kinetic energy. Thus:

$$E_1 = \frac{1}{2} k_s \theta_{\max}^2 + \frac{1}{2} J_s \omega_{step}^2$$

where is the rotation of the spring at the point where it is released,

is the moment of inertia of the spring and associated parts

The energy extracted from the pedestrian is:

$$E_{in} = \frac{1}{2} k_s \left(\theta_{\max}^2 - \theta_0^2 \right) + \frac{1}{2} J_s \omega_{step}^2 \qquad \textbf{Equation 5-1}$$

Phase 2 - Spring unwind to zero velocity (<t<). During this phase the angular position is governed by the equation:

$$J_s \ddot{\theta}_s = -k_s \theta_s - B_s \dot{\theta}_s - D_s \operatorname{sgn}\left(\dot{\theta}_s \right) \qquad \textbf{Equation 5-2}$$

where is the angle of rotation of the spring

is the viscous friction coefficient associated with the spring and

is the coulomb friction coefficient associated with the spring

with initial conditions $\theta_s(t_1) = \theta_{\max}$ and $\dot{\theta}_s(t_1) = \omega_{step}$. Phase 2 ends at time when the spring velocity reaches zero: $\dot{\theta}_s(t_2) = 0$. The spring angle at the end of Phase 2, $\theta_{s2} = \theta_s(t_2)$ can be determined by solving Equation 5-2 and the energy stored in the system at this time is.

$$E_2 = \frac{1}{2} k_s \theta_{s2}^2$$

Phase 3 - Spring drives generator (<*t*<). Once the velocity of the spring passes through zero, the sprag clutch connects the spring and flywheel/generator and so the generator velocity, $\dot{\theta}_g$ is equal to the spring velocity $\dot{\theta}_s$. Note that the rotation angles are not necessarily equal since the sprag clutch allows the flywheel/generator to rotate to any position $\theta_g \leq \theta_s$. However, the relative angles remain constant during this phase. The dynamics during Phase 3 are governed by:

$$\left(J_s + J_g\right)\ddot{\theta}_s = -k_s\theta_s - \left(B_s + B_g\right)\dot{\theta}_s - \left(D_s + D_g\right)\mathrm{sgn}\left(\dot{\theta}_s\right) - k_t i \qquad \textbf{Equation 5-3}$$

where is the moment of inertia of the generator, flywheel and associated parts

is the viscous friction coefficient associated with the generator/flywheel

is the coulomb friction coefficient associated with the generator/flywheel

is the torque constant of the generator and

i is the current flowing through the generator and into the load

The effect of generator inductance will be neglected in the model since the time constant associated with the inductance is typically much shorter than that associated with the mechanical behaviour. Hence the generator may be described as a voltage source proportional to angular velocity of the generator and a series resistance. The load will be assumed to be a constant resistance. Thus the generator current is:

$$i = \frac{k_e \dot{\theta}_g}{R_g + R_l}$$

where is the emf constant of the generator

is the winding resistance of the generator and

is the load resistance

The initial conditions at the beginning of phase 3 are $\dot{\theta}_s(t_2) = 0$ and $\theta_s(t_2) = \theta_{s2}$. Phase 3 ends when the spring angle returns to its initial value, $\theta_s(t_3) = \theta_0$. At this point the spring and generator velocities are equal $\dot{\theta}_s(t_3) = \dot{\theta}_g(t_3) = \dot{\theta}_{g3}$ and can be determined from the solution of Equation 5-3.

Phase 4 - Rundown of flywheel (<*t*<). When the spring reaches its end stop it is assumed that it stops rapidly and the flywheel continues to rotate. The precise behaviour of the spring during this phase is unimportant since it does not affect the output power. The dynamics of the flywheel and generator during Phase 4 is described by:

$$J_g \ddot{\theta}_g = -B_g \dot{\theta}_g - D_g \operatorname{sgn}(\dot{\theta}_g) - \frac{k_t k_e \dot{\theta}_g}{R_g + R_l} \qquad \textbf{Equation 5-4}$$

The initial conditions for phase 4 are $\theta_g(t_3) = \theta_0$ and $\dot{\theta}_g(t_3) = \dot{\theta}_{g3}$.

Power is generated and transferred to the load resistance during phases 3 and 4 and so the total energy delivered to the load is:

$$E_{out} = R_l \int_{t_2}^{t_4} i(t)^2 dt$$ **Equation 5-5**

5.3.1. Preliminary Mathematical Model Simulation

The four phases in the evolution of variables were illustrated in Figure 5-2 previously. The following section presents a validation of simulated results obtained from the mathematical model with those described in Figure 5-2. Position and velocity of the spring and flywheel generator are examined to show the validity of the mathematical model.

For the following comparison, the key optimised parameters are shown in Table 5-1. Experimental results showed an optimised load of 14Ω and an optimised inertia for the flywheel of $1.6x10^{-6}$. A more detailed examination of the parameters will be presented in Table 5-2 of the results Section5.5.5.

Key Parameters	**Value**
Moment of inertia of flywheel and generator	$1.6x10^{-6}$
Load resistance	14 Ω

Table 5-1 key optimized parameters

These key parameters where obtained through matching of model dynamics to optimized running of the prototype. The load resistance was matched to the equivalent resistance of the motor coil.

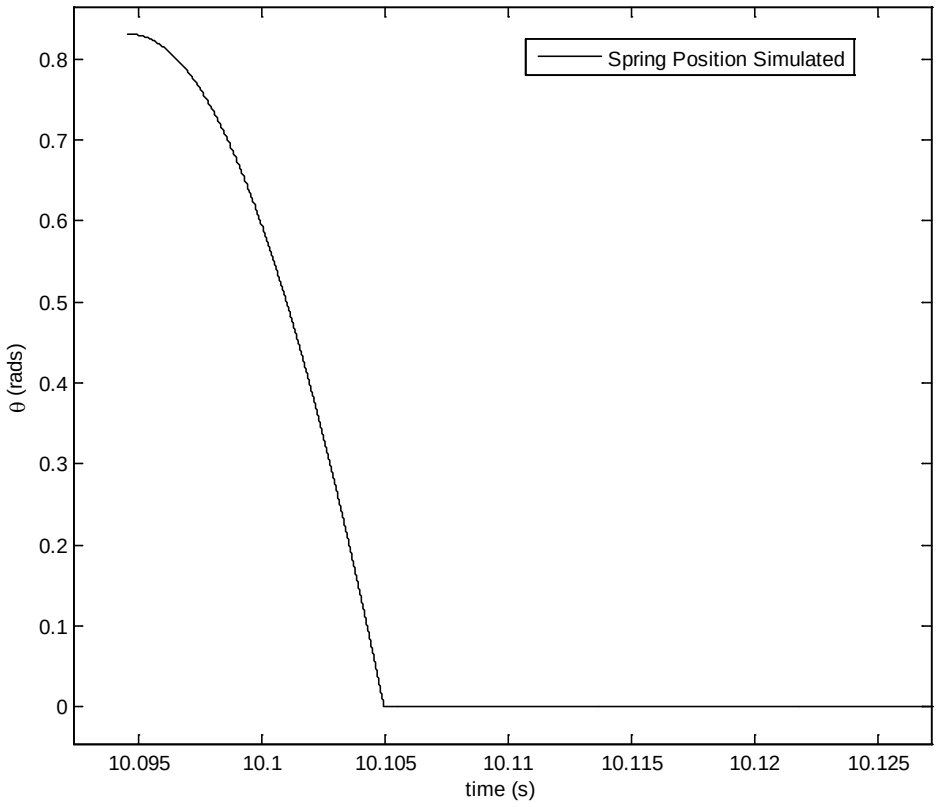

Figure 5-3 Simulated Spring Position in Phase 2 & 3

The simulated spring position during phase 2 & 3 is shown in Figure 5-3 above. As discussed previously, a constant velocity is assumed during phase 1 and so this phase is not shown. A good match is seen as the spring angle reaches at 0.85 radians & travels back to the end-stop at zero radians. The time scale is not critical here but it can be seen that the return to zero radians is achieved in no more than 10ms.

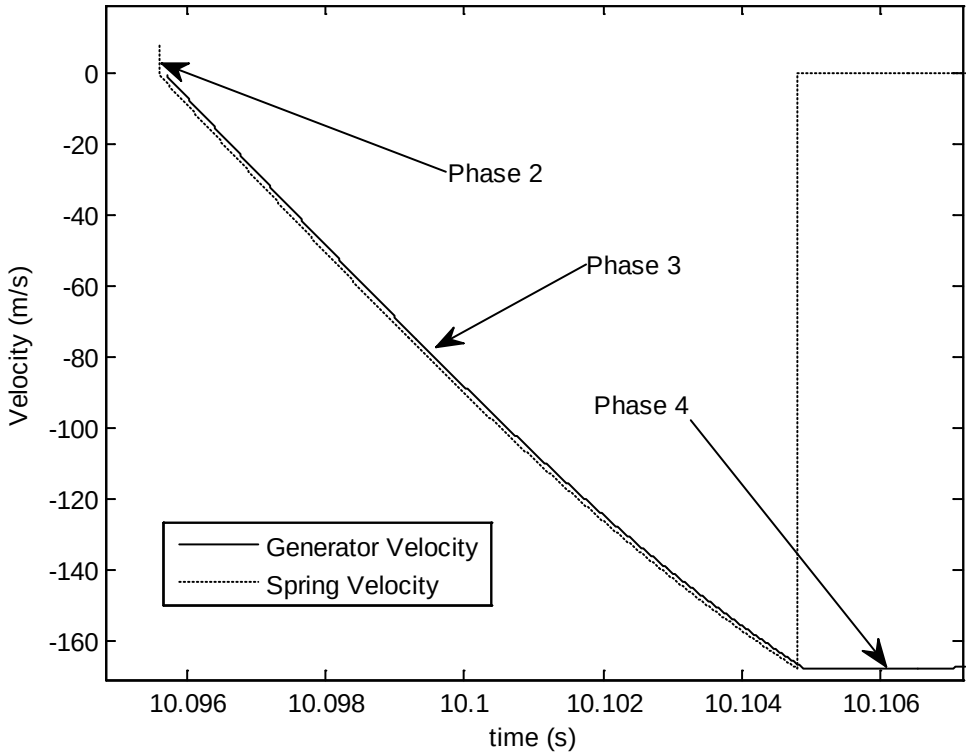

Figure 5-4 Simulated Spring & Generator Velocity in Phase 2 to 4

The simulated spring & generator velocity are shown in Figure 5-4 above, the dotted line indicating the generator velocity and the full line indicating the spring velocity. A good match is observed between the illustration in Figure 5-2 and Figure 5-4. The majority of the figure shows the evolution of the spring and generator velocity during phases 2 & 3, and a portion of phase 4 is also shown, discussed shortly. The phase 2 arrow pointing at the beginning of the dotted line shows a small time segment where phase 2 occurs, this is better illustrated in Figure 5-2 where the relationship between the variable is exaggerated. Here, it can be seen that this occurs before the springs return to zero and represents the spring unwind to zero velocity.

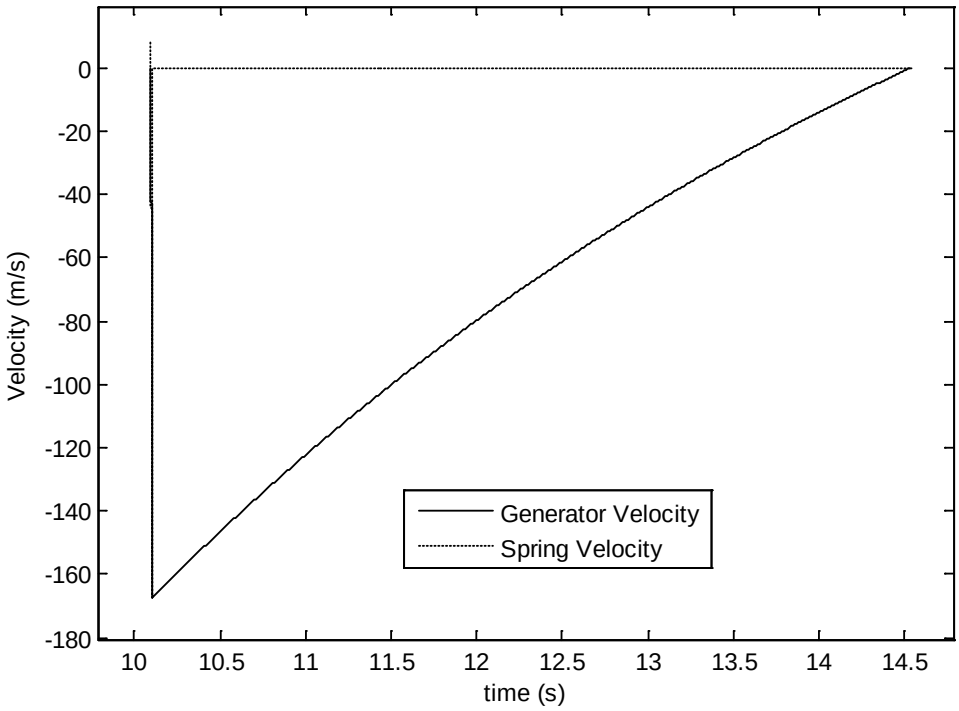

Figure 5-5 Simulated Spring & Generator Velocity during phase 2 to 3

To complete the comparison of the illustrated evolution of variables in Figure 5-2 and the simulated results, a final simulation of the spring and velocity profiles is shown in Figure 5-5. Here, the majority of the simulation shows the final phase 4 where the generator rundown is seen, phase 2 & 3 are also illustrated but accrue in such a short timescale that they cannot be seen closely. The spring and generator reach a maximum of around $170ms^{-1}$ (shown as a negative direction since it is in the opposite direction to the spring windup) from which, the generator runs down to zero velocity after a short period. This again matches well with the illustration in Figure 5-2 and therefore shows a good match between speculated description and the mathematically modeled simulation output for the spring.

The simulation results presented in Figure 5-3 to Figure 5-5 demonstrate that the model presented behaves as expected. Based on this model it is desirable to maximise the energy

delivered to the load for given input characteristics. The result of this optimisation and further analysis is given in the next section.

5.4. Parameter Optimisation

In order to optimise the power output from the system it is necessary determine the most appropriate system parameters given the constraints on the system. It is important to note that the aim is to optimise the output energy rather than to optimise the conversion efficiency. To maximise the output energy it is desirable to extract as much energy from the pedestrian as possible and then convert this to output energy as efficiently as possible. Thus the energy extracted from the pedestrian is considered. A conservative input stage was envisaged with 60-80kg pedestrian mass and 10mm deflection to capture the input energy.

The energy derived from the pedestrian depends on the force applied by the foot and the associated displacement of the spring. The force applied during walking clearly depends on the mass of the pedestrian but also on their gait. As described in section 4.1, during normal walking the peak reaction forces are approximately 25% greater than body weight while during running the peak reaction forces are typically 2.75 to 3 times body weight [53]. This was seen for the stair results of section 4. In a general environment there will be a range of pedestrian body weights and a variety of gaits encountered. For the purposes of this discussion however, a fixed body weight is assumed, Mg (where M is the pedestrian mass and g is the gravitational constant) and the reaction force is assumed to be equal to that body weight. The amount of deflection in the floor surface also determines the input energy but in order to avoid discomfort or distraction for the pedestrians this deflection must also be limited. As noted previously, the acceptable limit appears to be approximately 10mm in most environments. The relationship between the angular displacement of the spring and the torque

is shown in Figure 5-6. The additional potential energy stored in the spring, as a result of increasing the angle from . to . is equal to the shaded area in Figure 5-6 which is given by:

$$E_p = \frac{1}{2} k_s \left(\theta_{\max}^2 - \theta_0^2 \right) \qquad \textbf{Equation 5-6}$$

We wish to maximise this energy while satisfying the constraints:

$$k_s \theta_{\max} \le Mgr$$

and

$$\theta_{\max} - \theta_0 \le \frac{d_{\max}}{r}$$

where *r* is the radius of the input pivot arm and is the maximum allowable deflection of the step. The maximum energy occurs if $k_s \theta_{\max} = Mgr$ and $\theta_{\max} - \theta_0 = \frac{d_{\max}}{r}$ in which case Equation 5-6 may be written as:

$$E_{in} = k_s \left(\theta_{\max} - \theta_0 \right) \left[\theta_{\max} - \frac{1}{2} \left(\theta_{\max} - \theta_0 \right) \right] = Mgd_{\max} - \frac{1}{2} k_s \frac{d_{\max}}{r} \qquad \textbf{Equation 5-7}$$

This reaches a maximum value of $E_{in} = Mgd_{\max}$ as $k_s \to 0$. In this case $\theta_{\max} \to \infty$ so that the relationship $k_s \theta_{\max} = Mgr$ is maintained. In other words, the shaded area in Figure 5-6 approaches a rectangular shape. Thus the desirable spring characteristics are that it should have low stiffness but should have a large preload, . It should however be noted that as $k_s \to 0$ and $\theta_{\max} \to \infty$ the total amount of energy stored in the spring increases and hence

the amount of material required to make the spring increases. This, in turn, implies an increase in the mass and moment of inertia of the spring. The increase in inertia is undesirable (as will be seen later) and so a trade-off must be reached between spring inertia and input energy capture.

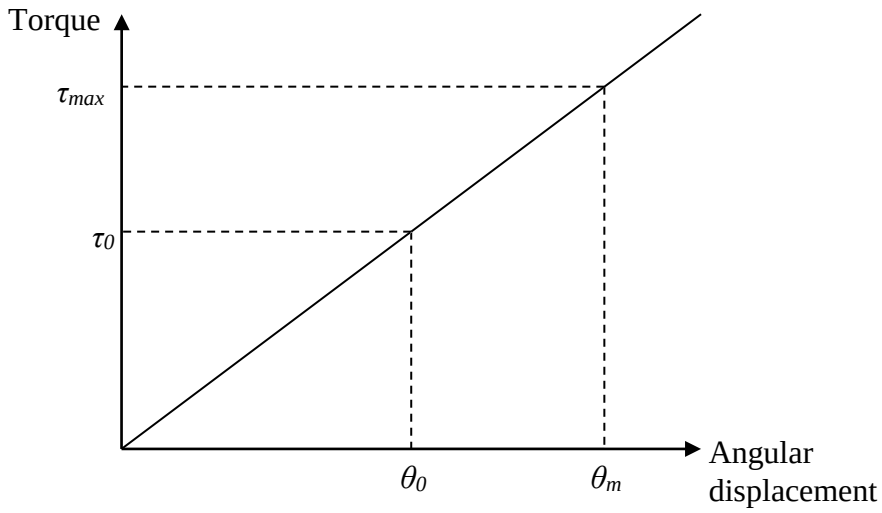

Figure 5-6 Torque-angle relationship for spring

The inertia of the spring is important because, at the end of phase 3, the spring and the generator are rotating with the same angular velocity, . and the energy is:

$$E_3 = \frac{1}{2}\left(J_s + J_g\right)\omega_g^2$$

while immediately afterwards, the velocity of the generator is . but the velocity of the spring is zero and so the energy is:

$$E_3^+ = \frac{1}{2} J_g \omega_g^2$$

Thus, a proportion of the energy $\frac{J_s}{J_s + J_g}$ is lost and to minimize this loss, must be minimized.

The losses due to friction and due to the internal resistance of the motor are more complex and are related to one another. Clearly, if friction could be eliminated, then the associated losses would also be zero but, typically, reducing friction requires more precise and hence more expensive construction or special devices, such as air or magnetic bearings, which themselves require energy. The transfer of energy from the generator to the load depends on the internal resistance of the generator and the load resistance. Conventionally, maximum power transfer between source and load is achieved for equal source and load resistance but in this system the situation is more complex. Since the current flowing in the generator produces a torque opposing the generator rotation (see Equation 5-3) the load resistance affects the generator speed (Equation 5-4). Therefore selecting a suitable value for the load resistance is important. From Equation 5-4 it can be seen that the viscous friction term $-B_g\dot{\theta}_g$ has a similar effect to the generator torque term $-\frac{k_t k_e \dot{\theta}_g}{R_g + R_l}$ in that both are dependent on generator velocity. Since the generator term represents useful work while the friction term purely relates to losses, it is necessary to ensure that the generator term dominates the friction term, while also minimising resistive losses in the generator. In the absence of friction, it is possible maximize the energy reaching the load by minimizing the effect of generator resistance and this is achieved by ensuring that $R_l >> R_g$. This has the effect of extending the time for which the generator continues to rotate. In the presence of friction, extending the

duration of phases 3 and 4 means that more energy is lost through friction and so the frictional losses must be balanced against the generator resistance losses. The relationship between load resistance and efficiency $\left(E_{out}/E_{in}\right)$ cannot be determined analytically but may be determined numerically, as shown in Figure 5-7 for a number of friction coefficient values.

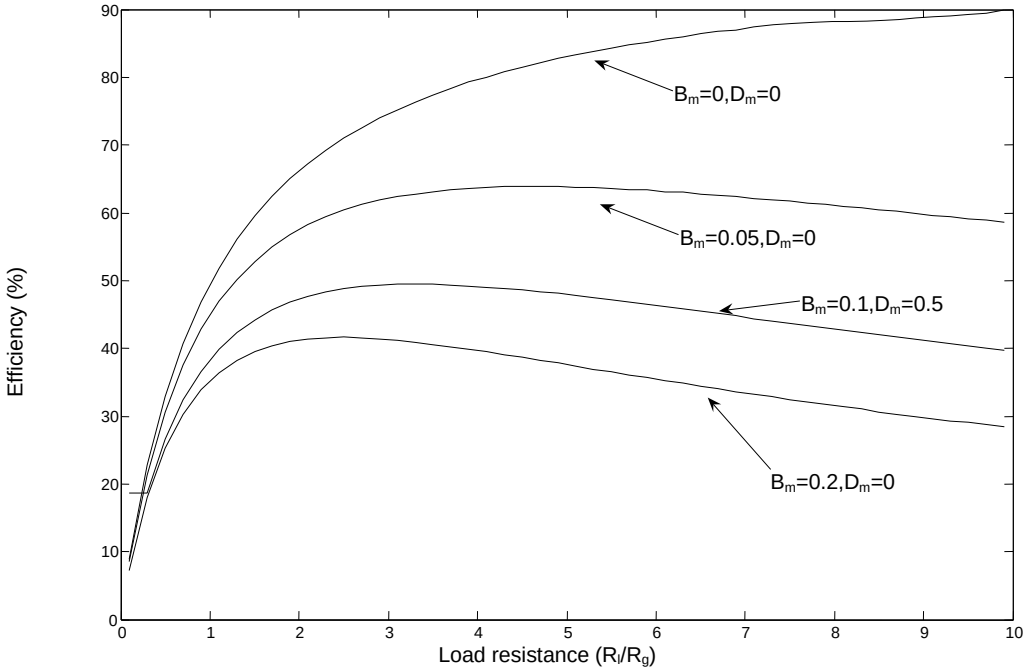

Figure 5-7 Effect of load resistance on efficiency for different friction coefficients

It can be seen that, as expected, as the friction increases, the system efficiency decreases but it can also be seen that the load resistance for which the efficiency is maximized depends on the friction coefficients. In all cases, the load resistance for maximum efficiency is significantly higher than the generator internal resistance. For the case where friction is zero, the maximum efficiency is obtained for infinite load resistance.

As noted above, efficiency is increased by making the term $\frac{k_t k_e \dot{\theta}_g}{R_g + R_l}$ much larger than $B_g \dot{\theta}_g$.

$\frac{k_t k_e \dot{\theta}_g}{R_g + R_l}$ may be maximised by increasing and or by minimising and adjusting to maintain maximum power transfer. However, these quantities cannot be varied independently. For a given magnetic field strength, and are both proportional to the number of turns per pole on the rotor coil. However, for a generator with given linear dimensions, the cross sectional area available for the coils is approximately fixed and so to increase the number of turns by a factor *n* implies a reduction in wire cross sectional area by a factor $1/n$ and an increase in total wire length of *n*. Thus, $k_t k_e$ increases by but, for a given wire resistivity, also increases by and the effects cancel out. If the linear dimensions are increased then and can be increased without altering but it should be noted that, in general, a larger generator will suffer from greater frictional forces.

The effect of spring friction terms and is more straightforward since it only affects behaviour during phase 3 and not phase 4. Thus, spring friction affects the generator velocity at the end of phase 3 but not subsequent behaviour. Because of this, the relationship between , and efficiency is less affected by the load resistance. Optimisation of these parameters during the prototype design proved effective and translated into increased efficiency of the converter. However, there is a limit to how much these parameters can be adjusted in experimentation. This is primarily a design limitation as the changing of the inertia flywheels leads to an indeterminate change in , for each flywheel whereby an update of the model is required before reliable data is recorded.

5.5. Experimental Results

To ensure correct mechanical operation and to provide manufacturing specifications, a CAD of the system was produced as shown in Figure 5-8. The CAD was particularly useful for the mechanical interaction of the striker mechanism to the pivot arm. For this, an optimum distance & length for pivot arm was key to ensuring a maximum 10-15mm deflection was achieved for the striker.

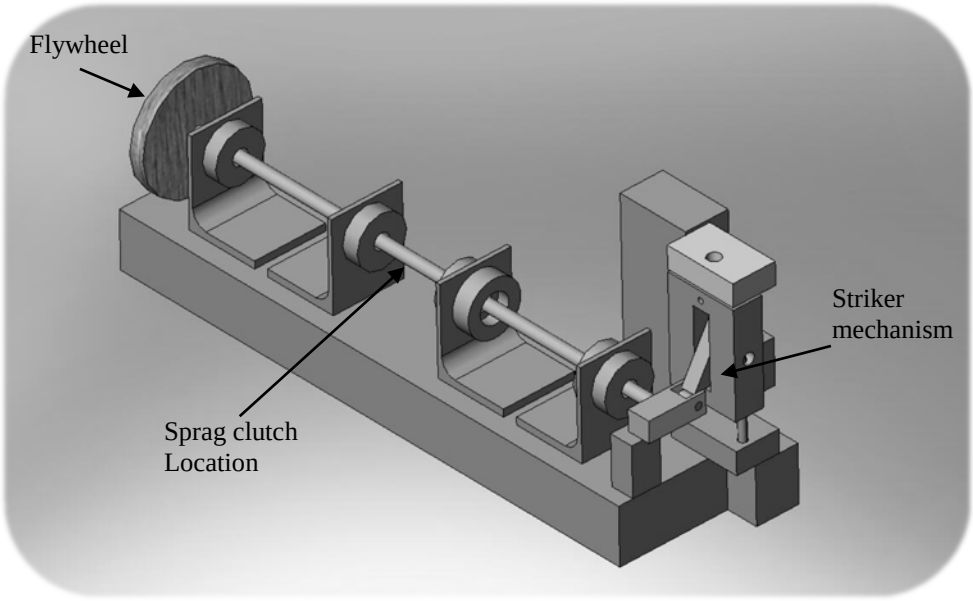

Figure 5-8 CAD of the Flyback Generator

The design process initially required the development of a prototype with a set of estimated parameters for the key variables. The moment of inertial of the flywheel/generator is a key parameter determining system efficiency; several flywheels were manufactured to obtain a rough estimate of performance for the output stage. An off the shelf high efficiency generator was attached to the flywheel to capture the rotational inertial energy. By varying the load resistance the maximum power transfer for the given parameters of the prototype were

assessed. The input energy stored in the spring could be adjusted by varying the amount of preload and the amount the twist during the input stage.

In order to assess the mechanism, a prototype device has been constructed as shown in Figure 5-9. In this case the mechanism is actuated through a stair tread rather than being mounted beneath a floor, allowing it to be easily inspected. The striker mechanism is attached through a plunger to the staircase allowing the energy to be transferred into the torsion spring via the spring pivot arm. The spring is attached to a shaft running through to the sprag clutch via two rotary bearings: one at the pivot end and the other at clutch end. During footfall or step deflection the sprag clutch freewheels and on release of the striker from the pivot arm the energy is transferred through to the output stage into the flywheel via two more bearings. The generator used is a precision DC motor [163] attached through a flexible coupling to the flywheel.

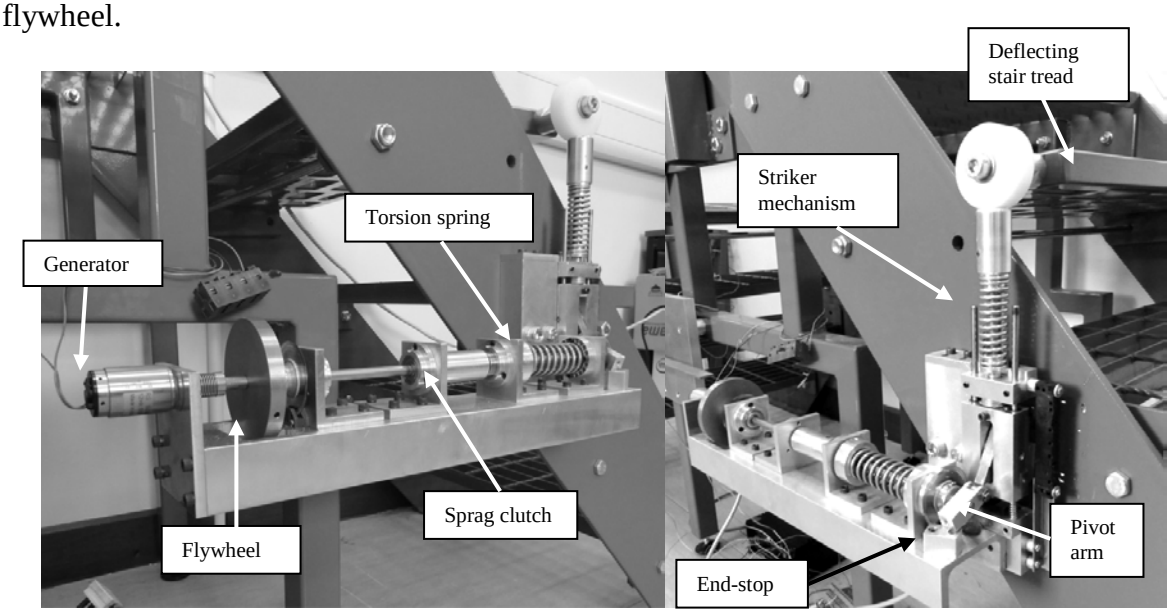

Figure 5-9 Prototype flyback generator mounted on a staircase

Several sensing devices are used to acquire the data from the system. The rotation of the flywheel and the angular position of the spring are measured using optical shaft encoders. The force applied through the plunger is measured using a button load cell and the linear

movement of the stair tread, attached to the striker mechanism, is measured using a linear potentiometer and calibrated to give a measurement for the displacement. The signals from the measurement devices were analysed through an ActiveX interface in a MATLAB script.

5.5.1. Parameter Identification

The parameters of the prototype mechanism were derived from a combination of data sheet information, physical measurement for parameters such as moment of inertia and spring constant and by fitting the simulation to measurements of dynamic behaviour of the system for the friction parameters. The parameters are listed in Table 5-2.

Parameter	**Symbol**	**Value**	**Units**	**Acquisition**
Spring constant		1.62	$N{\cdot}m{\cdot}rad^{-1}$	Measurement
Moment of inertia of spring mechanism		$25x10^{-6}$	kg·	Measurement
Viscous friction coefficient of spring mechanism		$5x10^{-6}$	$N{\cdot}m{\cdot}s{\cdot}rad^{-1}$	Simulation
Coulomb friction constant of spring mechanism		$1x10^{-6}$	N·m	Simulation
Moment of Inertia of flywheel/generator*		$1.6\ x10^{-4}$	kg·	Measurement
Viscous friction coefficient of flywheel/generator		$5x10^{-6}$	$N{\cdot}m{\cdot}s{\cdot}rad^{-1}$	Simulation
Coulomb friction constant of flywheel/generator		$4.2x10^{-3}$	N·m	Simulation
Generator winding resistance		5.95	Ω	Measurement
Load resistance*		14	Ω	Measurement
Spring pre-load		1.27	rad	Measurement
Spring maximum twist		2.10	rad	Measurement

Table 5-2 Parameters of prototype mechanism. Items marked * are the values used in the model validation but may be adjusted to maximise energy output

The value for the spring constant shown in the table was obtained using a combination of torque transducer and optical encoder. The signals were captured using a data acquisition

card and analysed and presented using MATLAB as seen in Figure 5-10. From the figure it can be seen that the spring exhibits the predicted linear behaviour according to Hooke's law with a slope of 1.62 Nm rad^{-1}. A value for the spring constant was found and is shown in Table 5-2.

Several flywheels manufactured from brass were used to capture the energy from footfall; these are listed in Table 5-3. The mass of the flywheels were measured using a digital weighing machine capable of weighting a maximum of 4kg at an accuracy of a of gram. . From this, the inertia $J = 1/2mr^2$ was calculated using the dimensions given in the table. The smallest and largest inertias were not used in the final presentation of the results and so were removed as sufficient information to inform the model was obtained using flywheels 2, 3 & 4.

Flywheel	Length (l)	Radius (r)	Mass (kg)	Inertia ( )
1	0.0100	0.0175	0.0808	0.00001
2	0.0100	0.0300	0.2375	0.00010
3	0.0150	0.0300	0.3563	0.00016
4	0.0100	0.0400	0.4222	0.00034
5	0.0250	0.0400	1.0556	0.00080

Table 5-3 Flywheels with Mass and Inertia Values

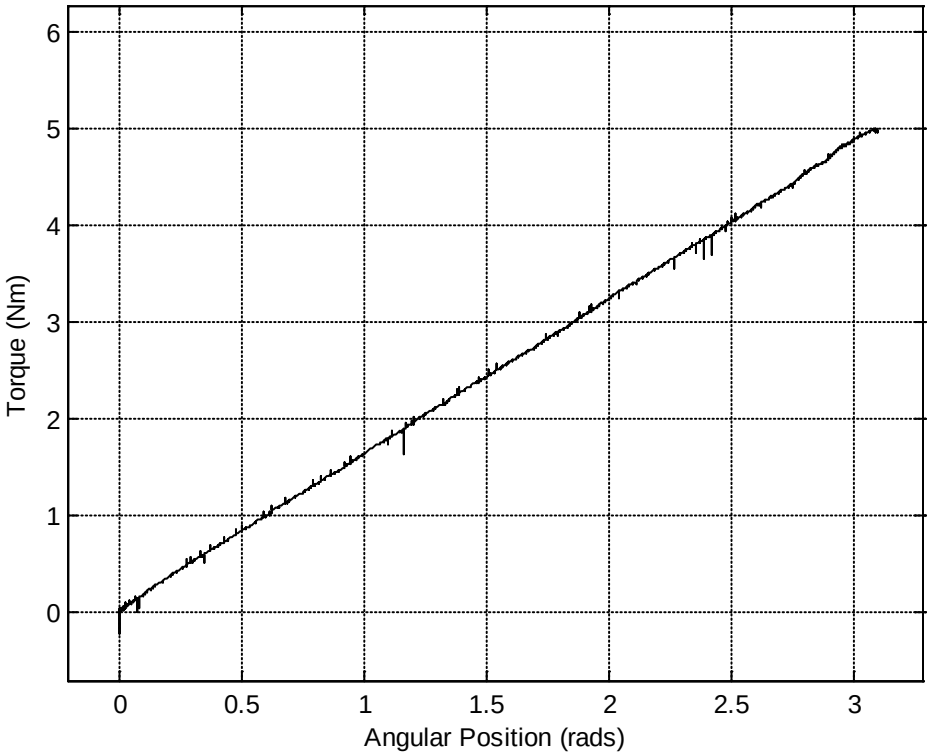

Figure 5-10 Spring constant measurement

5.5.2. Input Energy

The system input energy is obtained using a force transducer in the form of a load cell and linear potentiometer to capture the displacement. Using a cumulative summation of the force with respect to displacement the input energy e_{in} is obtained.

$$e_{in} = \int f(x)dx \qquad \textbf{Equation 5-8}$$

The input energy is the energy transferred during footfall on the tread into the spring, this takes place over phase1, as described in Figure 5-2 in Section 5.2.

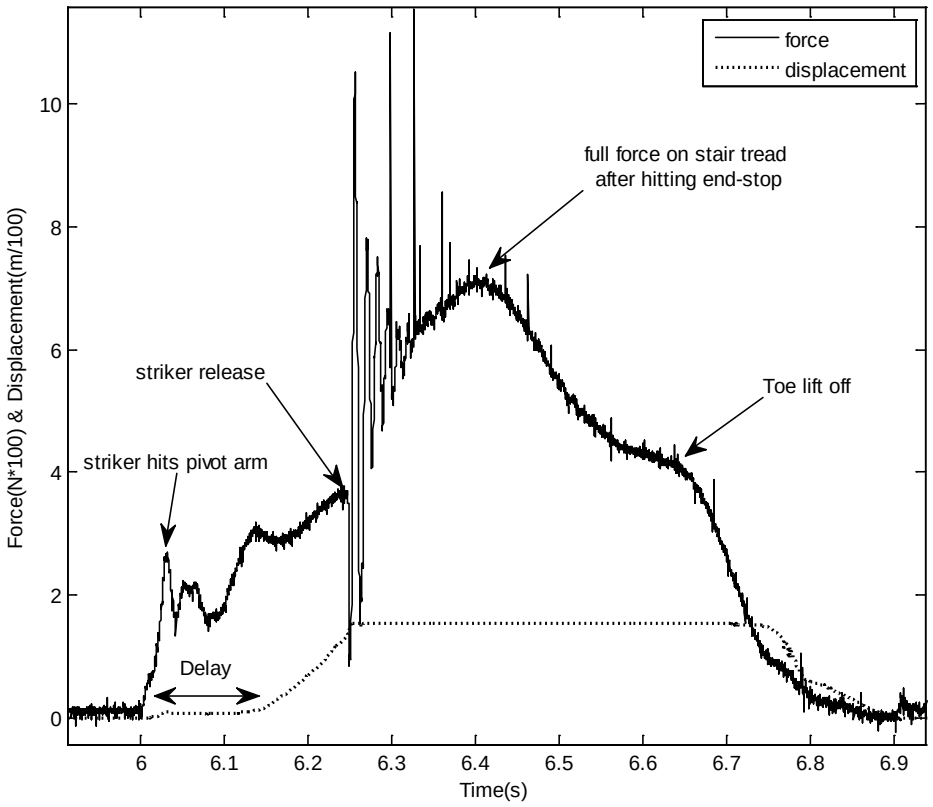

Figure 5-11 Force & Displacement profile during footfall – Phase 1

A typical footfall profile can be seen in Figure 5-11. There is a short delay in the displacement profile between 6.0 and 6.15, wherein the force is irregular. During this period the striker hits the pivot arm and a sharp increase in the force is seen and the displacement remains virtually unchanged. This is due to the angle of the pivot arm and will be discussed in more detail on page 87. The striker release occurs at 6.25s with a force of approximately 400N and 17mm displacement. For a short time the force drops but then the striker mechanism hits the end-stop and so the force increases to its maximum at over 700N. A gradual decrease in force is observed as the pedestrian's weight is transferred off the tread.

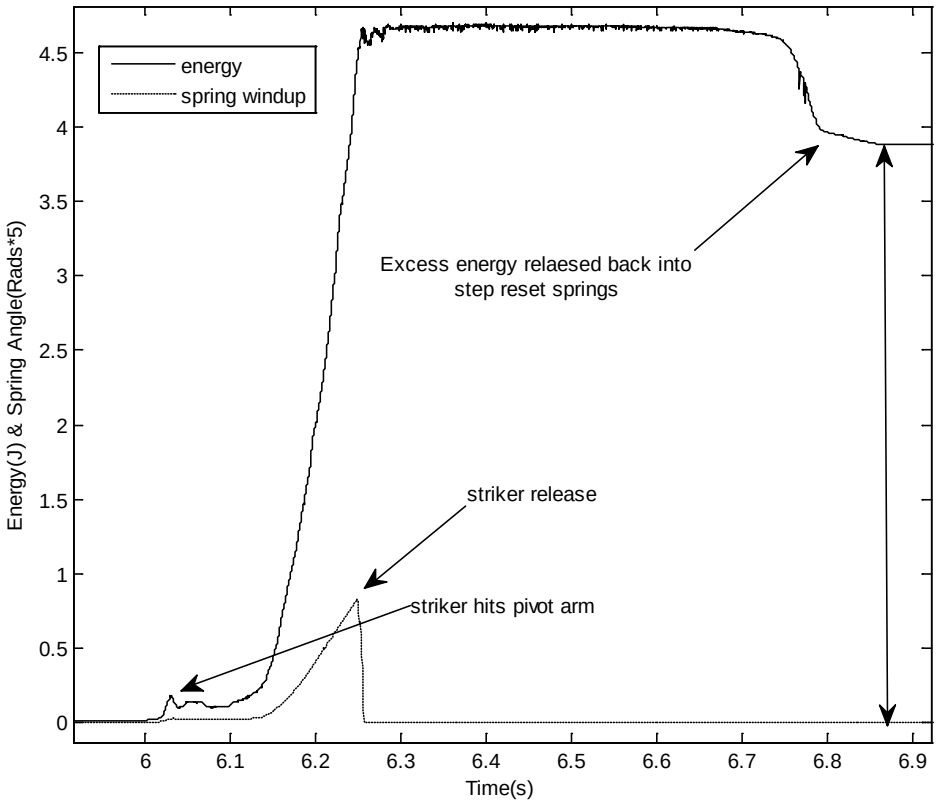

Figure 5-12 Spring Angle & Energy input profile

The force and displacement data in Figure 5-11can be used to determine the input energy profile using a discrete approximation of Equation 5-8 $e_{in}(i) \approx \sum F(i)\,[d(i) - d(i-1)]$, where F is the force d the displacement and i is the sample number. The spring angle during energy input & the energy profile is shown in Figure 5-12. Similar to the force/displacement curve, it can be seen that a short delay occurs during the initial energy input, starting at the point when the striker hits the spring pivot arm, at 6.03s. The spring angle is shown to emphasise the manner in which it tracks the energy profile, peaks at at approximately 0.8 radians, at then returns to zero as it slips of the striker mechanism and hits the end-stop at 6.25s. At this point, maximum energy is delivered into the spring, around 4 Joules; however, the energy profile proceeds to increase as the striker mechanism bottoms out as it hit the end-

stop. At the end of the profile the excess energy captured in the stair tread returns to the reset mechanism (spring). The remaining 4 Joules represents the energy delivered into the input stage of the mechanism.

Using the same data from the linear potentiometer and the load cell, a profile of the force & displacement can be generated as shown in Figure 5-13. It can be seen that the curve has a hysteresis effect; this is due to the mechanism having a return-spring as part of the striker configuration. This allows the parts to reset to enable the next step to be inputted.

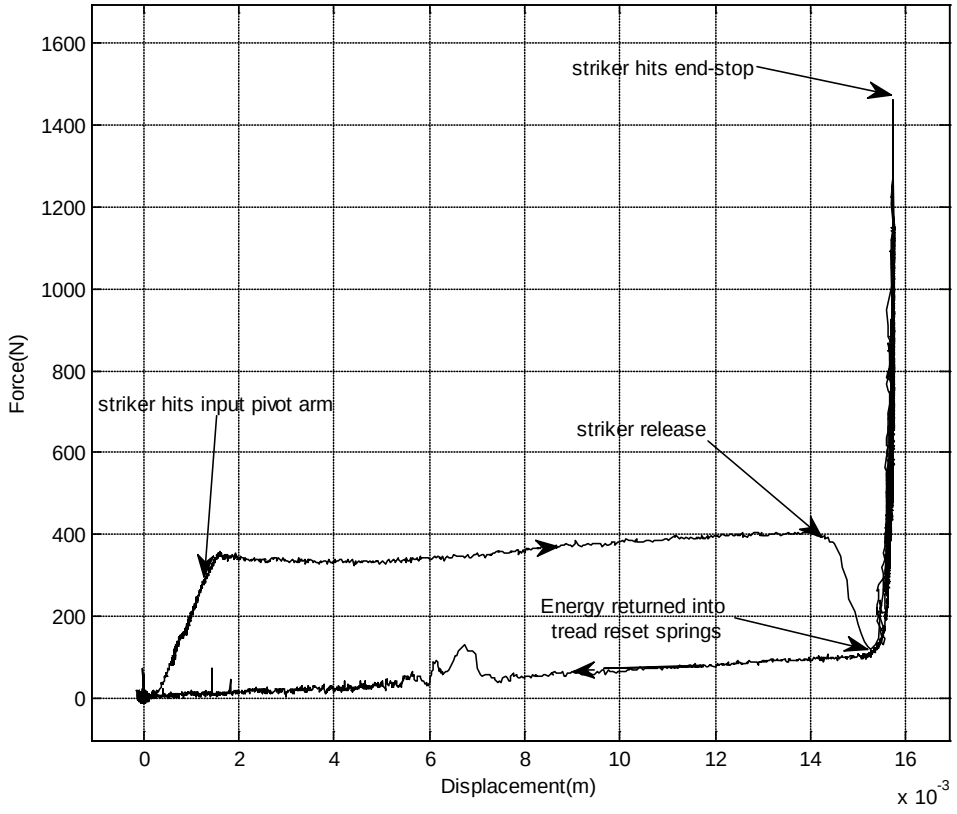

Figure 5-13 Force Displacement profile

At the beginning of the footstrike just as the step is actuated a sharp increase in force for a relatively small deflection is seen as the striker hits the spring pivot arm but for the rest of the step profile, a relatively small increase in force for a large deflection is seen until the striker is

released. Figure 5-14 shows the position of the pivot arm and striker mechanism, this was designed to minimise the abnormal effect of a step deflecting underfoot. The angles and are made small and are symmetrically arranged around the horizontal position so that the effective radius is constant and the torque applied to the spring is proportional to the applied force.

Due to the change in radius of the pivot arm being slightly raised the force required to move the striker is seen in Figure 5-13, as indicated by the arrow showing the point at which the striker hits the pivot arm.

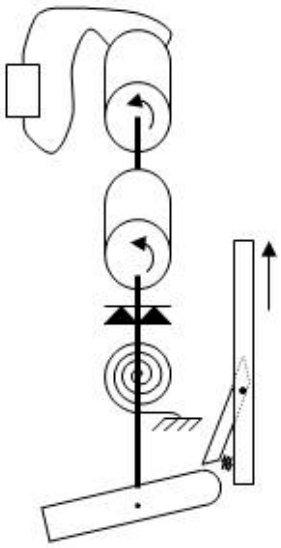

Figure 5-14 Striker arm position

The pivot arm in actuality was raised 5 to 8 mm above the horizontal to allow a 16 mm vertical travel. Although the step is horizontally balanced, the angle of the pivot arm causes some of the input energy to be lost in friction as the mechanism rotates past the horizontal and the subsequent release of the striker. This is precisely the effect seen at the beginning of the striker action in Figure 5-13.

The striker was designed to accommodate a level of adjustment and for this reason it can be seen that shortly after the striker is released, at approximately 14.5mm, the force drops dramatically only to spike at more than 1.5 times body weight of the subject, this is the effect of the step hitting the end-stop. After this spike the energy is released back into the return springs, as the pedestrian steps off the tread.

5.5.3. Comparison of Simulation & Experimental results

In this subsection the mathematical model is compared with the experimental results to show the validity of the model. The optimized parameters shown in Table 5-2 previously are still in use for these results. However, some adjustments to viscous and columbic friction parameters were made when flywheel inertia were changed. This was necessary because dismantling & reassembling the system resulted in changes in friction coefficient. The adjustments to these parameters can be seen in Table 5-4 below.

Flywheel Inertia			
	$1.0e^{-}$	$1.6e^{-}$	$3.4e^{-}$
Viscous Friction	$7.5e^{-6}$	$5e^{-6}$	$2.5e^{-6}$
Coulomb Friction	$6.3e^{-3}$	$4.2e^{-3}$	$6.3e^{-3}$

Table 5-4 Inertia viscous and coulomb variations

The spring position comparison is shown in Figure 5-15 was obtained through the use of optical encoders mounted on the shaft and simulation. It can be seen that the experimental spring position shows the entire sequence of footfall and release; however, the simulated result shows only phase 2. The simulation does not account for the phase 1 and assumes a constant velocity of 10ms for . Spring windup is seen to reach a value of approximately 0.84 radians showing a good agreement with simulation.

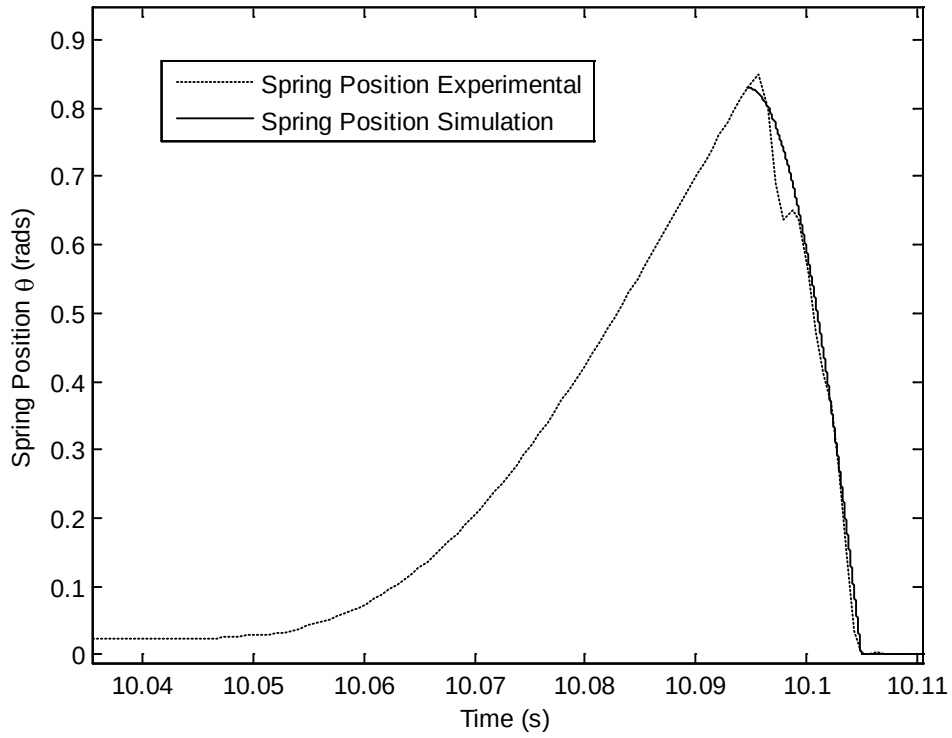

Figure 5-15 Spring position comparison

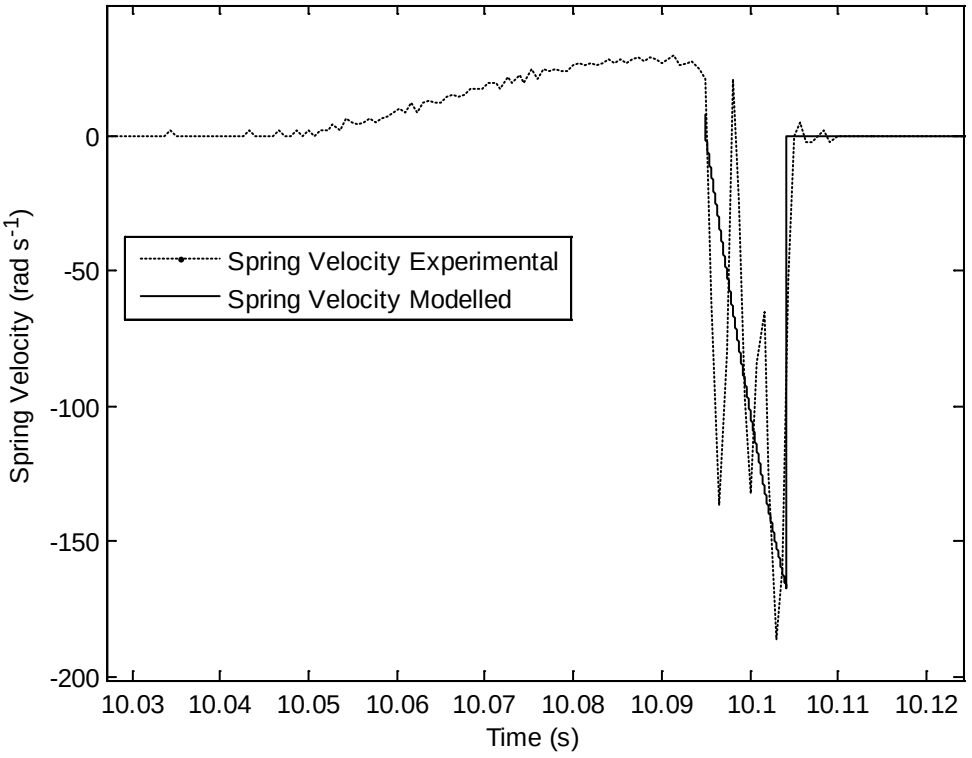

Figure 5-16 Spring velocity comparison

The spring velocity comparison is shown in Figure 5-16. The time taken for spring release from the striker and its eventual contact with the back stop is approximately 10ms and the entire sequence can be seen to take approximately 55ms. Also, from the figure it can be seen that sampling during this small segment was not sufficient to overcome differentiation.

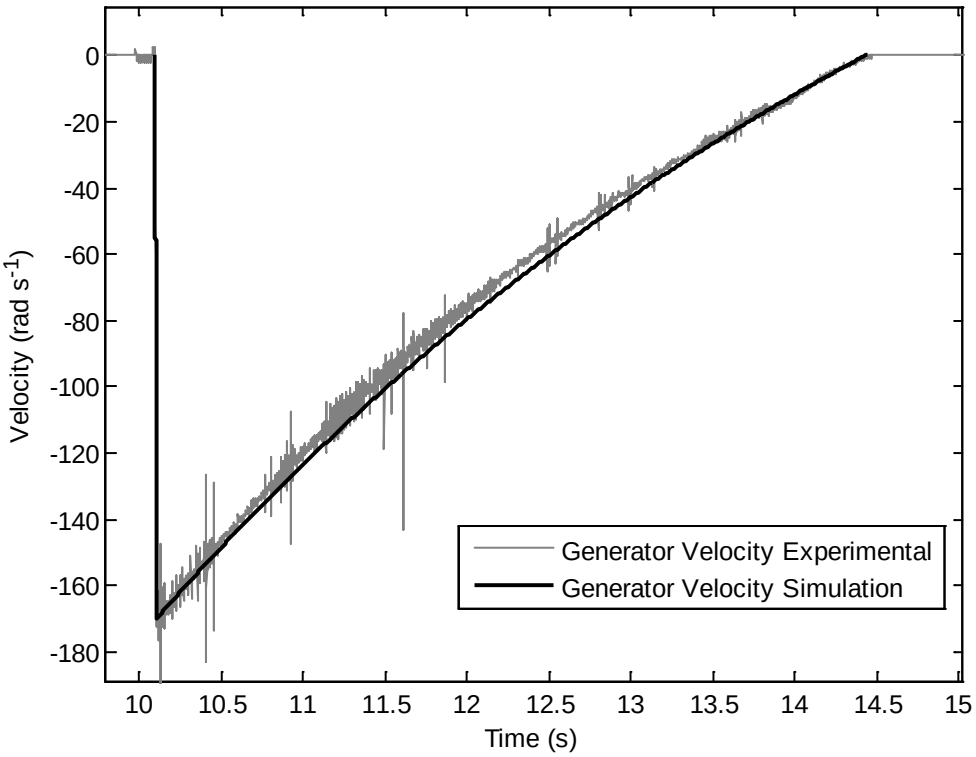

Figure 5-17 Generator velocity comparison

The Generator velocity comparison is shown in Figure 5-17, it can be seen that the velocity of the flywheel increases sharply reaching approximately 170 radians per second and a gradual rundown taking approximately 4.5 seconds. The simulation results can be seen to track the experimental results quite accurately, validating the modelled behaviour.

5.5.4. Conversion Power

The power output with respect to time, for the three inertias used for experimental analysis, is shown in **Figure 5-18.** As expected it can be seen that for the average input energy and an optimized 14Ω load resistance, the generator velocity is highest for the lowest inertia $1.0x10^{-}$ resulting in a higher voltage and higher power output. It can also be noted that the duration of the available power also varies according to the inertia used. As expected, it can be seen that the longest inertia provides the longest rundown. The duration of run down and the peak power output combined with how much energy is extracted by the load are key factors in the system efficiency.

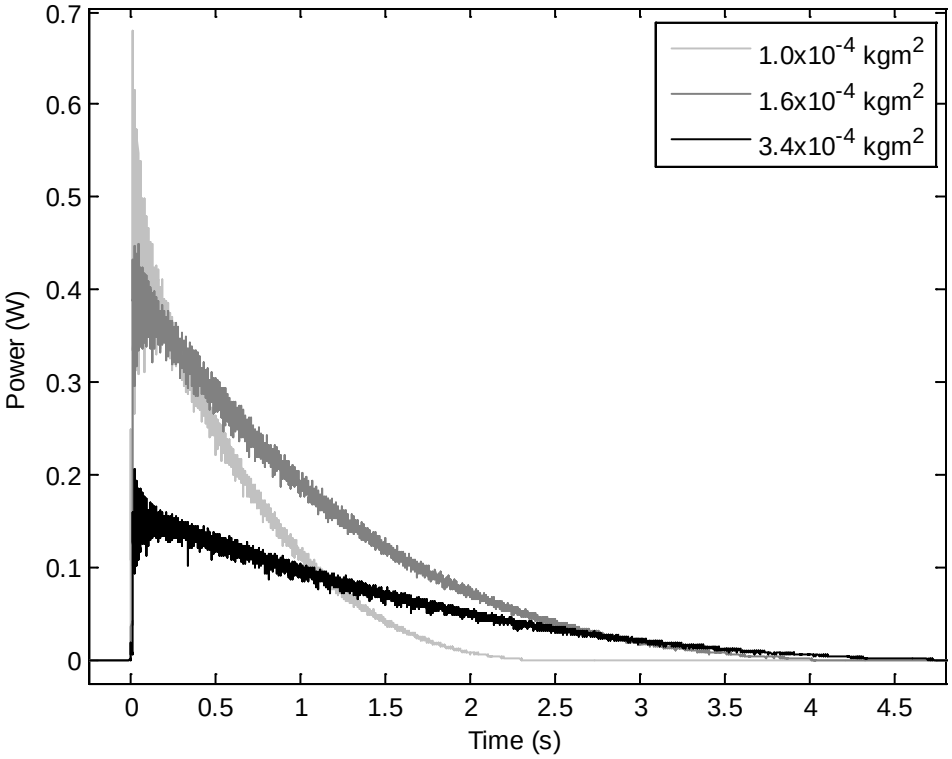

Figure 5-18 Power output for selected inertia

5.5.5. Energy Conversion

The energy output for a range of inertias and load resistances is shown in Figure 5-19. It can be seen that optimum energy in delivered to the load at approximately 14Ω for the 1.0x10^{-}. Also, the energy output from the other two inertias is lower.

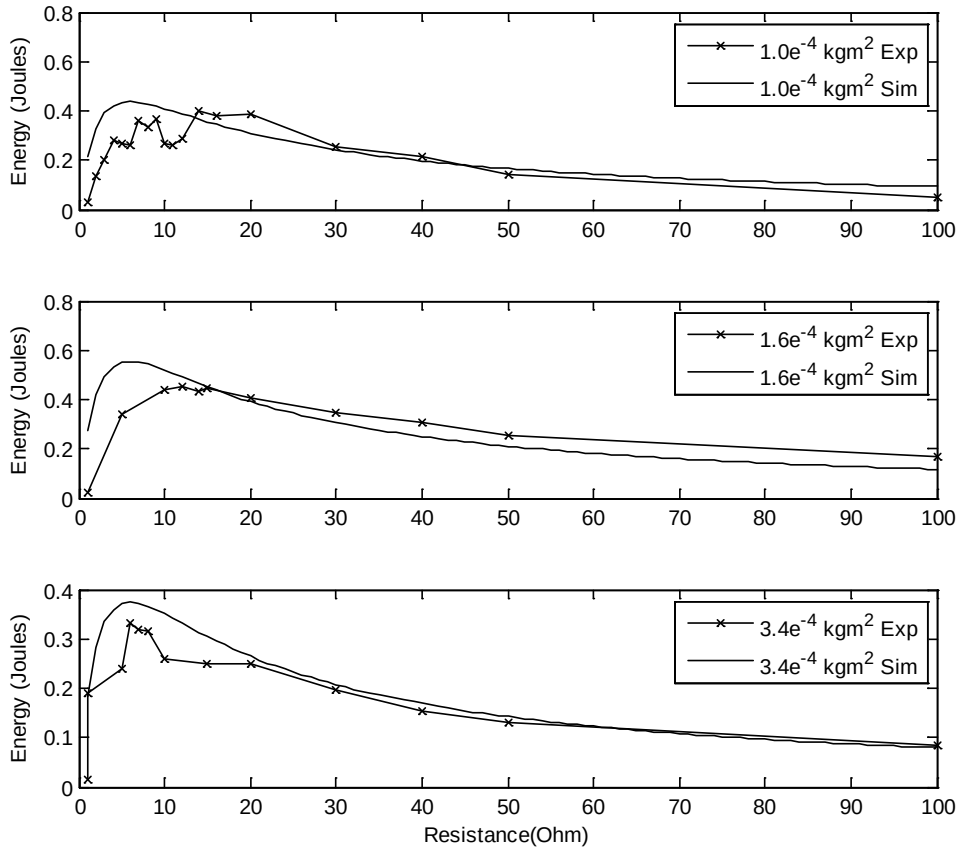

Figure 5-19 Flywheel inertia energy outputs for a range of load resistance values

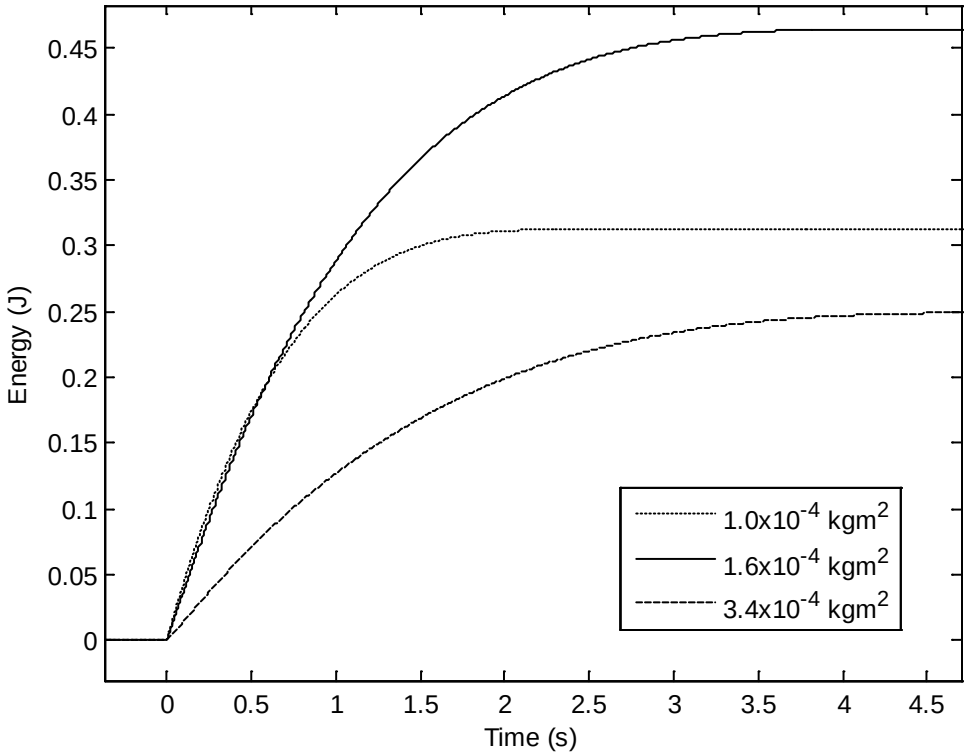

Figure 5-20 Energy output for selected inertia

The maximum energy output for a fixed load resistance as a function of time is shown in **Figure 5-20**. It can be seen that the energy delivered to the 14 Ω load resistance is greatest for the 1.6x10^{-} inertia.

5.5.6. Conversion Efficiency

The system efficiency is a key result; with this characteristic the overall performance of the system can be evaluated.

$$Efficiency\,\eta = \frac{OutputEnergy, e_{out}}{InputEnergy, e_{in}}$$

The efficiency for the three inertias is plotted against load resistances shown in Figure 5-21. It can be seen that the system is most efficient when the 1.6x10^{-} inertia is used, giving a peak efficiency close to 20%. The simulation results for the same inertia show slightly higher efficiency at close to 24%. This difference between the experimental efficiency results and the simulated results can be attributed to the changing friction values in the system for particular test runs. However, the overall match can be seen to track the experimental results. Inertia of 1.0x10^{-} and 3.4x10^{-} respectively, show a similar relationship between experimental & simulation results with good correspondence overall.

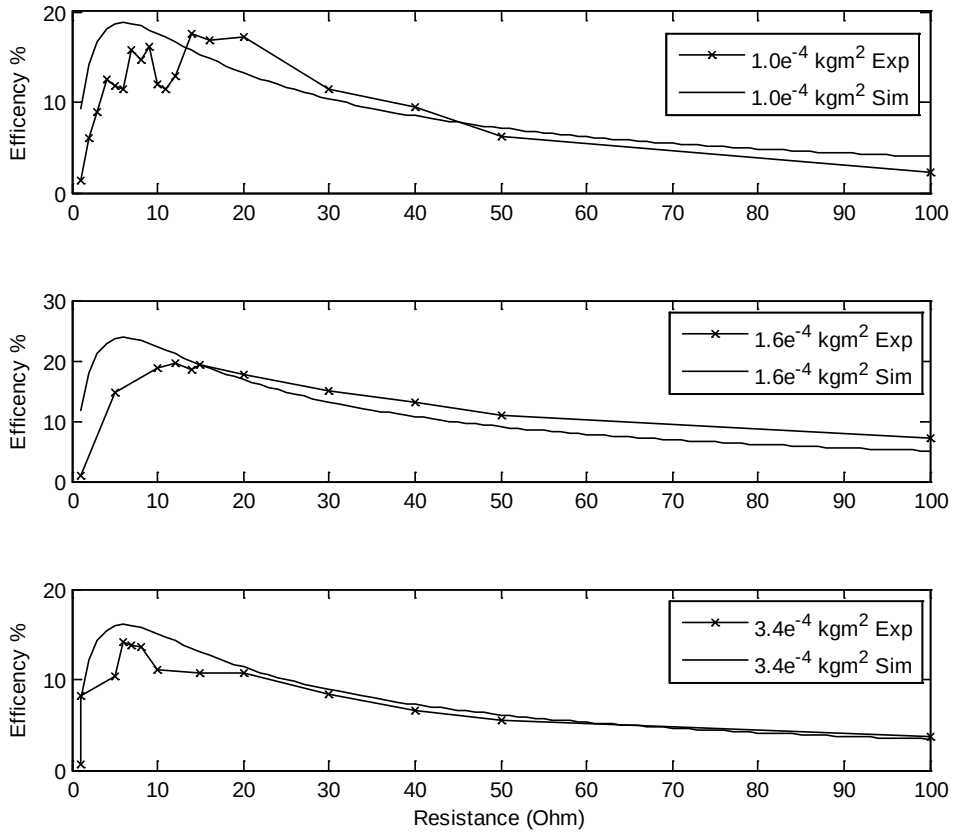

Figure 5-21 Flywheel Inertia Efficiencies

5.5.7. System Energy losses

For further development and manufacture of the next generation prototypes, establishing the system losses will allow the concentration of resources to be directed in an efficient manner. The energy losses can be evaluated by examining the energy available at key stages of delivery to the load. This is illustrated in Figure 5-22.

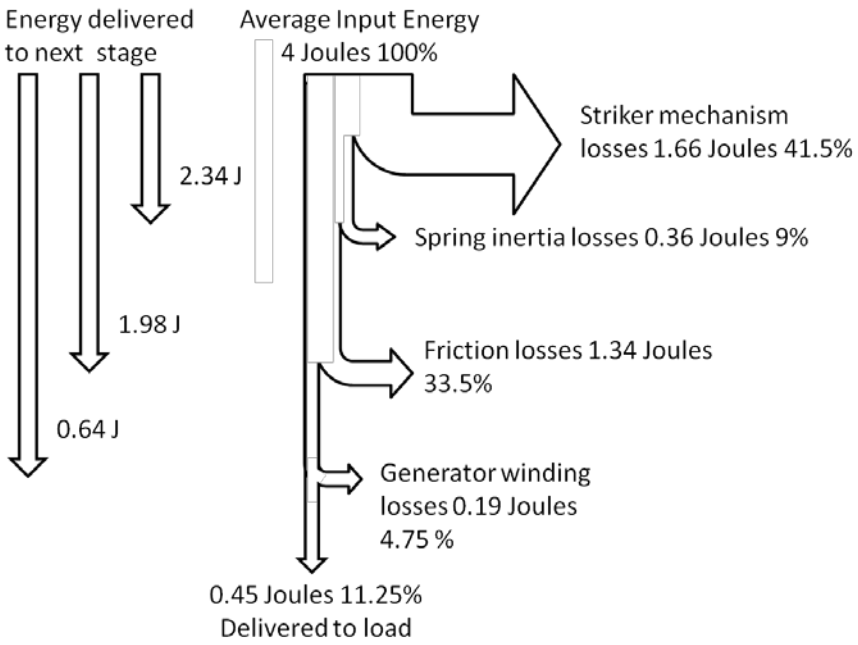

Figure 5-22 System losses and efficiency

From previous discussion, it was seen that on average approximately 4 Joules is delivered to the striker mechanism. For experimental purposes the stair tread was actuated many times and it was determined that the energy delivered to the input stage fluctuated and that the average input energy was 4 Joules.

The striker mechanism attached to the stair tread is used to transfer the energy from the pedestrian into the spring; as discussed previously, the energy delivered to the output stage is

$$E_{in} = \frac{1}{2} k_s \left(\theta_{\max}^2 - \theta_0^2 \right) + \frac{1}{2} J_s \omega_{step}^2$$

This energy can be calculated from the experimental data and the parameters given in Table 5-2. The losses at this stage are 1.66 Joules and account for 41.5% of the total energy available to the system. This is the greatest loss observed and originates from the input mechanism during the energy transfer from the input tread to the spring. The energy delivered to the next stage after the losses is 2.34J.

At the end of phase 3 as the spring is released from the striker, it accelerates and drives the spring and flywheel to the point at which the pivot arm hits the end-stop. A small loss is incurred and energy is lost into the end-stop, this can be calculated as;

$$E_s = \frac{1}{2} J_s \omega_{step}^2$$

Using the parameters provided in Table 5-2, the loss incurred at this point is 0.36 Joules or 9% of the total energy available in the system. The energy delivered to the next stage after the losses incurred is 1.98J.

The losses in the bearing are the next most significant losses at 1.34 Joules. This is 33.5% of the total energy available. The motor/generator losses can be found using

$$E_g = E_l \frac{R_g}{R_l}$$

The generator losses are 0.19 Joules and the energy delivered to the load is useful electrical energy of 0.45J.

5.6. Discussion

The mechanism provides a means of converting footfall energy to electrical energy in a manner which in an efficient manner. The behaviour of the system is described by the mathematical model developed with a good degree of accuracy and so it is possible to use this model as the basis for parameter optimisation. By suitable choice of spring constant and 'pre-load' it is possible to maximise the energy extracted from the pedestrian's footfall. This must be balanced against the need to minimise the inertia of the spring relative to that of the flywheel and generator. As with any mechanism, the efficiency is limited by the presence of friction but, for given friction values, it is possible to select other system parameters to minimise the effects of these frictional losses.

During footfall the applied force is only used to twist the spring and accelerate the striker mechanism. These parts may be designed to have minimal inertia and hence the dynamic forces during impact are not significant compared to the spring forces. The sprag clutch decouples the input and output side of the mechanism so that they may be designed separately, allowing greater freedom in the choice of parameters.

The mechanism has been designed to accept a specified input displacement (in this case 10mm) and applied force (600N). Assuming the ground reaction force is equal to the user weight, this input force corresponds to a pedestrian mass of approximately 60kg. For users with lower weight they will not produce sufficient displacement for the striker mechanism to release the spring and so no energy will be transferred to the output. Conversely, for heavier users, they only produce the same displacement, and hence input energy, as a 60kg user. It

would be possible to extract more energy from these heavier pedestrians by using a stiffer spring but this would prevent lighter users producing any energy. The choice of optimum 'cut-off' mass depends on the mass distribution among the user population. Selecting this cut-off for particular locations, along with methods of extracting maximum energy from a range of users, is a subject for further study.

The prototype mechanism has been designed for understair use but the same concept could be applied to in-shoe energy harvesting. This does, however, present significant challenges in terms of fitting the components within the confined space of a typical shoe. In particular, the two mechanical storage elements (spring and flywheel) require minimum physical dimensions in order to be capable of storing the requisite energy. It may thus be that it is necessary to reduce the energy extracted to a more modest level in this scenario.

5.7. Conclusions

A novel mechanism has been proposed which is capable of extracting significant levels of energy from normal human motion and converting this energy in an efficient manner into electrical energy. Based on a mathematical model of the mechanism, it has been possible to identify system parameters which optimise the output power and efficiency. Experimental results demonstrate an output energy of 450mJ with an efficiency of 24%. These figures compare favourably with other published devices discussed in Table 2-2 Summary of available technologies on page 40.

6. Chapter 6 – Cantilever Design

In this chapter a second generator is introduced as an alternative way of converting human footfall energy to usable electrical energy. With this approach a cantilever is configured to accept input energy through a striker mechanism attached to a stair tread on the same staircase. The chapter begins by discussing the mechanistic characteristics of the system and then develops the mathematical model governing its physical operation. Parameters are identified to enable a model to be generated in MATLAB to verify the prototypes operation. This model is then used to optimise the system efficiency. Results validating the model are presented and roots to increase efficiency are established.

6.1. Impulse vibration system

As with all the prototypes discussed in this work, the aim is to transform low cyclic or intermittent impulses of energy into longer pulses which can then be converted into electrical energy used to power sensor and actuator networks.

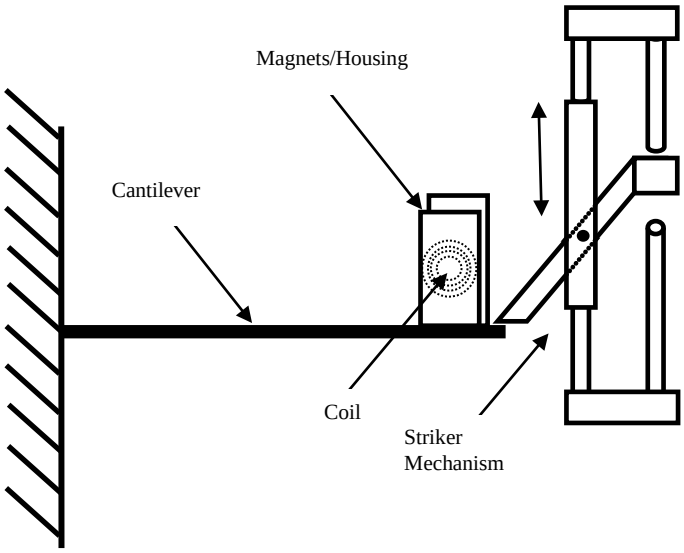

Figure 6-1 Vibrating cantilever footfall generator

This design will convert the heel strike of person walking on a flight of stairs or a floor into a vibration by the striker connecting with the cantilever. The mass on the end of the cantilever consist of high strength magnets, which when in a vibrating state will induce voltage in a coil placed between them as seen in Figure 6-2 below.

6.2. Mathematical Model

In this section we consider a beam with the dimensions shown in Figure 6-2.

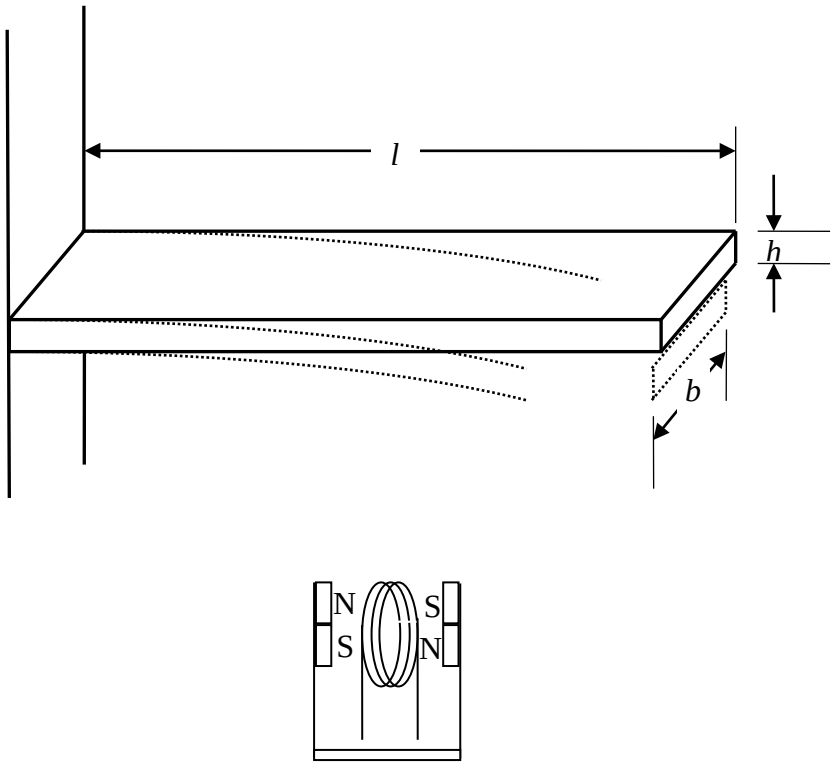

Figure 6-2 Cantilever Beam

The deflection at the end of the beam, δ, when subjected to a force F is given by:

$$\delta = \frac{Fl^3}{3EI}$$

Where E is the Young's modulus of the material used and I is the second moment of area which, for a rectangular section beam is $I = \frac{bh^3}{12}$. Thus the spring constant at the end of the beam is:

$$k = \frac{F}{\delta} = \frac{3EI}{l^3}$$

The mass of the cantilever is $m = \rho bhl$ where ρ is the material density. If the entire beam mass were moving then the resonant frequency would be $\omega = \sqrt{\frac{k}{m}} = \sqrt{\frac{3EI}{\rho hbl^4}}$. However not all of the mass moves and the resonant frequency is

$$\omega = 1.875^2 \sqrt{\frac{EI}{\rho hbl^4}}$$

If there is an additional mass at the tip of the cantilever the resonant frequency becomes [166]:

$$\omega = \sqrt{\frac{k}{m_{eff}}}$$

where the effective mass is $m_{eff} = m_{tip} + 0.23m_{beam}$.

The motion of the magnets relative to the coil induces an open circuit voltage, $v(t) = k_e \dot{x}(t)$ where is the emf constant. If the coil resistance is and the load resistance is , this voltage

results in a current $i = \frac{k_e \dot{x}}{R_C + R_L}$. This, in turn causes a reaction force in the cantilever equal to $k_t i$ where is the force constant. Thus the dynamics of the cantilever beam may be written as:

$$m_{eff}\ddot{x} = -kx - \left(b_m + \frac{k_e^2}{R_C + R_L}\right)\dot{x} \qquad \textbf{Equation 6-1}$$

where represents the mechanical damping and we use the fact that $k_t = k_e$.

For an initial displacement and zero initial velocity, the solution to Equation 6-1 is:

$$x(t) = \frac{x_0}{\beta} e^{-\omega\xi t} sin(\omega\beta t + \phi)$$

where $\omega = \sqrt{\frac{k}{m_{eff}}}$, $\xi = \frac{\left(b_m + \frac{k_e^2}{R_C + R_L}\right)}{2\omega m_{eff}}$, $\beta = \sqrt{(1 - \xi^2)}$, and $\phi = cos^{-1}(\xi)$ and the velocity is given by:

$$\dot{x}(t) = \frac{\omega}{\beta} e^{-\omega\xi t}\{\xi sin(\omega\beta t + \phi) + \beta cos(\omega\beta t + \phi)\}$$

The instantaneous power delivered to the load is:

$$p(t) = \frac{v(t)^2}{R_L}$$

And the energy supplied to the load is:

$$E = \int_0^\infty p(t)dt = \frac{kx_0^2}{2}\frac{R_L k_e^2}{b_m(R_C + R_L)^2 + k_e^2(R_C + R_L)}$$

Given that the mechanical energy stored in the cantilever is $E_{in} = \frac{kx_0^2}{2}$ it is straightforward to see that the efficiency converting this mechanical energy to electrical energy is:

$$\eta = \frac{E}{E_{in}} = \frac{R_L k_e^2}{b_m(R_C+R_L)^2+k_e^2(R_C+R_L)}$$

The load resistance for maximum output power can be determined from $\frac{dE}{dR_L} = 0$ as

$$\hat{R}_L = \sqrt{\frac{R_C(b_m R_C + k_e^2)}{b_m}}$$

And the peak efficiency is:

$$\hat{\eta} = \frac{\hat{R}_L k_e^2}{b_m\left(R_C + \hat{R}_L\right)^2 + k_e^2\left(R_C + \hat{R}_L\right)} \qquad \textbf{Equation 6-2}$$

Note that as $b_m \to 0$ and $R_L \to \infty$, $\eta \to 1$. Unfortunately, it is not possible to arbitrarily control the mechanical damping but we should aim for a material which has low loss coefficient such as spring steel. For a given value of b_m it appears that it would be advantageous to make R_C as small as possible and k_e as large as possible. However, it is not feasible to control these two quantities independently since they are both determined by the coil configuration and the wire used.

$$\gamma = \frac{R_C}{k_e^2}$$

Substituting for $\hat{R}_L$ and γ in Equation 6-2 gives:

$$\eta = \frac{\sqrt{\gamma^2 + \frac{\gamma}{b_m}}}{2\gamma(b_m+1)+(2b_m\gamma+1)\sqrt{\gamma^2+\frac{\gamma}{b_m}}}$$

6.3. Parameter Optimisation

The relationship between γ, and the efficiency is shown in Figure 6-4. It can be seen that the efficiency increases for decreasing γ and . As noted previously, can be reduced by appropriate choice of cantilever material. In order to maximise efficiency we should aim to minimise γ, within the constraints imposed by the coil structure and materials.

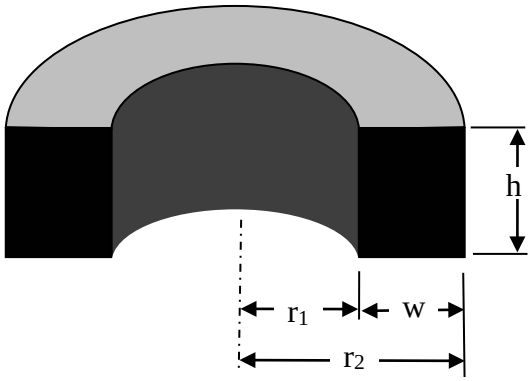

Figure 6-3 Coil Dimensions

Consider a circular coil with the dimensions shown in Figure 6-3 where the mean radius, $r = (r_2 + r_1)/2$, made up of wire with diameter *d*, operating in a magnetic field strength *B*. The emf constant, is

$$k_e = Bln$$

Where *l* is the effective length of wire, assumed equal to $2\pi r$ and *n* the number of turns.

Assuming that the coils are laid in uniformly distributed rows then the number of turns which can be fitted within the coil area is:

$$n = \frac{wh}{d^2}$$

and so

$$k_e = \frac{Brwh}{d^2}$$

The total length of wire in the coil is $l = 2\pi rn$ and for wire resistivity ρ the coil resistance is:

$$R_C = \frac{l\rho}{d^2} = \frac{2\pi\rho rhw}{d^4}$$

Substituting & back into γ we obtain:

$$\gamma = \frac{R_C}{k_e^2} = \frac{2\pi\rho}{B^2whr} \qquad \textbf{Equation 6-3}$$

From Equation 6-3, it can be seen that γ may be reduced by altering the magnet and coil characteristics. Reducing resistivity, ρ, reduces γ but this is limited by the material properties of the wire material, with copper offering the lowest resistivity at reasonable cost at normal operating temperatures. Increasing the physical dimensions of the coil, *w*, *h* and *r* all result in a decrease in γ, as does increasing the magnetic field strength, *B*. Making it bigger and needing bigger more expensive magnets.

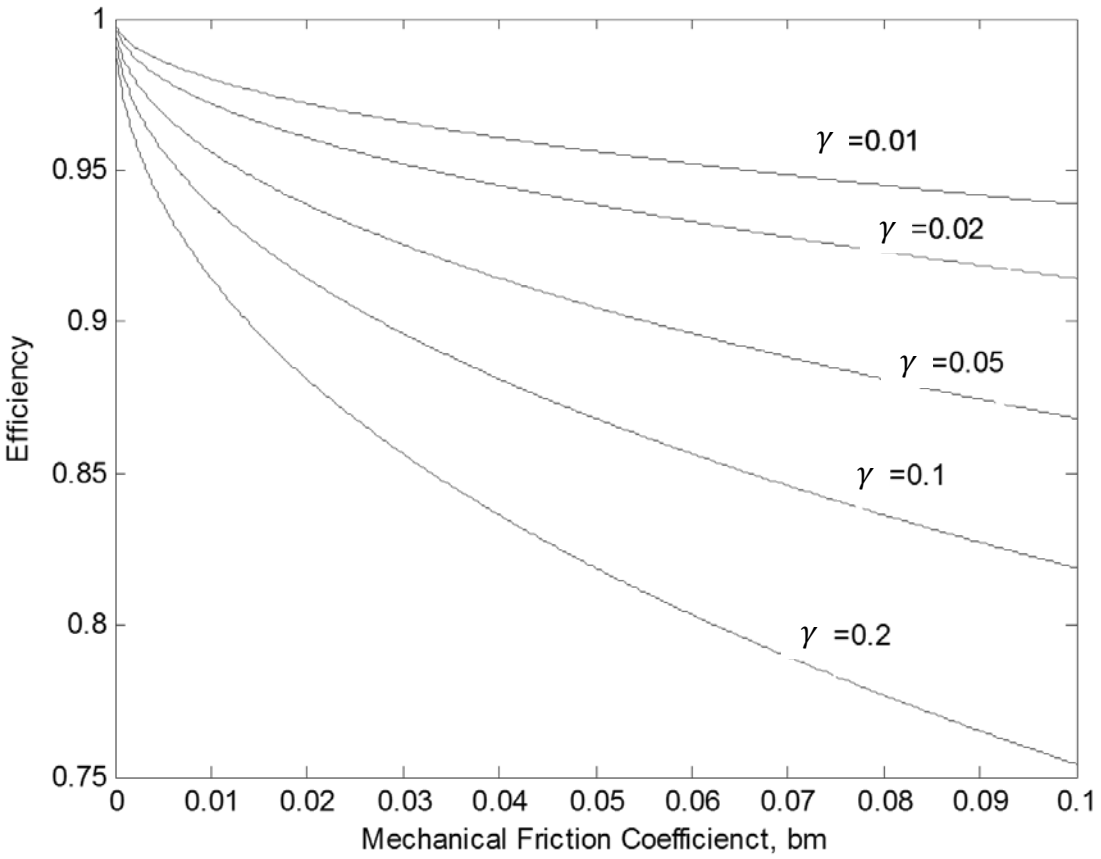

Figure 6-4 Effect of Mechanical Damping and gamma on Efficiency

6.4. Experimental Results

As with the flyback generator, the cantilever generator, shown Figure 6-6, was constructed to establish the concept and investigate the practicality of the proposed mechanism. Again as with the flyback generator, the energy is transferred through a stair tread on the bespoke staircase. However, a new striker mechanism has to be designed that would allow the cantilever to continue oscillating once it was actuated. Figure 6-5 shows the new striker. The striker block is attached to the stair tread and moves up & down. Adjustment rods on the rear of the mechanism can be seen which allow the vertical movement. The upper rod allows the force to be transferred into the cantilever on the downward stroke and the lower rod helps to remove the striker tip out of way of the oscillating cantilever so that the energy can be extracted by the coil and magnet configuration into electrical energy.

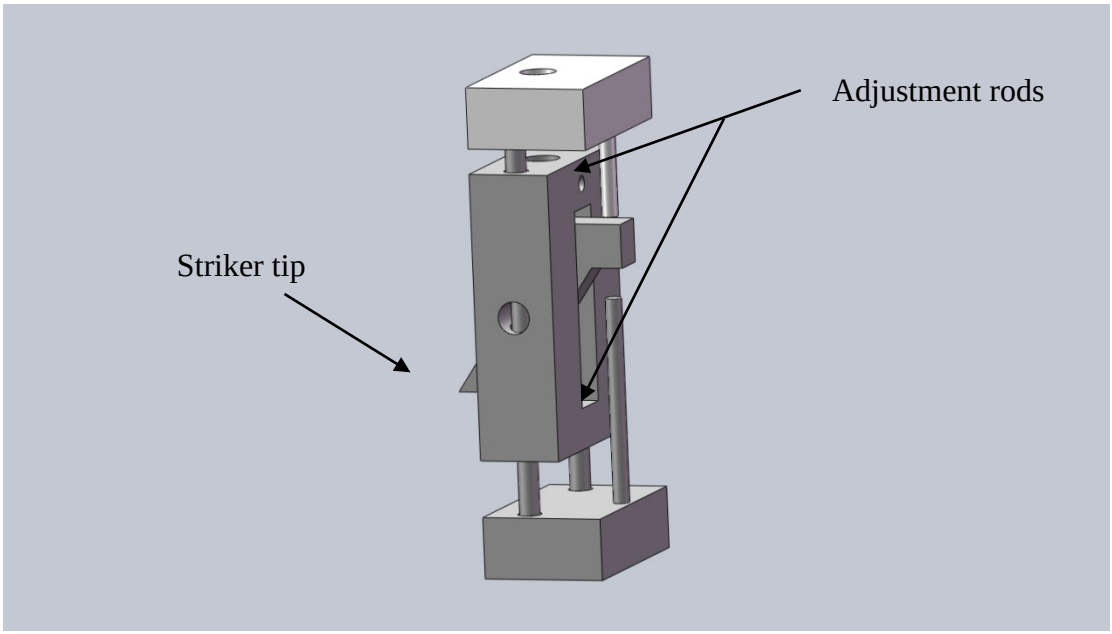

Figure 6-5 Cantilever striker mechanism

Figure 6-6 shows the generator attached to the side of the staircase. For this generator a coil and magnet configuration, which will be discussed in more detail later at the end of this

chapter, was used and can be seen in the image attached to the frame which is in turn attached to the staircase. Therefore while the cantilever oscillates, with the magnets forming the tip mass, the coil and coil housing remain stationary. For the experimental purposes the cantilever design is adjustable and allows the length of the cantilever to be adjusted. The staircase was instrumented with sensors to obtain reading for force, linear movement and voltage output from the bespoke generator.

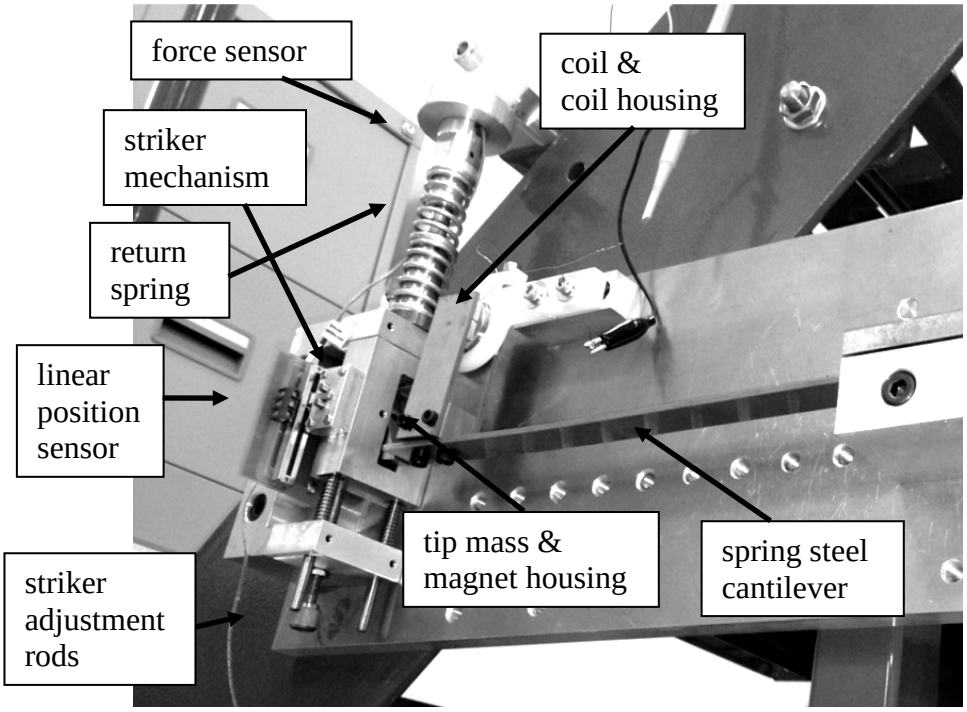

Figure 6-6 Prototype cantilever generator mounted on a staircase

The Cantilever was mounted on the side of the staircase, very similarly to the Flyback generator as discussed in chapter 5. The striker mechanism as discussed above can be seen in the figure and the coil & coil housing can be seen to be attached to the frame of the staircase while the beam can be actuated and oscillate freely inducing a voltage in the coil. The voltage

across the coil winding is measured and used to corroborate the validity of the mathematical model.

6.4.1. Parameter Identification

The parameters of the prototype generator were obtained from a combination physical measurement of parameters, the mass and spring constant of the beam and by fitting the simulation to measurements of dynamic behaviour of the system for the mechanical damping factor. The parameters are listed in Table 6-1. One spring steel beam was used for validating the mathematical model. However this single beam was actuated in three different lengths to ascertain the impact on the parameters governing the mathematical model.

Parameter	**Sym**	**Value**			**Acquisition**
Breadth	b	20mm			Measured
Height	h	3mm			Measured
Length	l	=127mm	=178mm	=254mm	Measured
Beam mass		59.8g	83.8g	119.6g	Measured
Tip mass		176g			
Deflection	x0	5mm	10mm	11mm	Measured
Beam Input Energy	Ein	0.8527 J	0.2992 J	0.0983 J	Measured
Frequency	ω	ω_1 = 299.2	ω_1 = 174.5	ω_1 = 89.2	Measured
Mechanical Damping	ξ	ξ_1 =0.0038 ξ_1 =0.0945	ξ_2 =0.0036 ξ_2 =0.0198	ξ_3 =0.0029 ξ_3 =0.0049	Measured Simulation
Spring Constant	k	17050 N/m	5984 N/m	1624 N/m	Simulation

Table 6-1 Cantilever generator parameter identification

From Table 6-1, the 3 beam lengths are 127mm, 178mm and 254mm. During actuation of the step the beam deflection was 5mm for the 127mm bean and 10mm for the 178mm beam and 11mm for the 254mm beam. The input energy, Ein, for each beam length was calculated

using its corresponding spring constant k obtained from the physical properties and dimensions of the beam. The simulated resonant frequency of the beam was matched to the measured value by tuning the spring constant value. Finally the damping factor ξ was first measured using the open circuit voltage decay profile of each beam.

6.4.2. Input Energy

The system input energy (as opposed to the beam input energy) was obtained using a force transducer in the form of a load cell and linear potentiometer to capture the displacement. Using a cumulative summation of the force with respect to displacement the input energy can be found, as discussed in 5.5.2.

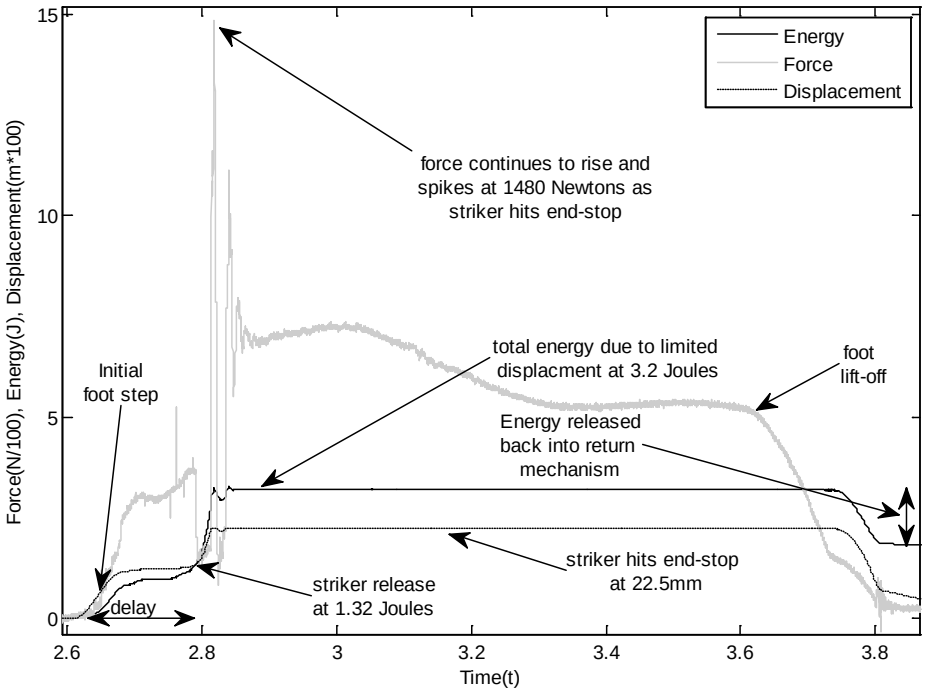

Figure 6-7 Force & Displacement profile during footfall for 178mm beam

Force, displacement and energy are shown in Figure 6-7 for a single actuation of the system. It can be seen that the force peaks at approximately 1480 Newton's at which point the striker has hits the end-stop. The figure shows that at the point of the release from the striker 1.32

Joules of energy are extracted from the user. A further portion of the energy is returned to the system via the return spring and this can be seen towards the end the profile at approximately 3.8 seconds as seen in the figure.

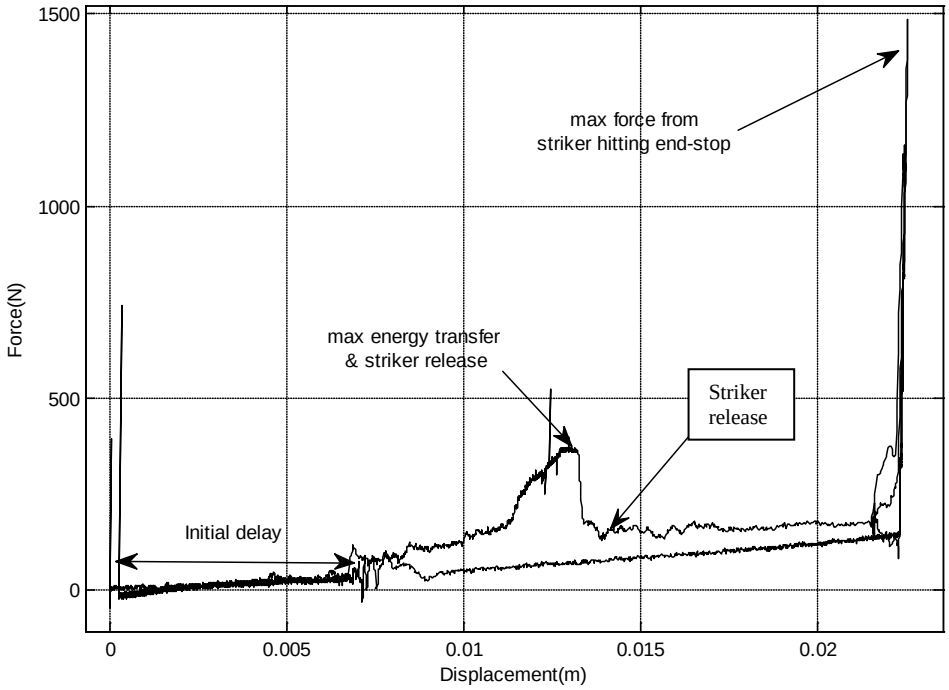

Figure 6-8 Force Displacement curve

The force displacement curve for an input profile can be seen in Figure 6-8. An initial delay can be seen before the cantilever and striker mate contact. After approximately 10mm of displacement the force can be seen to rise to around 300 Newton's and then fall when the striker releases the cantilever before spiking at the end of the profile to a maximum when the striker hits the end-stop.

6.4.3. Mechanical Damping

In order to determine the mechanical damping the open circuit profiles were used as this detaches the system from any load and confines the analysis to a closed system. The open circuit voltage profile for the 254mm length beam is shown in Figure 6-9. The initial peak voltage can be seen to be approximately 4 Volts and the decay of the voltage can be seen to occur over a 40 second period.

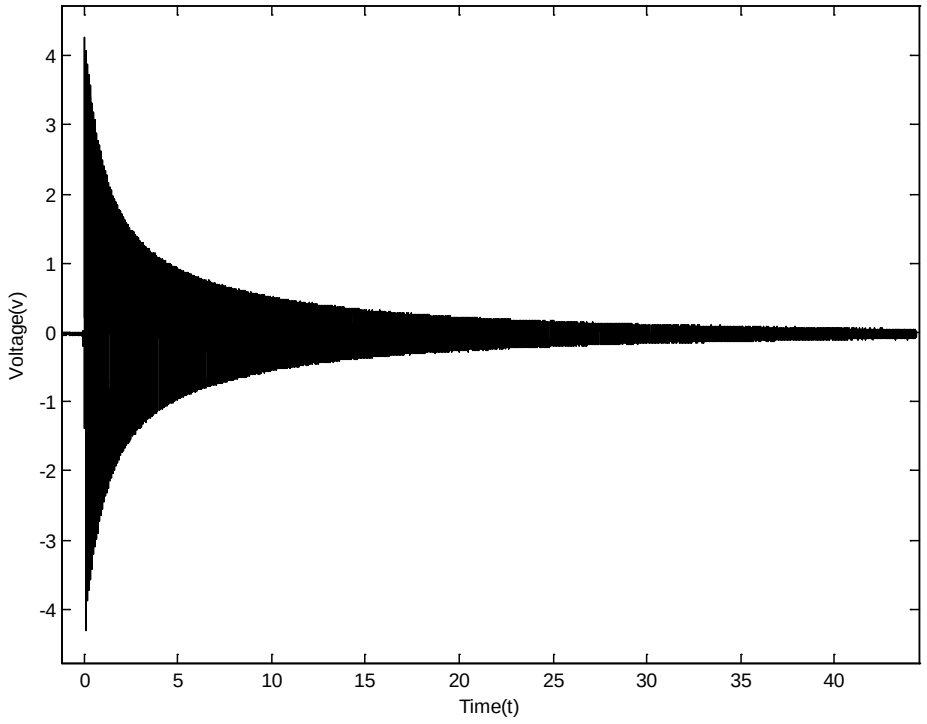

Figure 6-9 Open circuit voltage for the 254mm length beam

The decaying amplitude of voltage may be represented by

$$A(t) = A_0 e^{-\xi \omega t}$$

The amplitude of the second peak is then

$$A_1 = A_0 e^{-\xi 2\pi}$$

Therefore ξ can be found by taking the log of each side and rearranging to give

$$\xi = \frac{1}{2\pi}\log(\frac{A_1}{A_0}) \text{ or } \xi = \frac{1}{2\pi}[\log(A_1) - \log(A_0)]$$

Using this process, the mechanical damping ξ was found for each beam lengths and can be seen in Table 6-2. The sampling and log technique for acquiring ξ is shown in Figure 6-10 below.

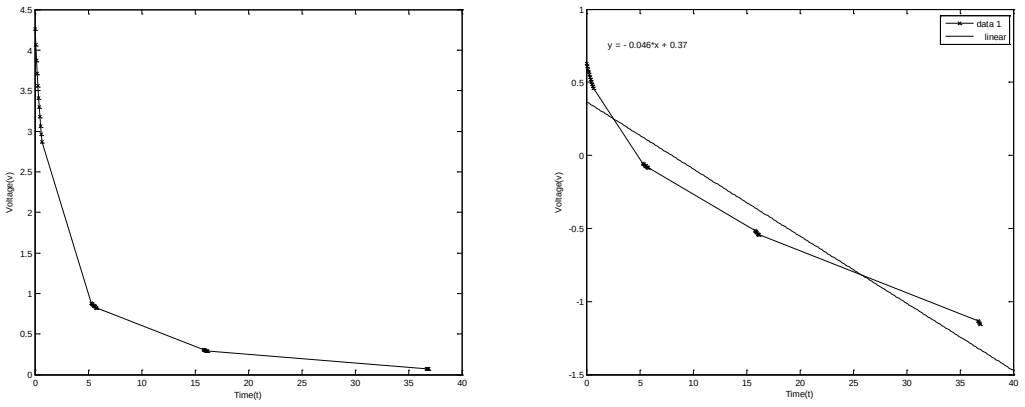

Figure 6-10 Sampling and log technique for acquiring ξ

Beam Length	ξ
254mm	ξ_1= 0.0029
178mm	ξ_2= 0.0036
127mm	ξ_3= 0.0038

Table 6-2 Mechanical damping found from time domain analysis

The mechanical damping obtained from the open circuit decay was then compared to the simulation to give a best fit as seen in Figure 6-11. This shows the open circuit experimental and simulation results for the 254 beam.

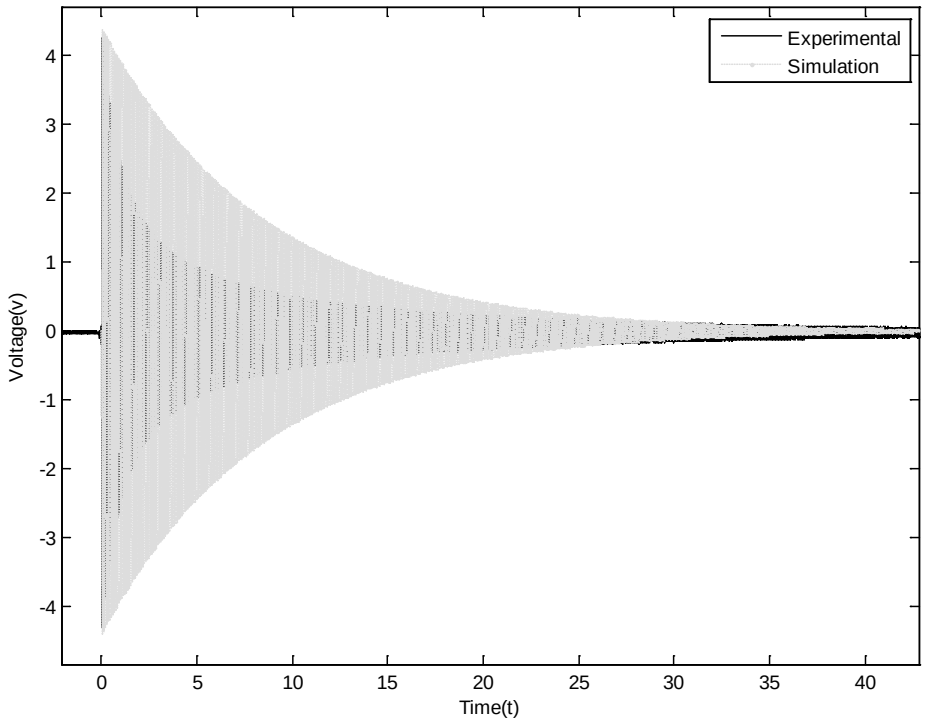

Figure 6-11 Open circuit voltage decay over time for the 254mm beam

The initial steps in matching the voltage decay of the simulation to the experimental result, shown in gray dotted plot, was to adjusting the resonant frequency ω of the simulation to the experimental results. The decay of induced voltage in the coil can be seen to end at around 40 seconds after the initial actuation. The simulation shows a good fit in relation to the decay and also to the mechanical damping of the system.

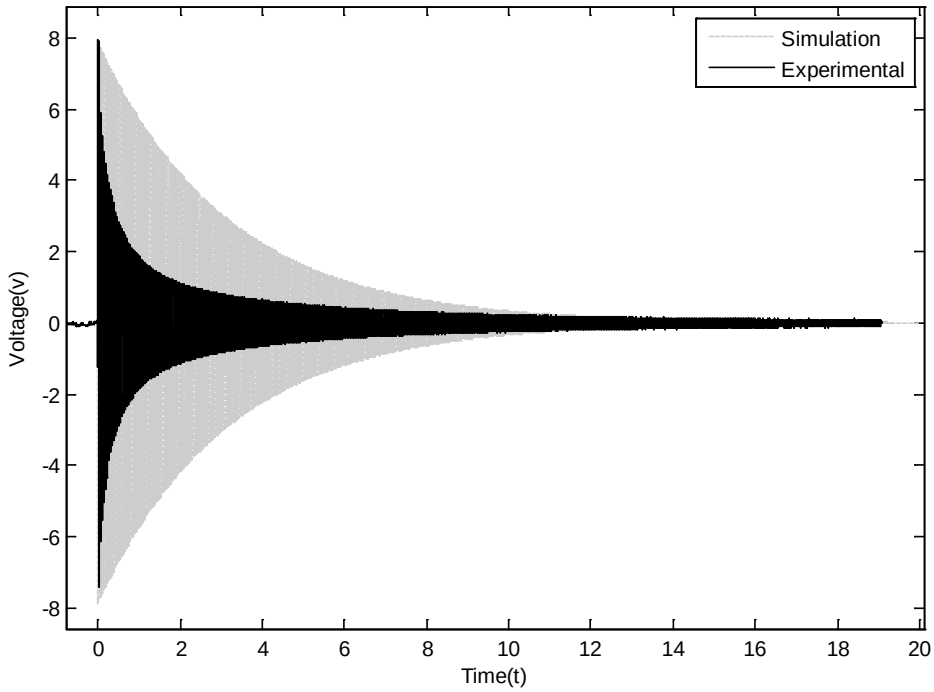

Figure 6-12 Open circuit voltage decay over time for the 178mm beam

The open circuit voltage decay for the 178mm beam can be seen in Figure 6-12. The mechanical damping can be seen to match the time domain but remarkably less than for the longer beam at 254mm.

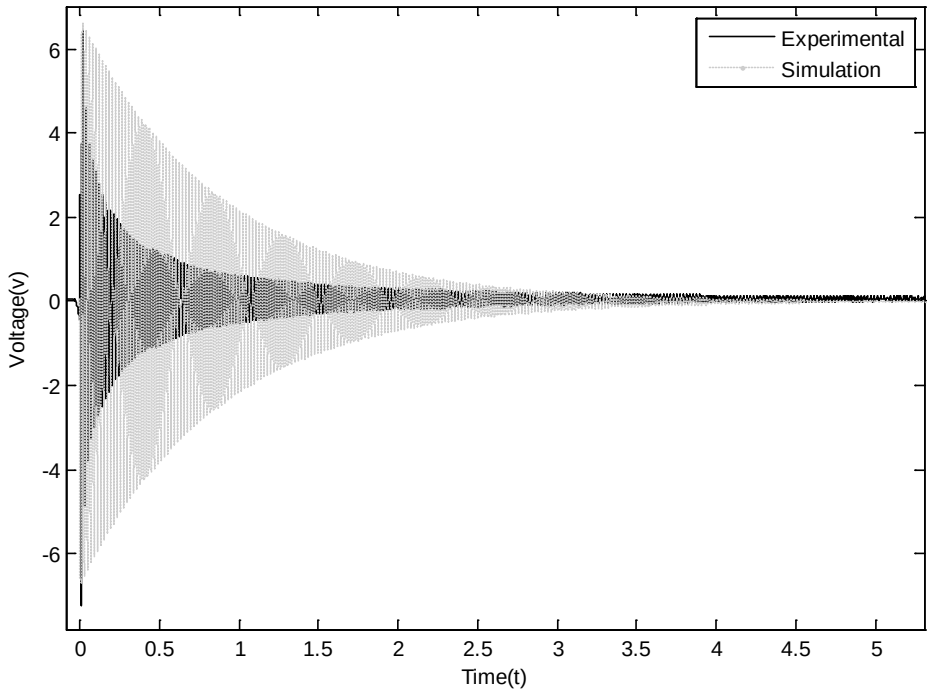

Figure 6-13 Open circuit voltage decay over time for the 127mm beam

The open circuit voltage decay for the 127mm beam can be seen in Figure 6-13. Again, the mechanical damping can be seen to be quite a mismatch in the time domain. This is more apparent for this beam length and is showing the worst fit to simulation from the three beam used.

Beam Length	ξ for time domain	ξ for varying load resistances	*factor bigger between ξ values
127mm	ξ_1= 0.0038	ξ_1= 0.0208	*5.5
178mm	ξ_2= 0.0036	ξ_2= 0.0198	*5.5
254mm	ξ_3= 0.0029	ξ_3= 0.0049	*1.7

Table 6-3 Mechanical damping found from time domain analysis

The mismatch in mechanical damping from the simulation to the experimental results for the shorter beam is due to the beam being subjected to deflection greater than its elastic limit and therefore the beam exhibits non-linear behaviour, placing it outside of a linear regions modelled in the simulation.

6.4.4. Power Conversion

The following results show simulation matches to power, energy and efficiency for the 3 beam lengths in experiments for a range of load resistance up to 100 Ohms. Table 6-3 shows the factor change in matched ξ values used in the simulation results.

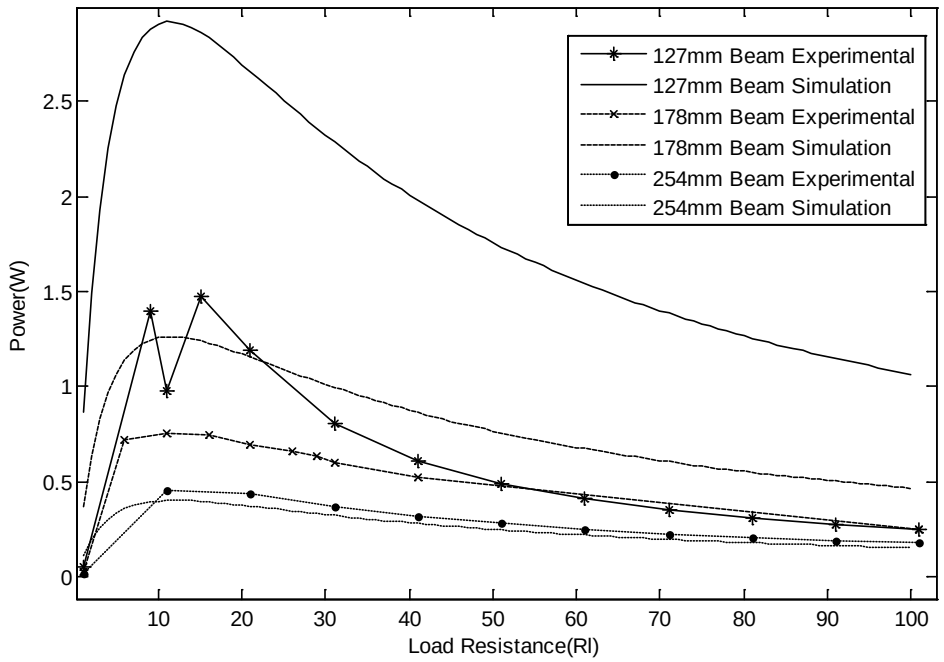

Figure 6-14 Max power output for the 3 beam lengths for varying load resistances

The experimental and simulation results for max power output for varying loads is shown in Figure 6-14. Best match to these results is seen for the 254mm beam length and progressive deviation to the experimental results can be seen for shorter beams at 178mm and 127mm beam lengths. Whilst some deviation is seen in the shorter beam the period of time that this

occurs is also very short and can be associated to some extent to the coil moving outside the magnetic field.

6.4.5. Energy Conversion

The experimental and simulation results for energy output for varying loads is shown in Figure 6-15. A good match in magnitude and slope to all beam lengths can be seen. Mechanical damping discussed in the previous section was a key parameter in the exceptionally good agreement between experimental and simulation results seen Figure 6-15.

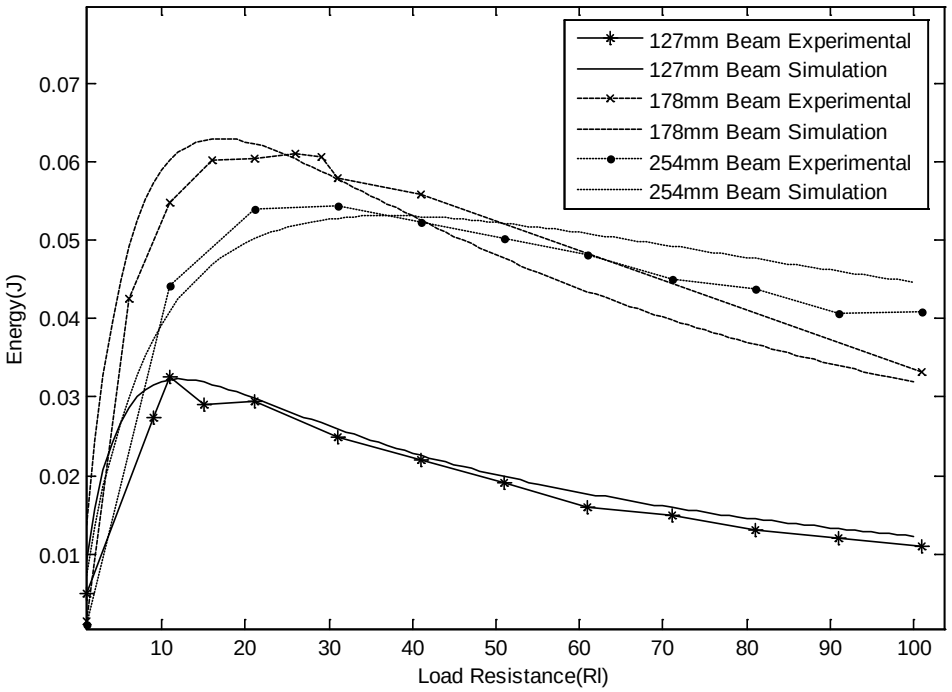

Figure 6-15 Energy output for the 3 beam lengths for varying load resistances

The highest energy output of 60mJ can be seen for the 178mm beam length. This is partly due to a larger input energy which will be seen to have an effect on the efficiency results discussed shortly.

6.4.6. Conversion Efficiency

The experimental and simulation results for conversion efficiency as a function of varying loads are shown in Figure 6-16. As with the energy values, these results show a good match to experimental results but are clearly due to ξ value quite different to those used for the time domain match to the simulation for shorter beams. This is also a good fit but worth noting that this is the ration of system energy-out to energy-in.

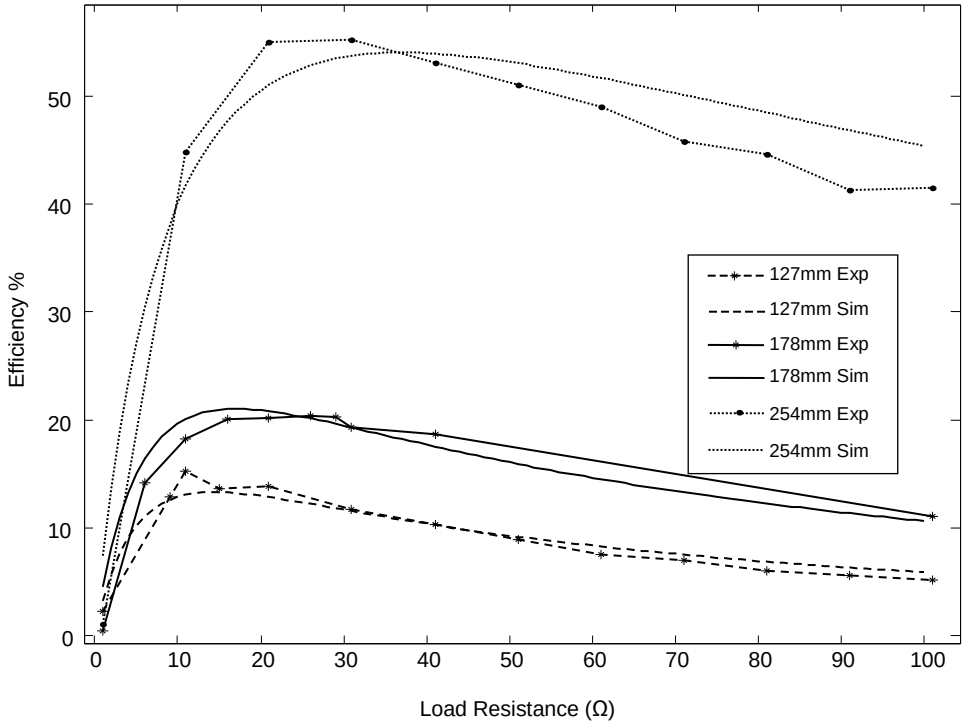

Figure 6-16 Efficiency output for the 3 beam lengths for varying load resistances

6.4.7. Energy Losses

The energy losses of the vibrating cantilever system are shown in Figure 6-17. The method of defining energy to each stage after losses are shown on the left side of the figure and energy losses for the striker, mechanical losses and coil losses are shown on the right of the figure.

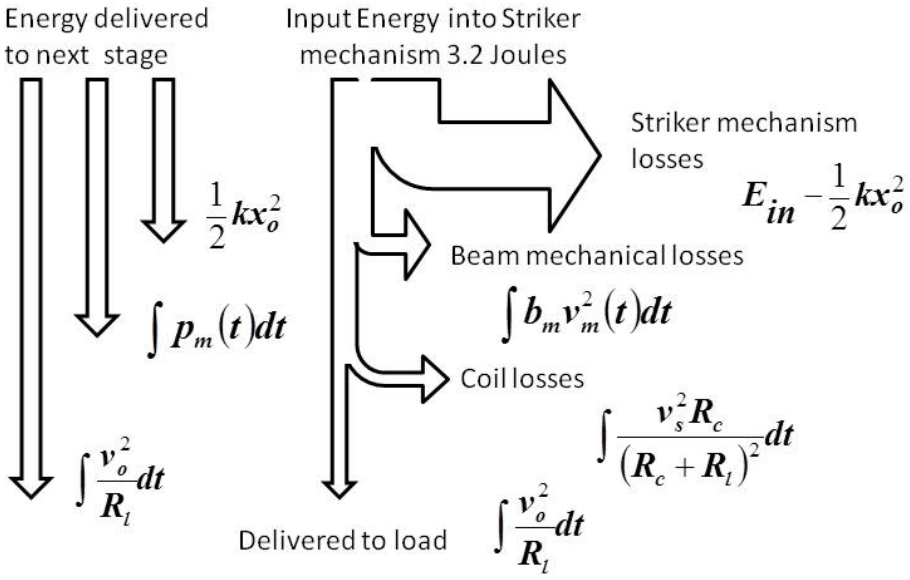

Figure 6-17 System energy losses

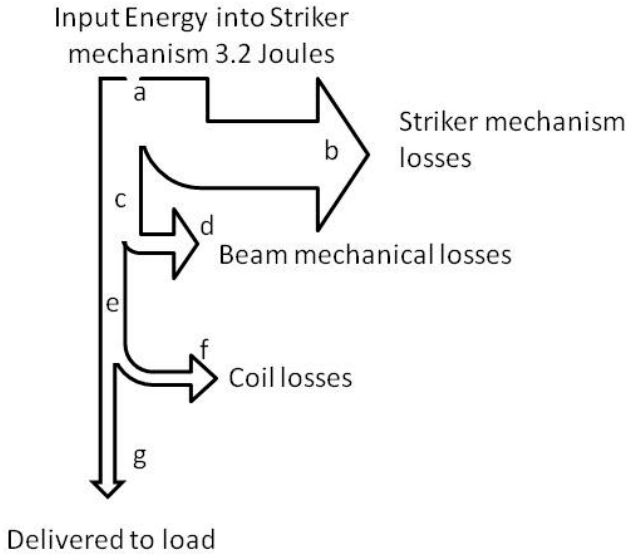

Figure 6-18 Energy values at specified points from a to g

Energy	Input (mJ) (c)	Mechanical (mJ) (e)	Output (mJ) (f)
254mm	100	71.6	52.8
178mm	309.7	109.8	64.4
127mm	213.2	60.2	29.7

Table 6-4 Energy available to stage

The energy delivered to each stage after losses for the 3 cantilever lengths are shown in Table 6-4. The longest beam at 254mm is the most efficient at converting the input energy. However, it can be seen that more energy can be delivered into the shorter beams and therefore more energy can be converted albeit less efficiently than the longer beam. It can be seen that less energy is inputted into the shortest beam at 127mm when it might be logically foreseeable to expect more energy into the shorter beam. The reduced energy is due to a shorter tip deflection of the beam at approximately 5mm as opposed to +10mm tip deflection for the longer beams. It was necessary to protect the beam from plastic deformation and its was and subsequent non-linear behavior outside of the modeled behavior.

Energy Losses	**Striker (J) (b)**	**Mechanical (mJ) (d)**	**Coil (mJ) (f)**
254mm	3.10	26.6	20.6
178mm	2.89	200	45.3
127mm	2.99	153	30.4

Table 6-5 Cantilever Energy losses

The system efficiency is determined from the energy delivered to the cantilever beam and so the losses incurred at the first stage which are attributed to the striker mechanism are not considered as system losses. However, it can be seen that for the longest beam length at 254mm, these losses are considerable and account for 96% of the energy being lost being lost from the stair tread to the beam. As expected the mechanical losses seen for shorter beam lengths are considerable at 6.25% for the 178mm beam length, compared to 0.8% for the longer beam at 254mm. The losses through the coil are minimal and in a very small percentage for all the beam lengths.

6.5. Discussion

The vibrating cantilever mechanism provides a means of converting footfall energy to electrical energy. The short linear impulse motion is converted to a longer vibration motion allowing efficient conversion by the coil and magnet arrangement. The behaviour of the system is described by the mathematical model developed with a good degree of accuracy and so it is possible to use this model as the basis for parameter optimisation. By suitable choice of spring constant and scaling up of the cantilever dimensions, it would be possible to maximise the energy extracted from the pedestrian's footfall. This must be balanced against the need to minimise the mechanical damping of the system by selecting appropriate materials for the cantilever.

6.6. Conclusion

A mechanism has been developed which is capable of extracting good levels of energy from normal human motion and converting this energy in an efficient manner into electrical energy. Based on a mathematical model of the mechanism, it has been possible to identify system parameters which optimise the output power and efficiency. Experimental results demonstrate an output energy of 53mJ with an efficiency of 55%.

7. Chapter 7 – Design Comparisons and Manufacture

In this chapter the two energy conversion systems are compared to one another in terms of efficiency, mechanism and energy input. Further discussion on complexity and reliability of the mechanisms is presented and a projected breakdown of the volume costs associated with manufacture for both mechanisms is examined. Also, some indications of power generation for footfall, road and rail use are presented. Finally, the design process and optimisation strategies for further development are presented.

7.1. System Efficiency and Input Energy

The efficiency of the systems being compared can be determined from several input stages. For clarity, it is desirably to compare the conversion systems after the striker mechanism as both systems have almost identical mechanisms up to this point and show similar losses through these stages. A more detailed explanation of the losses for stair tread and striker mechanisms can be seen in the chapter for the particular conversion system.

Conversion System	**Efficiency (%)**	**Power (Watt)**	**Energy (Joules)**	**Input Energy (Joules)**
Flyback				
$1.0e^{-}$	18	0.80	0.40	2.33
$1.6e^{-}$	20	0.45	0.45	2.33
$3.4e^{-}$	14	0.30	0.30	2.33
Cantilever				
127mm	14	1.50	0.03	0.21
178mm	20	0.75	0.06	0.31
254mm	55	0.50	0.05	0.10

Table 7-1 Conversion Systems Comparison

The efficiency for the conversion mechanisms in terms of the constraints governed by the prototype designs are shown in Table 7-1. The optimum efficiency under these constraints is 20% for the flyback converter and 55 % for the vibrating cantilever converter. It can be seen that the flyback converter accepts a much higher input energy at 2.33 Joules, in contrast to the input energy delivered into the cantilever converter, which is much lower at 0.31 Joules. These results show that under these constraints the flyback converter performs less efficiently but is able to convert more of the input energy into usable electrical energy. The flyback converter allows the input energy to be tuned through a preload facility; where additional energy can be stored into the spring. For lower input energy conditions the cantilever performs more favourably, converting more of the energy available, more efficiently. Finally, for conditions where short bursts of relatively 'high power' are required the smaller inertia for the flyback and shorter cantilever can be used as greater rotational/linear velocity is achieved resulting in a higher voltage output.

7.2. Prototype costs and volume manufacture estimates

Many applications of energy harvesting are price critical and so it is worthwhile considering the likely cost of the devices developed. At this stage of the development these can only be estimates. The cost of producing the two prototype devices is split into the purchase price of components and an estimate of the labour cost. The costs are for the mechanism only and do not include the cost of the step or associated fittings. The component cost is for one off purchase from a distributor and an estimate has been made for the cost in volume. A volume of 10000 units has been assumed. Labour costs are more difficult to predict for volume manufacture since these depend on the precise processes used and where the manufacture is done.

Item	Unit Price (£)	Quantity	Total Price (£)	Estimated unit price for 10000 off purchase (£)
Main bearings	2.13	3	4.26	1.20
Lever bearings	2.06	1	4.12	1.20
Striker bearing	10.77	2	23.54	2.00
Spring	2.00	1	2.00	1.50
Clutch	3.51	1	3.51	2.50
Shafts	0.50	2	1.00	0.25
Flywheel	5.00	1	5.00	3.00
Generator	49.55	1	49.55	25.00
Support materials etc	15.0	-	15.00	5.00
Total			**107.98**	**41.65**
Labour cost	**£1200**			

Table 7-2 Cost estimates for flyback converter

Item	Unit Price (£)	Quantity	Total Price (£)	Estimated unit price for 10000 off purchase (£)
Cantilever	2.80	1	2.80	1.00
Striker bearing	10.77	2	23.54	2.00
Magnets	0.46	4	1.84	0.30
Coil	0.50	1	0.50	0.10
Support materials etc	10.0	-	15.00	4.00
Total			**43.68**	**7.40**
Labour cost	**£800**			

Table 7-3 Cost estimates for vibrating cantilever converter

7.3. Critical Components and lifetime estimates

Accurate calculation of the reliability of electromechanical systems is a complex and time consuming process. In addition, it requires precise knowledge of operating conditions, such as temperature, humidity and the presence of dust, which are not currently known. This section, therefore is restricted to the identification, based on engineering judgment, of those components most likely to fail in service and, for these, an estimate of the likely operating

life. The operating life is given in terms of the number of cycles and, from this, the lifetime in years is calculated assuming a rate of 1 footfall per second for 12 hours per day (15million footfalls per year). In some cases, it is possible to identify alternative components which may provide extended operating life but at the expense of performance or additional purchase cost. The advantages and disadvantages of these alternatives will be outlined.

7.4. Flyback Converter

Being the most complex of the two mechanisms, the flyback converter has the most potential failure modes. The components of the system most likely to fail in the prototype device, the estimated lifetime and the source of data upon which the lifetime estimate is based are presented in Table 7-4. Most of the components have acceptable lifetime predictions and their lifetimes may be extended without significantly affecting performance. In the case of the spring, there is a trade-off between spring volume (the large the spring volume, the longer its service life) and the efficiency of the mechanism (a larger spring retains more of the stored energy and hence less is transferred to the output). The element with the shortest predicted life is the generator. The estimate given is conservative but precise prediction is difficult because of the complex nature of the movement involved. The main failure modes in the generator are in the bearings and brushes but the lifetime of these may be extended by the use of higher specification components or a higher power rated device.

7.5. Vibrating Cantilever Converter

Being a relatively simple mechanism, there are fewer critical components. These are listed in Table 7-5. Wear in the tip of the striker mechanism and the end of the cantilever arise because of the sliding motion which occurs as the striker slides off the end of the cantilever. The wear rate may be reduced by the use of alternative materials, such as bronze or nylon, which typically wear 100 times more slowly than steel under similar conditions. Alternatively

a lubricant could be used but this might require regular maintenance. Fatigue failure in the cantilever results from repeated bending but provided the volume of material used is sufficient, the stress may be limited to less than 40% of the ultimate strength in which case the fatigue life is effectively infinite, providing factors such as corrosion are avoided.

Component Name	**Failure mode**	**Failure effect**	**Estimated operating life (Cycles)**	**Estimated operating life (years)**	**Source of estimated lifetime**	**Lifetime extension options**
Striker tip bearing	Wear	Gradual deterioration in performance	116 000 000	7.8	Manufacturers calculation [171]	Increase bearing size
Bearing 1	Fatigue	Gradual deterioration in performance or Catastrophic failure	116 000 000	7.8	Manufacturers calculation [171]	Increase bearing size
Spring	Fatigue	Catastrophic failure	~Infinite	~Infinite	Design equations/ manufacturers calculations	Assumes appropriate safety margin in spring dimensions.
Generator	Various – primarily brush wear	Gradual deterioration in performance or Catastrophic failure	18 000 000	1.2	Manufacturers data	More expensive generator with improved bearings & brushes

Table 7-4 Critical Components in Flyback Converter

Component Name	Failure mode	Failure effect	Estimated operating life (Cycles)	Estimated operating life (years)	Source of estimated lifetime	Lifetime extension options
Striker tip	wear	Gradual deterioration in performance then catastrophic failure	1 000 000	0.06	Archard law of adhesive wear [167], [168]	Use bronze tips (increase life to 6 years) or lubricants
Striker friction device	wear	Catastrophic failure	unknown	unknown		Would require more detailed analysis but design could be readily modified to extend lifetime
Cantilever tip	wear	Gradual deterioration in performance then catastrophic failure	2 000 000	0.12	Archard law of adhesive wear [167], [168]	Use bronze tips (increase life to 12 years) or lubricants
Cantilever	Fatigue	Catastrophic failure	~Infinite	~Infinite	S-N curves	Assumes appropriate safety margin in cantilever dimensions.

Table 7-5 Critical Components in Vibrating Cantilever Converter

7.6. Design calculations for pedestrian use

In this section the potential power output for pedestrian use is considered, the mass of a pedestrian and frequency of footfall are the key considerations in this application. It is therefore assumed that a deflection of 10mm is permissible in these scenarios and that an efficiency of 30% of the potential power is achievable. It will also be assumed that the energy harvesting device is only able to capture a fixed amount of energy from pedestrians above a threshold weight and cannot extract additional energy from heavier people.

It is estimated that in a busy London transport exchange 10 million people pass through these stations over a year. Therefore, to estimate the amount of electrical energy generated by the energy harvesting modules with a footfall of, for example, 30,000 persons on a daily basis, certain assumptions have to be made. In this example, it is assumed that the energy

harvesting modules are placed in the walkway at the entrance of a building where people are funnelled into a walkway in and out every day:

- every person who enters leaves through this entrance as well
- each person steps on 20 modules each on entrance and exit, 40 steps/person/day
- each module generates 2.4 Joules per step of electrical power

This would indicate that 30.000 * 40 * 2.4 = 2,880,000 Joules is generated daily. 1 Watthour = 3600 Joules per 3600 seconds, therefore 2,880,000/3600 = 800 Watthours. If for example, the application using the power generated, is operational for an average of 9 hours a day, the total power consumption of the application should not exceed 800/9 = 88.9 Watt on average.

7.7. Design calculations for Rail/road use

In this section, the potential power output for a scaled up energy harvesting device used in a road or rail application is considered. The key elements in these calculations relate to the vehicle mass and the traffic density. The characteristics of road and rail transportation may introduce additional constraints on the system (for instance the permissible deflection may be limited due to safety concerns) or may allow greater energy extraction (for instance because larger electrical machines typically possess significantly higher efficiency than small ones) These constraints and opportunities cannot be determined at this time and would require further study. It is therefore assumed that a deflection of 10mm is permissible in these scenarios and that an efficiency of 30% of the potential power is achievable. It will also be assumed that the energy harvesting device is only able to capture a fixed amount of energy

from vehicles above a threshold weight and cannot extract additional energy from heavier vehicles.

7.7.1. Rail Transport

The weight of a train carriage/power car is typically in the range 25-50T, typically distributed between 8 wheels. The average weight per wheel is thus 5T. The number of cars per train varies from 1 for local passenger transport up to 50-100 for freight. For this analysis an average of 5 cars per train will be assumed. The number of trains using a particular line is also highly dependent on the location, with as few as 2 trains per day in some locations. For Kings Cross station there are approximately 20 train movements per hour during working hours, although these are spread across several lines. If it is assumed that this traffic is carried on 4 lines then there is an average of 5 train movements per hour on each line.

Based on these assumptions, the average power may be calculated as follows:

- For a 10mm deflection caused by a 5T load, the energy per wheel is 500J
- For a train consisting of 5 cars, each with 8 wheels, the total energy per train is 20kJ
- For 5 train movements per hour the average available power is 28W
- Assuming a conversion efficiency of 30%, the average output power 8.3W

As with pedestrian systems, this estimate is based on a single energy harvesting device. If multiple units were employed then the average power would scale accordingly.

7.7.2. Road Transport

Similar assumptions to those above may be made for the case of road vehicles. A greater variety of vehicle weights is encountered in road transport compared to rail but, as noted above, the conversion devices developed will extract the same energy from a car of 1T as a

40T truck, if the threshold weight is set to 1T. In scenarios where the majority of traffic is freight (for example in certain toll plazas where traffic streams are separated), it would be appropriate to increase the threshold weight to that of an average truck. For this estimate, it will be assumed that the threshold weight is set to 1T and that this is distributed between 2 pairs of wheels. Vehicle traffic density, once again, depends on location but a single lane of congested motorway carries 15000 vehicles per day [174].

Completing the same calculations as above, the following is obtained:

- For a 10mm deflection caused by a 0.5T load, the energy per wheel pair 50J or 100J per vehicle
- For 15000 vehicle movements per day the average available power is 17W
- Assuming a conversion efficiency of 30%, the average output power 5.2W

In the case of road traffic, there appears to be more potential for increasing the permissible deflection to, say 30mm, without causing undue effects on vehicle safety/passenger comfort. Thus it may be possible to increase the average power by a factor of 3.

It may be found more publically acceptable if such energy harvesting devices are restricted to locations where vehicles are already braking in order to avoid the, justified, accusation that energy is being taken from the vehicle.

7.8. Conclusions

The price and viability of the two mechanisms for the conversion of human footfall have considered. The two mechanisms presented can be used for a range of kinetic energy applications such as pedestrian, rail and road traffic applications. Efficiencies for both

systems compare favourable to existing technologies in academic and commercial use. In terms of complexity, the cantilever mechanism scores favourably as the flyback mechanism incorporates many moving parts and friction if difficult to manage. Cost for both mechanisms is considerable due to labour costs, however, for volume production it possible to reduce these to comparatively reasonable estimates.

Pedestrian, rail and road use offer good applications the mechanisms developed. Considering the energy lost in these examples and potential for harvesting the energy to provide power for off-grid wireless sensing and monitoring systems, these mechanical systems seem to be a reasonable solution for the cost and benefits perceived.

8. Chapter 8 – Conclusions and Further Development

In this chapter the overall thesis conclusions are presented and routes for further development are discussed.

8.1. Thesis Conclusions

Wireless sensing and monitoring devices offer an attractive solution to many environmental, security and process monitoring problems but one barrier to their fuller adoption is the need to supply electrical power over extended periods of time without the need for dedicated wiring. Energy harvesting provides a potential solution to this problem in many applications. In this work the characteristics and energy requirements of typical sensor network nodes were investigated and an assessment of a range of potential ambient energy sources were carried out, along with the characterisation of a wide range of energy conversion devices.

An area of academic research and commercialisation which has seen some attention in recent times is Footfall Energy Harvesting (footfall harvesting). This is the conversion of kinetic energy in footfall to useable electrical energy. Footfall harvesting has been researched for many applications, particularly for bodyworn systems where the motion of footfall can be harvested to power electronic devices. This study investigates a closely related concept to bodyworn systems, where footfall is used to power off-body electronic devices using footfall harvesting mechanisms in spung flooring and stairwells. Some early stage commercial products have been developed in this space but very little academic literature can be found on the subject.

In this work, two mechanisms that convert the linear motion of low frequency, high amplitude pulses of energy into rotational motion and vibrational motion have been

prototyped and tested. Computer models that simulate the mechanical behaviour of the prototypes have been developed, these mechanisms have allowed the devices to be optimised and configured for the applications scenarios envisaged.

From investigations into ground reactions forces, it has been seen that the forces available when walking up and down stairs are much more than those seen for level walking. These forces can exceed 2-3 times body weight and so suggest that coupling a harvesting mechanism within a stair would see a greater amount of energy transferred to a mechanism and provide a better source of energy. It was also observed that, firstly, there is more energy obtained from climbing and descending staircases than there is available from a level floor situations and secondly that the maximum energy exerted was at the front of the staircase tread, validating the stair-tread design being pivoted at the rear, which allowed the majority of the force to be coupled into the harvesting mechanism via a striker arrangement.

One of the mechanism prototyped for testing and validation coupled the footfall energy through a spring and ratchet mechanism to a flywheel and generator configuration. In the development of this Flyback converted it was seen that the mechanism was capable of extracting significant levels of energy from normal human motion and converting this energy in an efficient manner into electrical energy. It was seen that with the mathematical model of the mechanism, it was possible to identify system parameters which optimised the output power and efficiency. Experimental results demonstrated an output energy of 450mJ with an efficiency of 24%.

The second device prototyped was the vibrating cantilever mechanism. This device also provided a means of converting footfall energy to electrical energy with good efficiency. The

short linear impulse motion characteristic of footfall energy was converted to a longer vibration motion through the use of a striker mechanism allowing efficient conversion by the bespoke coil and magnet arrangement. The behaviour of the system was similarly described by the mathematical model with a good accuracy allowing the model to be used for parameter optimisation. It was seen that by suitable choice of spring constant and scaling up of the cantilever dimensions it was possible to maximise the energy extracted from the pedestrian's footfall. However, it was observed that this had to be balanced against the need to minimise the mechanical damping of the system by selecting appropriate materials for the cantilever. The mechanism was capable of extracting good levels of energy from normal human motion and converting this energy in an efficient manner into electrical energy. Experimental results demonstrated that an output energy of 53mJ with an efficiency of 55% was possible for the cantilever vibrational generator.

Efficiencies for both systems compared favourable to existing technologies in academic and commercial use. In terms of complexity, the cantilever mechanism scored favourably as the flyback mechanism incorporates many moving parts and friction was found to be difficult to manage. However, the flyback mechanism provides a mean of more easily tuning for different input forces and is able to convert the energy efficiently. Also, it is envisaged that the costs associated with the generator used in the mechanism can be offset by attaching several striker mechanism into a single generator flywheel arrangement thereby reducing the component costs. The costs for manufacturing both mechanisms is considerable due to the cost associated with labour, however, for volume production it would be possible to reduce these costs.

Pedestrian, rail and road use offers good applications for these prototype devices. Considering the potential in capturing the energy available in footfall, and the motion of vehicles in providing power for off-grid wireless sensing and monitoring systems, these mechanical systems seem to be a reasonable solution for the cost and benefits perceived.

8.2. Further Development

In this subsection some recommendations are suggested for further development of the flyback and vibrating cantilever mechanism. Area of focus are the losses observed in the striker mechanism, a multi input striker to allow one generator to be used in the flyback generator and further development of the cantilever in terms of beam material selection and mechanical to electrical conversion in the generator design.

8.2.1. Striker Mechanism

A critical component in the the conversion of mechanical energy into the two conversion devices has been the striker mechanism. However, in each device a considerable amount of energy is lost into this part of the conversion process. It is recommended that losses of the overall system can be reduced by improving the design of the striker mechanism to reduce the friction in the linear motion by use of better bearing or lubrication. Furthermore, it is suggested to analyse the pivot arm connected to the spring and reduce the frictional losses in this element.

8.2.2. Multi input concept device for Flyback

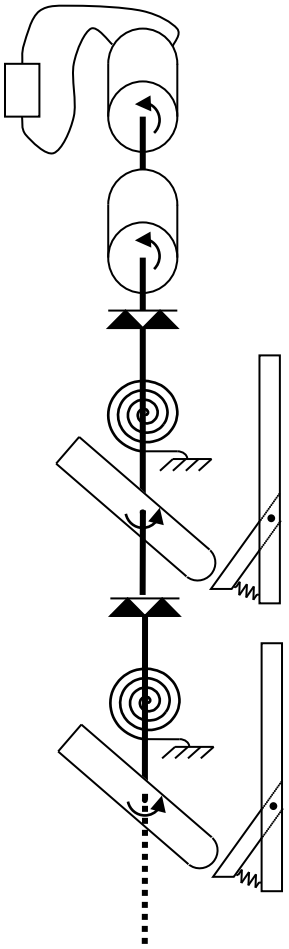

Figure 8-1 Multi input under-floor energy harvester

A multi input prototype based on the current device would also be beneficial. This would reduce component cost of the flyback system and make it a more attractive solution for volume production. An illustrated of the proposed mechanism is presented Figure 8-1 above. For this upgrade each stair on a flight of stairs could have a striker attached to it allowing energy to be extracted from multiple stairs.

8.2.3. Vibrating Cantilever material tests

As noted in chapter 6, the mechanical damping of the cantilever limits the efficiency of the mechanism. It would be beneficial to test for other suitable materials that could be used for the cantilever. At present only spring steel has been tested in experimentation. Some materials may perform better in terms of fatigue and durability and so a survey of suitable materials for the cantilever would be beneficial. The conversion of mechanical energy to electrical energy has been seen to be quite efficient, however when scaling the device to accept higher input forces or equally to accept lower forces it would be beneficial to study the latest generator design literature to optimise the mechanical to electrical conversion components of the system.

9. References

[1] U. Hansmann, L. Merk, M. S. Nicklous and T. Stober. Pervasive Computing: The mobile world. Springer, 2003.

[2] E. H. Callaway, Jr. Wireless Sensor Networks: Architectures and Protocols. CRC Press, 2003.

[3] ://www.elizabethredmond.net/images/images/project_description.html, Accessed September 2008.

[4] Power generating dance floor hit UK Club, http://www.engadget.com/tag/piezoelectric, Accessed September 2008.

[5] Club Surya London, http://www.club4climate.com/news/dr-earth-launches-his-manifesto-for-planet-earth/, Accessed September 2008.

[6] http://www.sustainabledanceclub.com/, Accessed September 2008.

[7] Jain, R. and Wullert, J. (2002). Challenges: environmental design for pervasive computing systems. In Proc. of the 8th Annual international Conference on Mobile Computing and Networking. ACM Press, New York, NY. 263-270.

[8] Stojmenovic. Handbook of Sensor Networks: Algorithms and Architectures. Wiley, 2005.

[9] Kay Romer and Friedemann Mattern. The design space of wireless sensor networks. IEEE Wireless Communications Magazine, 11(6):54-61,2004.

[10] K. Martinez, R. Ong, J. K. Hart, and J. Stefanov. GLACSWEB: A Sensor Web for Glaciers. In *Adjunct Proc. EWSN2004*, Berlin, Germany, January 2004.

[11] I. W. Marshall, C. Roadknight, I. Wokoma, and L. Sacks. Self-Organizing Sensor Networks. In *UbiNet 2003*, London, UK, September 2003.

[12] Roemmich, D., S. Riser, R. Davis and Y. Desaubies. 2004. Autonomous profiling floats; workhorse for broadscale ocean observations. Mar Tech SocJ.38(2).

[13] R. Beckwith, D. Teibel, and P. Bowen. Pervasive Computing and Proactive Agriculture. In *Adjunct Proc. PERVASIVE 2004*, Vienna, Austria, April 2004.

[14] A. Mainwaring, J. Polastre, R. Szewczyk, D. Culler, and J. Anderson. Wireless Sensor Networks for Habitat Monitoring. In *WSNA*, Atlanta, USA, September 2002.

[15] P. Juang, H. Oki, Y. Wang, M. Martonosi, L. S. Peh, and D. Rubenstein. Energy-Efficient Computing for Wildlife Tracking: Design Tradeoffs and Early Experiences with ZebraNet. In *Proc. ASPLOS X*, San Jose, USA, October 2002.

[16] Z. Butler, P. Corke, R. Peterson, and D. Rus. Networked Cows: Virtual Fences for Controlling Cows. In *WAMES 2004*, Boston, USA, June 2004.

[17] F. Michahelles, P. Matter, A. Schmidt, and B. Schiele. Applying Wearable Sensors to Avalanche Rescue. *Computers and Graphics*, 27(6):839–847, 2003.

[18] The 29 Palms Experiment: Tracking vehicles with a UAV-delivered sensor network. http://robotics.eecs.berkeley.edu/~pister/29Palms0103/ accessed April 2008

[19] W. M. Meriall, F. Newberg, K. Sohrabi, W. Kaiser, and G. Pottie. Collaborative Networking Requirements for Unattended Ground Sensor Systems. In *Proc. IEEE Aerospace Conference*, March 2003.

[20] G. Simon, A. Ledezczi, and M. Maroti. Sensor Network Based Countersniper System. In *Proc. SenSys*, Baltimore, USA, November 2004.

[21] S-H. Yang & P. Frederick, SafetyNET - A wireless sensor network for fire protection and emergency responses, *Measurement and Control*, Vol 39, Iss 7, 218-219, 2006

[22] N. Noury, T. Herve, V. Rialle, G. Virone, E. Mercier, G. Morey, A. Moro, T. Porcheron, Monitoring behavior in home using a smart fall sensor, IEEE-EMBS Special

Topic Conference on Microtechnologies in Medicine and Biology, October 2000, pp. 607–610.
[23] Rangarajan, S., Kidane, A., Qian, G., Rajko, S. And Birchfield, D. 2007. The design of a pressure sensing floor for movement-based human computer interaction. *Proceedings of the 2nd European conference on Smart sensing and context*.
[24] Infineon Technology: Walk this way for the smart floor. IEE Electronics systems and software, June/July 2003.
[25] B.G. Celler et al., An instrumentation system for the remote monitoring of changes in functional health status of the elderly, International Conference IEEE-EMBS, New York, 1994, pp. 908–909.
[26] G.Z.Yang (Ed.), Body Sensor Networks, Springer-Verlag, March 2006.
[27] N. F. Timmons and W. G. Scanlon. Analysis of the performance of IEEE 802.15.4 for medical sensor body area networking. *Proc. Annual IEEE Communications Society Conference on Sensor and Ad Hoc Communications and Networks*, October 2004.
[28] C. Kappler and G. Riegel. A Real-World, Simple Wireless Sensor Network for Monitoring Electrical Energy Consumption. In *Proc. EWSN 2004*, Berlin, Germany, January 2004.
[29] L. Benini, E. Farella and C. Guiducci, Wireless sensor networks: Enabling technology for ambient intelligence, *Microelectronics Journal*, 37(12):1639-1649, December 2006.
[30] N. Correal & N. Patwari, Wireless Sensor Networks: Challenges and Opportunities, *Proc. MPRG/Virgina Tech Wireless Symposium*, 2001
[31] P. Baronti, P. Pillai, V. Chook, S. Chessa, A. Gotta, and Y. F. Hu, Wireless sensor networks: a survey on the state of the art and the 802.15.4 and zigbee standards, *Computer Communications*, 30:1655-1695, 2007.
[32] http://www.z-wavealliance.org/modules/start/ accessed 23 April 2008
[33] http://www.enocean.com/en/home/ accessed 23 April 2008
[34] S. C. Ergen, *ZigBee/IEEE 802.15.4 Summary*, http://www.eecs.berkeley.edu/ csinem/academic/publications/zigbee.pdf. accessed March 2008
[35] http://www.xbow.com/Products/productdetails.aspx?sid=164, accessed May 2008
[36] http://www.xbow.com/Products/productdetails.aspx?sid=253, accessed May 2008
[37] http://www.jennic.com/products/index.php?productID=0000000002, accessed May 2008
[38] S. Roundy, Energy scavenging for wireless sensor nodes with a focus on vibration to electricity conversion. *PhD Thesis*, University of California, 2003.
[39] S. Roundy, D. Steingart, L. Frechette, P. Wright & J. Rabaey, Power Sources for Wireless Sensor Networks, *Wireless Sensor Networks*, Springer, Volume 2920/2004, pp 1-17, 2004.
[40] I. Stojmenovic (Ed). Handbook of Sensor Networks: Algorithms and Architectures; S. Roundy and L. Frechette. Energy Scavenging and Nontraditional Power Sources for Wireless Sensor Networks. John Wiley and Sons, 2005.
[41] P. Glynne-Jones, N.M. White, Self-powered systems, a review of energy sources, Sens. Rev. 21 (2) (2000) 91–97.
[42] [L. Mateu & F. Moll, Review of Energy Harvesting Techniques and Applications for Microelectronics, *VLSI Circuits and Systems II. Ed. J.F. Lopez, F.V. Fernandez, J.M. Lopez-Villegas, J.M. de la Rosa, Proc SPIE*, Vol. 5837, pp. 359-373, 2005
[43] A. Jenson, S. Fridstedt, and A. Weernick, A batteryless remote control for Volvo, results of a feasibility study. ISATA 2000 conference on Automotive and transportation technology 25-29 September 2000.
[44] T. von Büren, Body-Worn Inertial Electromagnetic Micro-Generators, *Dissertation ETH 16466, Swiss Federal Institute of Technology, Zurich,* 2006

[45] B. Linden and T.B. Reddy. Handbook of Batteries. New York: McGraw-Hill, 2002.
[46] P.H. Cope and Y. Podrazhansky, The art of battery charging, IEEE *Fourteenth Annual Battery Conference on Applications and Advances*, January 12-15, 1999, pp. 233-235.
[47] J.L. Gonzalez, A. Rubio & F. Moll, Human Powered Piezoelectric Batteries to Supply Power to Wearable Electronic Devices, Int. J. Soc. of Materials Engineering for Resources, Vol. 10, No.1, pp. 34-40, 2002
[48] T.E. Starner, Powerful change part 1: batteries and possible alternatives for the mobile market, *IEEE Pervasive Computing*, Vol. 2, Iss. 4, pp. 86 – 88, 2003
[49] J. Lopez, M. Gonzalez, J.C. Viera and C.Blanco. Fast-charge in lithium-ion batteries for portable applications. *Annual International Telecommunications Energy Conference. 2004*, pp 19-24.
[50] J.B Bates, N.J. Dudney, B. Neudecker, A. Ueda and C.D. Evans. Thin-film lithium-ion batteries. *Solid State Ionics*, 135: 33-45.
[51] http://www.infinatepowersolutions.com/, accessed May 2008.
[52] J. F. Randall. On the ambient energy sources for powering indoor electronic devices. *PhD Thesis*, Ecole Polytechnique Federale de Lausanne, Switzerland, May 2003.
[53] T. Starner, Human powered wearable computing, *IBM Systems Journal*, V.35, 3&4, 1996, pp. 618-629.
[54] D. Morton, Human Locomotion and Body Form, The Williams and Wilkins Co., Baltimore, 1952.
[55] T. Starner & J.A. Paradiso, Human-Generated Power for Mobile Electronics, *Low-Power Electronics Design, Ed. C. Piguet*, CRC Press, ch. 45, pp. 1–35, 2004
[56] M. Stordeur & I. Stark, Low power thermoelectric generator - self-sufficient energy supply for micro systems, *Proc Int. Conf. Thermoelectrics XVI*, pp 575 - 577, 1997.
[57] http://www.poweredbythermolife.com/ accessed 17 April 2008.
[58] Y. Yumita & H. Kumagai, Hydraulic Power Generating Device, US patent 7005758 B2, Feb 2006.
[59] A.S. Holmes, G. Hong, K. R. Pullen & K. R. Buffard, Axial-Flow Microturbine with Electromagnetic Generator: Design, CFD Simulation, and Prototype Demonstration, *Proc. 17th IEEE Int'l Micro Electro Mechanical Systems Conf. (MEMS 04)*, 2004, pp. 568–571
[60] C. Federspiel and J. Chen, Air-Powered Sensor, available at http://repositories.cdlib.org/cedr/cbe/cit/Federspiel2003_AirPoweredSensor.
[61] L. Mateu & F. Moll, Review of Energy Harvesting Techniques and Applications for Microelectronics, *VLSI Circuits and Systems II. Ed. J.F. Lopez, F.V. Fernandez, J.M. Lopez-Villegas, J.M. de la Rosa, Proc SPIE*, Vol. 5837, pp. 359-373, 2005.
[62] C.B. Carroll. 5,814,921: Frequency multiplying piezoelectric generator. US Patent, September 1998.
[63] M. Toda. Shoe generator: Power generation mechanism. Technical report, AMP Sensors, 1997.
[64] J.C. Kendall. Parasitic power collection in shoe mounted devices. *Bachelor's Thesis*. MIT Physics Department, 1998.
[65] J. Kymissis, C. Kendall, J. Paradiso & N. Gershenfeld, Parasitic Power Harvesting in Shoes, *IEEE Int. Conf. on Wearable Computing*, pp. 132-139, October 1998.
[66] N.S. Shenck. A demonstration of useful electric energy generation from piezoceramics in a shoe. *Master's thesis*, MIT EECS Department, Cambridge, MA, May 1999.
[67] N.S. Shenck and J.A. Paradiso. Energy scavenging with shoe-mounted piezoelectrics. IEEE Micro, 21(3):30-42, May 2001.

[68] J.F. Antaki, G.E. Bertocci, E.C. Green, A. Nadeem, T. Rintoul, R.L. Kormos & B.P. Griffith, A gait-powered autologous battery charging system for artificial organs, *J. American Society for Artificial Internal Organs*, Vol. 41, No. 3 M588-M595, 1995.
[69] N.W. Hagood et al, Development of Micro-Hydraulic Transducer Technology, *Int. Conf. on Adaptive Structures and Technologies*, Paris, France, pp. 71–81, 1999.
[70] S. Meninger, J. Mur-Miranda, J. Lang, A. Chandrakasan, A. Slocum, M. Schmidt & R. Amirtharajah, Vibration to electric energy conversion, *IEEE Trans VLSI Systems*. Vol. 9 No. 1, pp. 64–76, 2001.
[71] M. El-hami, P. G. Jones, E. James, S. P. Beeby, N. M. White, A. D. Brown, & M. Hill, Design and fabrication of a new vibration based electromechanical generator, *Sensors and Actuators A*, Vol. 92 . pp. 335-342, 2001
[72] N.G. Stephen, energy harvesting from ambient vibration. *Journal of Sound and Vibration*, , (-2), -425,
[73] S. Beeby, M. Tudor and N. White, Review paper: Energy harvesting vibration sources for microsystems applications, *Measurement Science and Technology*, Vol. 17, No. 12, Dec. 2006, pp. R175-R195.
[74] J. J. Sparks. Semiconductor devices, second edition. Chapman and Hall, 1994.
[75] http://www.hughesresearch.co.uk/index.htm accessed May 20th 2008
[76] P. Sanchez. 6,494,144 B1: Energy transfer assembly. US Patent, December 2002.
[77] M. B. Gott et al. 6,858,952 B2: Power conversion system. US Patent, February 2005.
[78] R. L. Lundgren. 4,250,395: Device for generating electricity by pedestrian and vehicular traffic. US Patent, February 1981.
[79] F. F. Ghassemi. 7,067,932 B1: System for generating electricity by using gravitational mass and/or momentum of moving vehicle. US Patent June 2006.
[80] M. Trew & T. Everett, Human Movement, Churchill Livingstone, 2001.
[81] McDowell MA, Fryar CD, Hirsch R, Ogden CL. Anthropometric reference data for children and adults: U.S. population, 1999–2002. Advance data from vital and health statistics; no 361. Hyattsville, MD: National Center for Health Statistics. 2005. Available at http://www.cdc.gov/nchs/data/ad/ad361.pdf, accessed 23 September 2008
[82] J. Barbieri. 1,506,282: Electric shoe. US Patent, August 1924.
[83] N. Lakic. 4,674,199: Shoe with internal foot warmer. US Patent, June 1987
[84] N. Lakic. 4,845,338: Inflatable boot liner with electrical generator and heater. US Patent, July 1989
[85] S-H Chen. 5,495,682: Dynamic shoes. US Patent, March 1996.
[86] J.C. Kendall. Parasitic power collection in shoe mounted devices. *Bachelor's Thesis*. MIT Physics Department, 1998.
[87] J. Hayashida. Unobtrusive integration of magnetic generator system into common footwear. *Bachelor's Thesis*, MIT Department of Mechanical Engineering, 2000.
[88] J.M. Gilbert, R.S. Oldaker, J.E. Grindley, P.M.Taylor, Control of a novel switched mode variable ratio drive, *Int. Conf. UKACC 96*, Vol. 1, pp. 412 – 417, 1996.
[89] J. M. Donelan, Q. Li, V. Naing, J. A. Weber, A. D. Weber, A. D. Kuo. Biomechanical energy harvesting: Generating electricity during walking with minimal user effort. Science Vol. 319. no. 5864, pp. 807 – 810, Feb 2008.
[90] L. C. Rome, L. Flynn, E. M Goldman, T. D. Yoo. Generating Electricity while walking with loads. Science Vol 309. no. 1725-8, 2005.
[91] Y. Takefuji, Known and unknown phenomena of nonlinear behaviors in the power harvesting mat and the transverse wave speaker, Proc. of international symposium on nonlinear theory and its applications, sept. 7-10, 2008. Available at http://www.neuro.sfc.keio.ac.jp/publications/pdf/nolta.pdf, accessed September 2008.

[92] Y. Takefuji, And if public transport does not consume more of energy?, Le Rail, pp31-33, April 2008(commercial). Available at http://www.neuro.sfc.keio.ac.jp/publications/pdf/rail.pdf, accessed September 2008.
[93] T. Starner, J. A. Paradiso. Human-generated Power for Mobile Electronics. Low-Power Electronics Design, C. Piguet (ed.), CRC Press, Chapter 45, pp. 1-35, 2004.
[94] J. F. Antaki, G. E. Bertocci, E. C. Green, A. Nadeem, T. Rintoul, R. L. Kormos, B. P. Gri±th. A Gait-powered Autologous Battery Charging System for Arti¯cial Organs. Journal of American Society for Artificial Internal Organs, vol. 41, no. 3, pp. 588-595, 1995.
[95] N. W. Hagood IV, D. C. Roberts, L. Saggere, M. A. Schmidt, M. Spearing, K. S. Breuer, R. Mlcak, J. A. Carrerero, et al. Development of Micro-hydraulic Transducer Technology. In Proceedings of the 10th International Conference on Adaptive Structures and Technologies, Paris, France, pp. 71-81, 1999.
[96] http://www.dtic.mil/cgibin/GetTRDoc?AD=ADA414020&Location=U2&doc=GetTRDoc.pdf accessed 20 September 2008
[97] R. Pelrine, R.D. Kornbluh, J. Eckerle, P. Jeuck, S. Oh, Q. Pei, & S. Stanford, Dielectric elastomers: generator mode fundamentals and applications, Proc. SPIE Vol. 4329 Smart Structures and Materials 2001: Electroactive Polymer Actuators and Devices, Ed. Yoseph Bar-Cohen, 2001, pp. 148-156
[98] US Pat. 6812624 - Filed Jul 20, 2000 - SRI International
[99] R. McLeish and J. Marsh. *Human Locomotor Engineering*, chapter Hydraulic Power from the Heel, pages 126–132. Inst. of Mechanical Engineers Press, London, 1971.
[100] J. Marsden and S. Montgomery. *Human Locomotor Engineering*, chapter Plantar Power for Arm Prosthesis Using BodyWeight Transfer, pages 277–282. Inst. of Mechanical Engineers Press, London, 1971.
[101] N. Landry, 6201314 B1: Shoe-sole with liquid powered electrical generator. US Patent, March 2001
[102] R. Komarechka, 623501 B1: Footwear with hydroelectric generator assembley. US Patent, May 2001
[103] R. L. Lundgren, 4250395: Device for generating electricity by pedestrian and vehicular traffic. US Patent, Febuary 1981
[104] F. F. Ghassemi, 7067932 B1: Systems for generating electricity by using gravitational mass and/or momentum of moving vehicle. US Patent, June 2006
[105] A.M. Perez Sanchez, 6494144 B1: Energy transfer assembly. US Patent, December 2002
[106] Highway Energy Systems LTD. http://www.hughesresearch.co.uk/, Accesssed September 2008
[107] N.S. Shenck & J.A. Paradiso, Energy Scavenging with Shoe-Mounted Piezoelectrics, *IEEE Micro*, Vol 21, No 3, pp30-42, 2001
[108] J. M. Gilbert & F. Balouchi Comparison of Energy Harvesting Systems for Wireless Sensor Networks, International Journal of Automation and Computing, Vol 5, No 4, pp334-347, 2008.
[109] MIT duo sees people-powered “Crowd Farm”. Available at http://web.mit.edu/newsoffice/2007/crowdfarm-0725.html. Accessed on 30th September 2008
[110] L. Mateu & F. Moll, Review of Energy Harvesting Techniques and Applications for Microelectronics, *VLSI Circuits and Systems II. Ed. J.F. Lopez, F.V. Fernandez, J.M. Lopez-Villegas, J.M. de la Rosa, Proc SPIE*, Vol. 5837, pp. 359-373, 2005
[111] T. Starner Human-Powered Wearable Computing, *IBM Systems Journal*, Vol. 35, No. 3/4, pp. 618-629, 1996

[112] S. Beeby, M. Tudor and N. White, Review paper: Energy harvesting vibration sources for microsystems applications, *Measurement Science and Technology*, Vol. 17, No. 12, Dec. 2006, pp. R175-R195.
[113] C.D. Richards M.J. Anderson, D.F. Bahr & R.F. Richards, Efficiency of energy conversion for devices containing a piezoelectric component, *J. Micromech. Microeng.* Vol. **14** pp. 717-721, 2004
[114] P. Glynne-Jones, S. P. Beeby & N. M. White, Towards a piezoelectric vibration-powered microgenerator, *IEE Science Measurement and Technology*, Vol. 148, No 2, pp. 68-72, 2001
[115] S.J. Roundy, P. K. Wright & J. Rabaey, A Study of Low Level Vibrations as a Power Source for Wireless Sensor Nodes, *Computer Communications*, Vol. 26, No. 11, pp. 1131 – 1144, 2003
[116] S.J. Roundy & P. K. Wright A piezoelectric vibration based generator for wireless electronics, *Smart Mater. Struct.* Vol. **13** pp. 1131-1142, 2004
[117] H.A. Sodano, E.A. Magluila, D.J. Inman & G. Park Sodano, Electric Power Generation Using Piezoelectric materials, *Proc Int. Conf. on Adaptive Structures and Technologies*, pp 153-161, 2002
[118] H.A. Sodano, D.J. Inman & G. Park, A Review of Power Harvesting from Vibration Using Piezoelectric Materials, *The Shock and Vibration Digest*; Vol. 36 pp. 197-205 2004
[119] S.J. Roundy et al, Improving Power Output for Vibration-Based Energy Scavengers, IEEE Pervasive Computing Vol 4 , Iss. 1, pp. 28 – 36, 2005
[120] J. Baker, S. Roundy and P.K. Wright, Improvements in Vibration Energy Scavenging for Wireless Sensor Networks, *Int. Energy Conversion Engineering Conf.*, San Francisco, 2005
[121] T. H. Ng & W. H. Liao, Sensitivity Analysis and Energy Harvesting for a Self-Powered Piezoelectric Sensor, *J. Intelligent Material Systems and Structures*, Vol. 16, No. 10, pp. 785-797, 2005
[122] K. Mossi, C. Green, Z. Ounaies & E. Hughes, Harvesting Energy Using a Thin Unimorph Prestressed Bender: Geometrical Effects, *J. of Intelligent Material Systems and Structures*, Vol. 16, No. 3, pp. 249-261, 2005
[123] A. D. Danak, H.S. Yoon & G.N. Washington, Optimization of Electrical Output in Response to Mechanical Input Piezoelectric Laminated Shells, *ASME International Mechanical Engineering Congress*, 2003, Paper #43185
[124] H.S. Yoon, G.N. Washington & A. Danak, Modeling and Design of Efficient Initially-Curved Piezoceramic Unimorphs for Energy Harvesting Applications, *J of Intelligent Material Systems and Structures*, Vol.16, pp: 877-888, 2005
[125] S.R. Anton & H.A. Sodano, A review of power harvesting using piezoelectric materials (2003–2006), *Smart Mater. Struct.* **16** R1-R21, 2007
[126] P. J. Cornwell, J. Goethal, J. Kowko, & M. Damianakis, Enhancing Power Harvesting using a Tuned Auxiliary Structure, *Journal of Intelligent Material Systems and Structures*, Vol. 16: pp. 825 – 834, 2005.
[127] S.J. Roundy & Y. Zhang, Toward self-tuning adaptive vibration-based microgenerators**,** *Smart Structures, Devices, and Systems II. Ed. S.F. Al-Sarawi, Proc. SPIE*, Vol. 5649, pp. 373-384, 2005
[128] W.J. Wu, Y.Y. Chen, B.S. Lee, J.J. He, & Y.T. Peng, Tunable resonant frequency power harvesting devices, *Smart Structures and Materials 2006: Damping and Isolation. Ed. W.W. Clark, M. Ahmadian & A. Lumsdaine, Proc. SPIE*, Vol. 6169, pp. 55-62 2006

[129] S.M. Shahruz, Design of mechanical band-pass filters for energy scavenging, *J. of Sound and Vibration*, Vol. 292, Iss. 3-5, pp. 987-998, 2006
[130] S.M. Shahruz, Limits of performance of mechanical band-pass filters used in energy scavenging, J. of Sound and Vibration**,** Vol. 293, Iss. 1-2, pp. 449-461, 2006
[131] J. Rastegar, C. Pereira & H.L Nguyen, Piezoelectric-based power sources for harvesting energy from platforms with low-frequency vibration, *Smart Structures and Materials 2006: Industrial and Commercial Applications of Smart Structures Technologies. Ed. E.V. White, Proc. SPIE*, Vol. 6171, pp. 1-7, 2006
[132] M. El-hami, P. G. Jones, E. James, S. P. Beeby, N. M. White, A. D. Brown, & M. Hill, Design and fabrication of a new vibration based electromechanical generator, *Sensors and Actuators A*, Vol. 92 . pp. 335-342, 2001
[133] N.G. Stephen, On energy harvesting from ambient vibration. *Journal of Sound and Vibration*, 293, (1-2), 409-425, 2006
[134] C.B. Williams, C. Shearwood, M.A. Harradine, P.H. Mellor, T.S. Birch & R.B. Yates, Development of an electromagnetic micro-generator, *IEE Proc. - Circuits, Devices and Systems*, Vol. 148, No. 6, pp. 337-342, 2001
[135] C. Shearwood & R.B. Yates, Development of an electromagnetic microgenerator, *Electronics Letters*, Vol 33, Issue 22, pp.1883 – 1884, Oct 1997
[136] H. Kulah and K. Najafi, An Electromagnetic Micro Power Generator for Low-Frequency Environmental Vibrations, *IEEE Conf. on Micro Electro Mechanical Systems - MEMS 2004, Maastricht, Netherlands*, pp. 237 – 240, 2004.
[137] P. Glynne-Jones, M.J. Tudor, S.P. Beeby, N.M. White, An electromagnetic, vibration-powered generator for intelligent sensor systems, *Sensors and Actuators A*, Vol. 110 No. 1, p.344-349, 2004
[138] http://www.perpetuum.co.uk/ accessed March 2008
[139] Beeby, S. P., Torah, R. N., Tudor, M. J., Glynne-Jones, P., O'Donnell, T., Saha, C. R. and Roy, S. A micro electromagnetic generator for vibration energy harvesting. *Journal of Micromechanics and Microengineering*, 17 (7). pp. 1257-1265, 2007
[140] S.J. Roundy, Energy Scavenging for Wireless Sensor Nodes with a Focus on Vibration to Electricity Conversion, PhD Thesis, University of California, Berkeley, 2003.
[141] S. Meninger, J. Mur-Miranda, J. Lang, A. Chandrakasan, A. Slocum, M. Schmidt & R. Amirtharajah, Vibration to electric energy conversion, *IEEE Trans VLSI Systems*. Vol. 9 No. 1, pp. 64–76, 2001
[142] W. Ma, M. Wong & L. Ruber, Dynamic simulation of an implemented electrostatic power micro-generator, *Proc. Design, Test, Integration and Packaging of MEMS/MOEMS*, pp 380–5, 2005
[143] G. Despesse et al, Fabrication and characterisation of high damping electrostatic micro devices for vibration energy scavenging, *Proc. Design, Test, Integration and Packaging of MEMS/MOEMS*, pp 386–90, 2005
[144] R. Tashiro, N. Kabei, K. Katayama, F. Tsuboi & K. Tsuchiya Development of an electrostatic generator for a cardiac pacemaker that harnesses the ventricular wall motion, *J. Artif. Organs* Vol. 5, No. 4, pp. 239–45, 2002
[145] T. Starner & J.A. Paradiso, Human-Generated Power for Mobile Electronics, *Low-Power Electronics Design, Ed. C. Piguet*, CRC Press, ch. 45, pp. 1–35, 2004
[146] J.F. Antaki, G.E. Bertocci, E.C. Green, A. Nadeem, T. Rintoul, R.L. Kormos & B.P. Griffith, A gait-powered autologous battery charging system for artificial organs, *J. American Society for Artificial Internal Organs*, Vol. 41, No. 3 M588-M595, 1995
[147] N.W. Hagood et al, Development of Micro-Hydraulic Transducer Technology, *Int. Conf. on Adaptive Structures and Technologies*, Paris, France, pp. 71–81, 1999

[148] J. Kymissis, C. Kendall, J. Paradiso & N. Gershenfeld, Parasitic Power Harvesting in Shoes, *IEEE Int. Conf. on Wearable Computing*, pp. 132-139, October 1998
[149] http://handle.dtic.mil/100.2/ADA414020 accessed 2 April 2008
[150] R. Pelrine, R.D. Kornbluh, J. Eckerle, P. Jeuck, S. Oh, Q. Pei, & S. Stanford, Dielectric elastomers: generator mode fundamentals and applications, *Proc. SPIE Vol. 4329 Smart Structures and Materials 2001: Electroactive Polymer Actuators and Devices, Ed. Yoseph Bar-Cohen*, 2001, pp. 148-156
[151] F.M. Discenzo, D. Chung, K.A. Loparo, Power scavenging enables maintenance-free wireless sensor nodes, *Int. Conf. on Complex Systems (ICCS)*, Boston, 2006
[152] S. Roundy, D. Steingart, L. Frechette, P. Wright & J. Rabaey, Power Sources for Wireless Sensor Networks, *Wireless Sensor Networks*, Springer, Volume 2920/2004, pp 1-17, 2004
[153] P.D. Mitcheson, E.K. Reilly, P.K. Wright & E.H. Yeatman, Transduction Mechanisms and Power Density for MEMS Inertial Energy Scavengers, *Proc. Power MEMS 06*, pp: 275 - 278, 2006
[154] N.S. Shenck & J.A. Paradiso, Energy Scavenging with Shoe-Mounted Piezoelectrics, IEEE Micro, Vol 21, No 3, pp30-42, 2001
[155] M. Marzencki, S. Basrour, B. Charlot, A. Grasso, M. Colin, L. Valbin, Design and Fabrication of Piezoelectric Micro Power Generators for Autonomous Microsystems, *Design, Test, Integration and Packaging of MEMS/MOEMS*, Montreux, Switzerland, June 01-03, pp 299-302, 2005
[156] P.D. Mitcheson, P. Miao, B.H. Stark, A.S. Holmes, E.M. Yeatman, T.C. Green, Analysis and Optimisation of MEMS Electrostatic On-Chip Power Supply for Self-Powering of Slow-Moving Sensors. *Eurosensors XVII*, Portugal, 21-24 Sept, pp 48-51, 2003
[157] E M Yeatman, Energy harvesting from motion using rotating and gyroscopic proof masses, Proc. IMechE Vol. 222 Part C: J. Mechanical Engineering Science, Vol 222, pp 27-36, 2007.
[158] R. McLeish and J. Marsh. *Human Locomotor Engineering*, chapter Hydraulic Power from the Heel, pages 126–132. Inst. of Mechanical Engineers Press, London, 1971.
[159] N. Landry, 6201314 B1: Shoe-sole with liquid powered electrical generator. US Patent, March 2001.
[160] R. Komarechka, 623501 B1: Footwear with hydroelectric generator assembley. US Patent, May 2001.
[161] I. W. Griffiths, Principle of Biomechanics and Motion Analysis, Lippincott Williams & Wilkins, 2006.
[162] M. Trew & T. Everett, Human Movement, Churchill Livingston, 2001.
[163] McDowell MA, Fryar CD, Hirsch R, Ogden CL. Anthropometric reference data for children and adults: U.S. population, 1999–2002. Advance data from vital and health statistics; no 361. Hyattsville, MD: National Center for Health Statistics. 2005. Available at http://www.cdc.gov/nchs/data/ad/ad361.pdf, accessed 23 September 2008.
[164] Motor/generator manufacturer data sheet: http://www.dracon-eltron.com/EN/mechatronics/ironless_core_brushed_dc_motors/datasheets/28L28.pdf accessed on 13 July 2009.
[165] Specification for sustainable energy floor systems: http://issuu.com/sustainabledanceclub/docs/sustainable_energy_floor_specifications/8 accessed on 08 September 2012.
[166] http://www.imechanica.org/node/2226
[167] http://personal.stevens.edu/~ffisher/nanolab/Challa-Fisher-IWSHM07.pdf - interesting looking paper – may have useful references

[168] Principles of Tribology, J Halling, Macmillan Education Ltd, 1978
[169] Materials Selection in Mechanical Design, MJ Ashby, Pergamon Press, 1992
[170] M. Trew & T. Everett, Human Movement, Churchill Livingstone, 2001.
[171] Motor/generator manufacturer data sheet: http://www.dracon-eltron.com/EN/mechatronics/ironless_core_brushed_dc_motors/datasheets/28L28.pdf accessed on 13 July 2009.
[172] http://www.skf.com/files/151316.pdf
[173] E.O. Doebelin, 'Measurement Systems, Design and Applications, Ed', |Mc Graw Hill, 1983
[174] B.S. Massey, 'Mechanics of fluids Ed' Van Nostrand Reinhold, 1989.
[175] Traffic indices for the use of the Belgian motorway network, http://www.tmleuven.be/project/verkeersindices/200301_paper.pdf
[176] http://www.innowattech.co.il/
[177] http://www.newenergytechnologiesinc.com/#top
[178] http://www.guardian.co.uk/environment/2009/jun/15/sainsburys-kinetic-plates-speed-bumps
[179] http://www.inhabitat.com/2008/12/10/energy-generating-revolving-door-by-boon-edam/
1

[1] Ref [166] – [179] accessed on 09/12

10. Appendix A - Device concepts generation

This section summarises the concepts generated during a series of brainstorming sessions and a review of available technologies. A number of concepts were generated but discarded at an early stage as not being appropriate for this application and so those presented here are those which are more suitable. There are a number of variants on several of the concept, not all of which are described in detail here. The major perceived advantages and disadvantages of each concept are listed against each concept. These assessments are based on information available in the scientific literature and engineering judgement. In some cases, experimental work has been conducted to make an initial assessment of the concepts[2].

10.1. Piezo electric material based systems

Concept 1. Direct compression of piezo material

Here an appropriate piece of piezo material would be placed under the floor/step and would generate a voltage when walked over. Given the displacements expected, it would be likely that PZT materials would be damaged but that PVDF would be more appropriate. This does however imply a lower efficiency. Comparing to the shoe inserts described in [148] it is anticipated that the output power for such a device would be relatively low.

[2] The following concept generation and brainstorming was carried out with the author's supervisor. Sketches were made by the author's supervisor.

Advantages

- Simple construction
- Low space requirement
- Easy to scale up
- Reliable
- No know IP issues

Disadvantages

- Low efficiency
- High cost

Concept 2. Direct bending of a cantilever of piezo material

There are a number of variants on this basic concept including use of a cantilever arrangement of the form shown in Figure 10-1 where the applied force is converted into bending of the cantilever. This reduces the strain on the piezo material and makes it possible to use more efficient, lower cost PZT material. A variation of this concept uses a prestressed bimorph but the anticipated level of output power, although greater than for Concept 1, remains low [148]. Similar limitations apply to the piezo speaker based device described in [91].

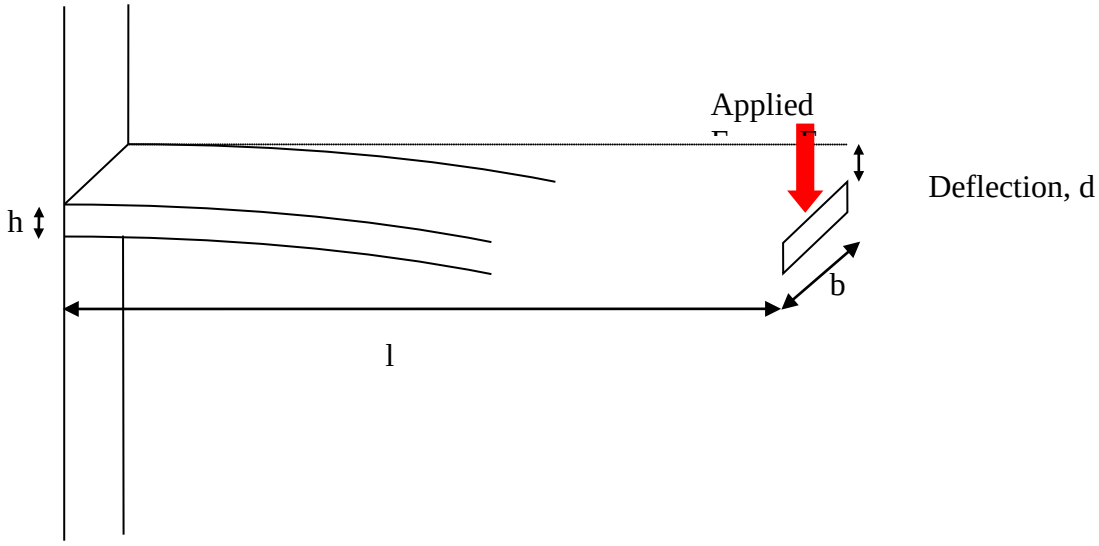

Figure 10-1 Cantilever beam

Advantages

- Simple construction
- Moderate space requirement
- Reliable
- No know IP issues

Disadvantages

- Low efficiency
- Moderate cost

Concept 3. Conversion to vibration of piezo cantilever

Piezo materials generally provide greatest efficiency when used in vibration mode, typically in a cantilever arrangement of the form shown in Figure 10-1. The challenge in this device is to convert the linear translation of the floor/step to vibration in an efficient manner. A rotational device has been proposed by Yeatman [157] but this appears complex. A simple striker mechanism has previously been proposed by the author as illustrated in the sketch of Figure 10-2. As the step moves up and down in response to pedestrian travel, the striker tip follows the trajectory shown. On the downstroke, it 'flicks' the end of the cantilever, initiating vibration, but then, on the upstroke, it retracts to avoid the cantilever.

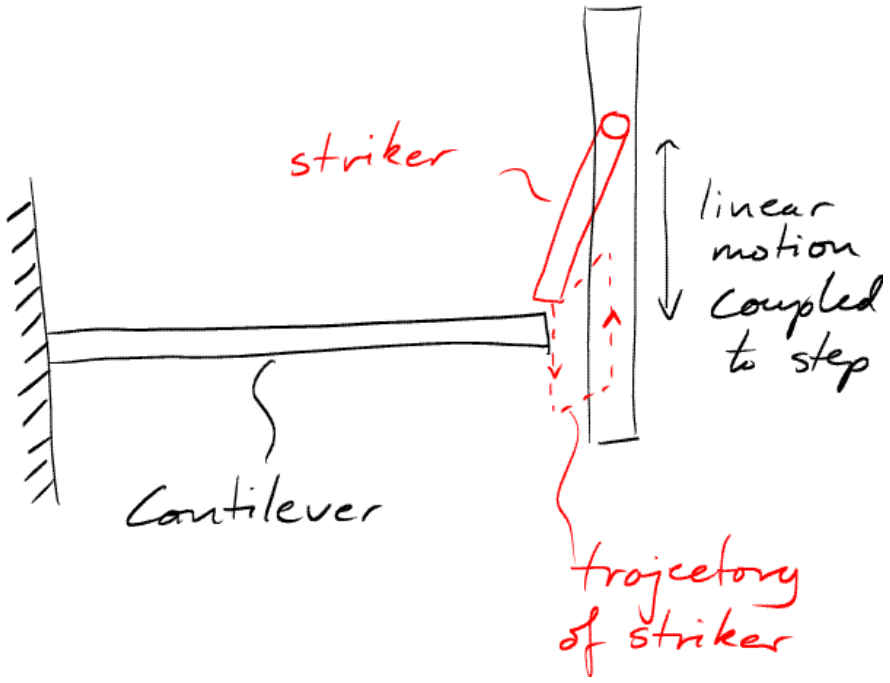

Figure 10-2 striker mechanism for linear to vibration conversion

Advantages

- Fairly simple construction
- Moderate space requirement
- Fairly reliable
- Background IP owned by UoH

Disadvantages

- Low efficiency
- Moderate cost

10.1.1. Electro active polymer based systems

Concept 4. Direct compression of EAP

Electro active polymers are attractive in that they could be placed directly below the floor surface/step, as shown in Figure 10-3.

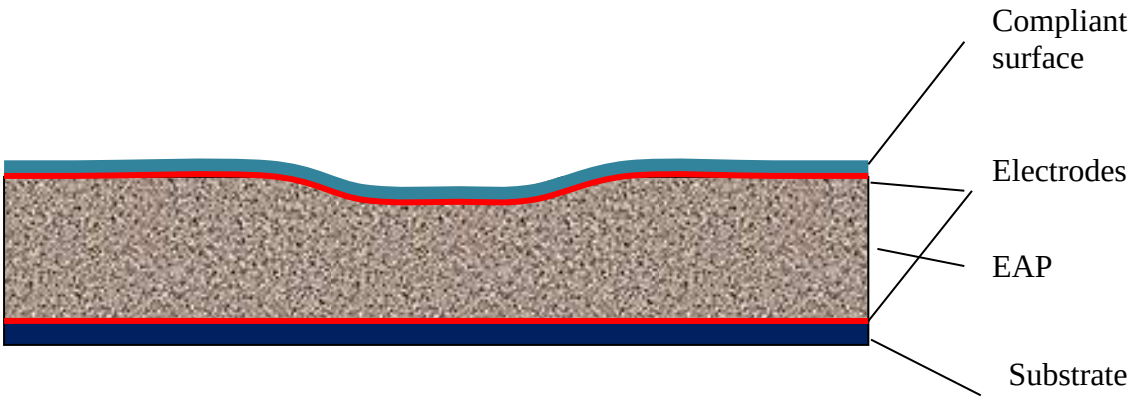

Figure 10-3 EAP based footfall generator

Advantages

- Simple construction
- Low space requirement

Disadvantages

- Low output power
- Uncertain cost
- Uncertain reliability
- Requires initiation voltage
- High voltage level

Concept 5. Contour Stretching EAP

It is believed that EAPs provide improved conversion when stretched and so a preferred structure may be of the form shown in Figure 10-4 derived from the device described in [148]. Although the reported output power from EAP shoe inserts is high, there is little documentation of the materials or the performance and hence there is uncertainty about its suitability.

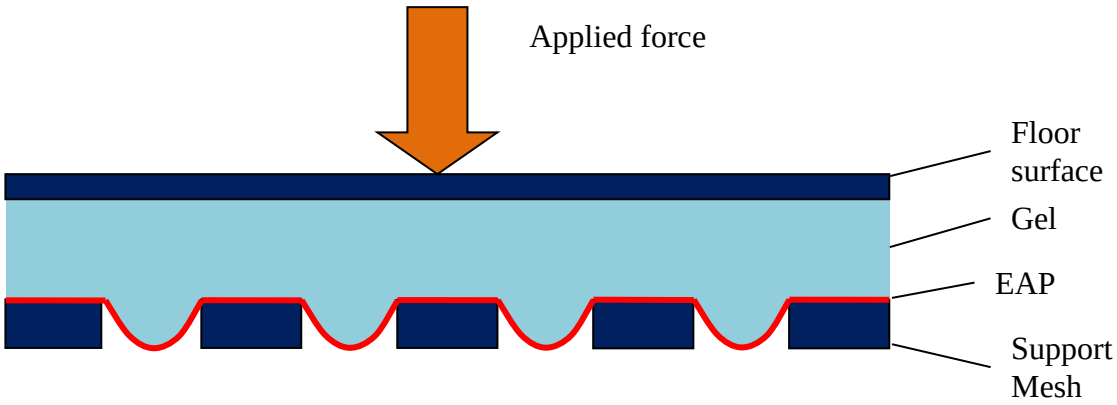

Figure 10-4 Contour stretching EAP

Advantages

- Simple construction
- Low space requirement
- High output power

Disadvantages

- Uncertain cost
- Uncertain reliability
- Requires initiation voltage
- High voltage level

10.1.2. Electromagnetic systems

Electromagnetic conversion is the longest established technology available but, as noted in report 1, electromagnetic conversion is most efficient for relatively high speed motion. This is inherently mismatched with the characteristics of footfall. Hence there is a requirement to

convert from the low speed footfall motion to high speed motion at the electromagnetic converter. The electromagnetic conversion based concepts are grouped into those which use a rotational converter and those based on vibration.

Rotational Electromagnetic systems

Although it is possible to construct a rotary generator, it is generally considered preferable, in terms of performance, simplicity and cost, to make use of commercial generators where possible. The majority of generators operate most efficiently at speeds of the order of 3000rpm. Although lower speed devices are available, they tend to be more expensive. The majority of concepts below adopt off the shelf generators.

Concept 6. Rack and pinion coupling

In this concept the linear motion of the step/floor panel is converted into rotation motion using a rack and pinion mechanism. A return spring would be required to lift the step/floor panel to its original position following footfall. This is relatively simple and has a fairly low space requirement. It is, however, difficult to achieve a high rotational speed and the rack and pinion components would need to be large and robust in order to withstand the large shock loads during heel strike. This will tend to result in high frictional forces and hence relatively poor overall efficiency.

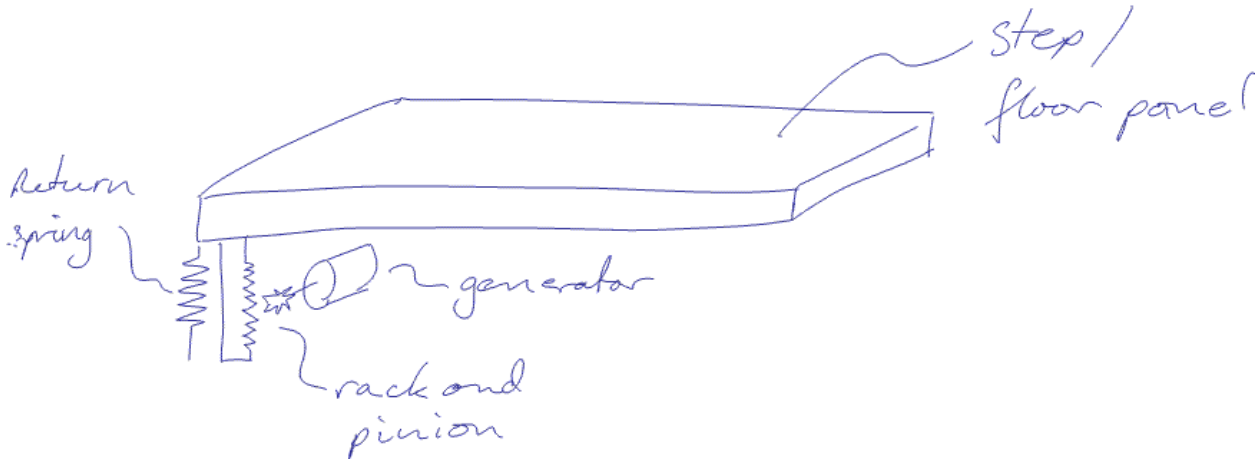

Figure 10-5 Rack an pinion conversion

Advantages

- Fairly Simple construction
- Low space requirement
- Moderate output power

Disadvantages

- Moderate reliability
- Moderately expensive components

Concept 7. Rack and pinion with additional gearing

This is a development of the previous concept but includes an additional gearing stage to give a better match to the optimum generator speed. This will improve the generator efficiency but this benefit may be lost due to additional losses in the gears.

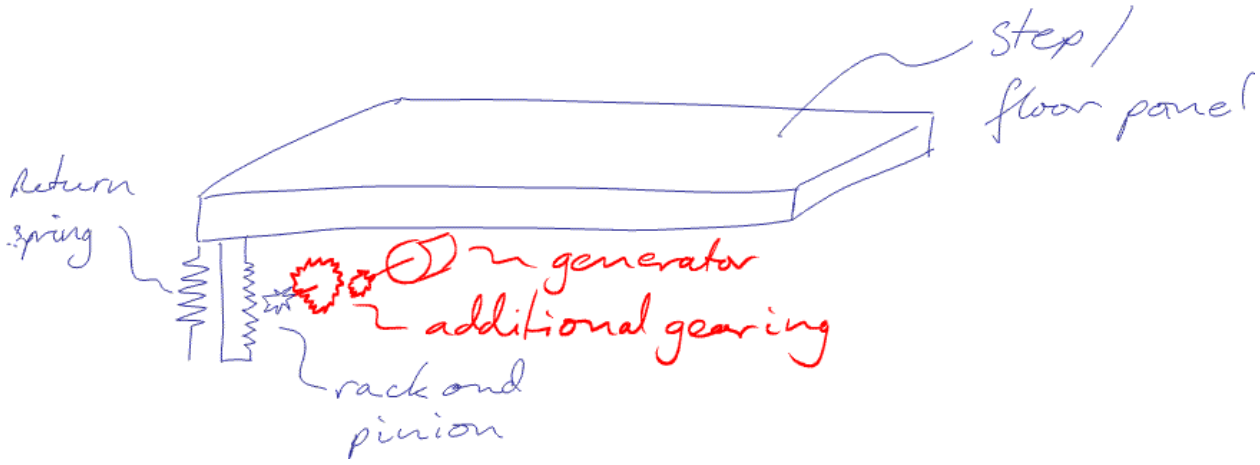

Figure 10-6 Rack and pinion with additional gearing

Advantages

- Fairly Simple construction
- Low space requirement
- Moderate output power

Disadvantages

- Moderate reliability
- Moderately expensive components

Concept 8. Rack and pinion with freewheel

A freewheel mechanism may be added to the above concepts to allow the generator to continue rotating after the end of the floor movement. A flywheel may also be added after the one way clutch to increase the duration of this continued rotation. Although this may give an increase in output energy the mechanism still suffers from some of the limitations of the preceding devices. A similar concept is used for harvesting energy from road vehicles [105] but the IP ownership is not clear for pedestrian use.

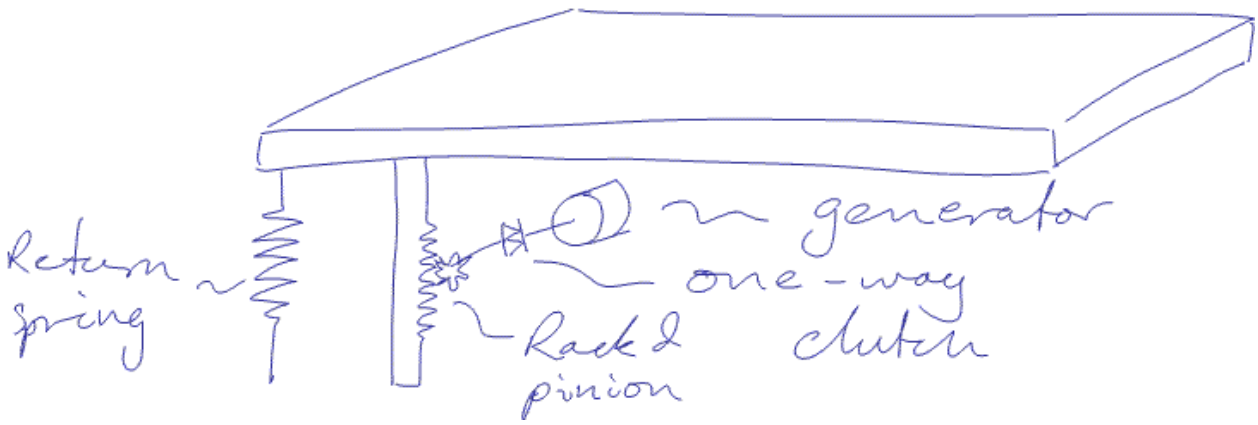

Figure 10-7 Rack and pinion with freewheel

Advantages

- Fairly simple construction
- Low space requirement
- Moderate output power

Disadvantages

- Moderate reliability
- Moderately expensive components

Concept 9. Spinning top mechanism

Rather than use a rack and pinion, this concept makes use of a spinning top type mechanism to give high speed rotation. This may include a free-wheel and flywheel mechanism to allow rotation to continue after the initial applied force. The system illustrated in Figure 10-8 shows the generator constructed as part of the spinning top but it would be possible, with slight

adaptation, to use an off-the-shelf generator. This suffers from similar problems to the previous three concepts in terms of the robustness required and the relatively poor efficiency due to the need to accommodate heel strike forces.

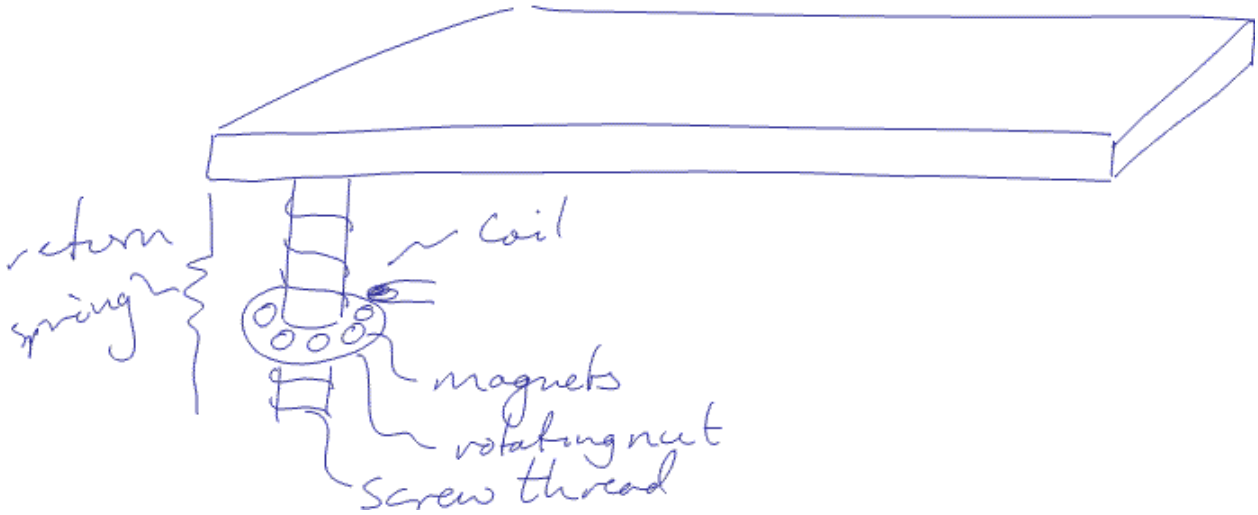

Figure 10-8 Spinning top mechanism

Advantages	Disadvantages
• Fairly Simple construction	• Moderately expensive components
• Moderate space requirement	• Moderate reliability
• Moderate output power	

Concept 10. Spring-freewheel converter

The major limitation of the preceding mechanisms is that they attempt to convert mechanical to electrical energy during the brief foot impact period. This results in large forces being applied to the mechanism and hence the need for large and robust components. These tend to limit efficiency. This concept, developed for the electric shoe project [107], makes use of a spring to store energy during the foot impact and then convert this stored energy over an extended period, allowing a smaller, more efficient mechanism. In the embodiment shown in Figure 10-9, a compression spring is used to store the input energy and once the foot is lifted

from the step the return motion is coupled through a crank and one way clutch to a gearbox which converts the motion to a higher speed matched to the generator. A flywheel may also be added to the generator shaft to allow the speed profile to be shaped to optimise the generator efficiency. Because the conversion occurs as the step returns to its starting position, it is not capable of fully capturing subsequent footsteps until this conversion is complete. Thus if footfall occurs at high frequency the captured energy level may be lower than expected.

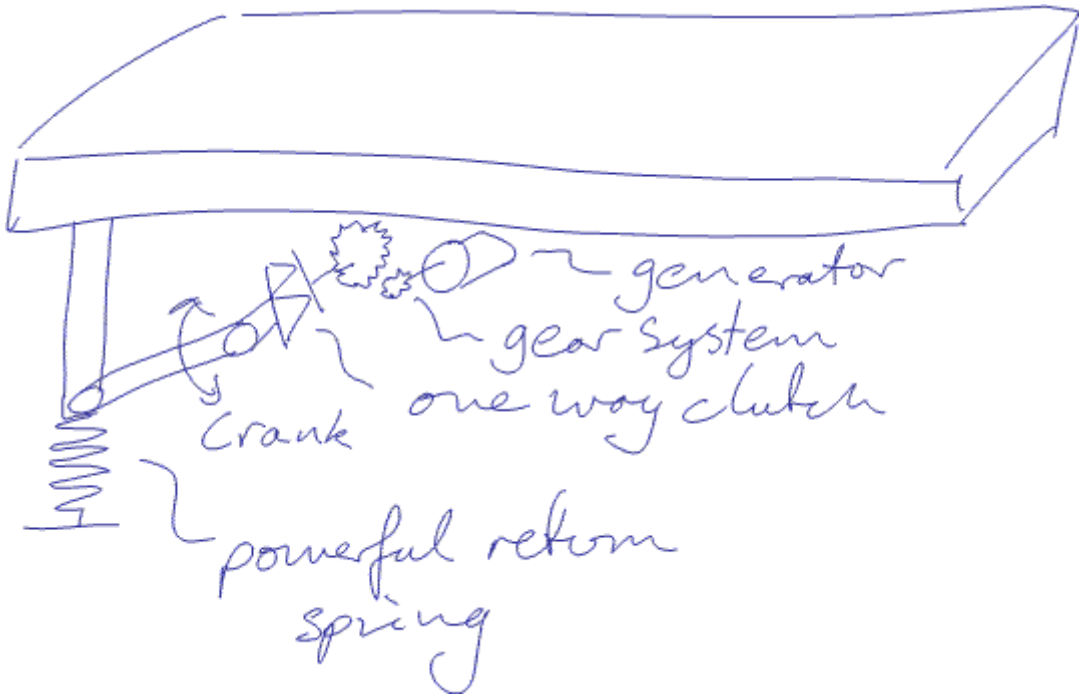

Figure 10-9 Spring-freewheel mechanism

Advantages

- High output power
- Good reliability

Disadvantages

- Fairly complex mechanism
- May miss steps in high traffic levels

Concept 11. Flyback Converter

This device, based on an electrical analogue of a switched mode power supply and studied extensively by the author as part this study, uses a striker mechanism which couples the linear motion of the step into a torsion spring during the footfall but then, at a defined displacement, allows the spring to fly back rapidly. This rapid motion is coupled, via a one way clutch, to a flywheel and the generator. The benefit of this mechanism is that it does not contain gears and so should give greater conversion efficiency. The mechanism has been extensively modelled and a prototype system constructed. This is currently being evaluated and optimised.

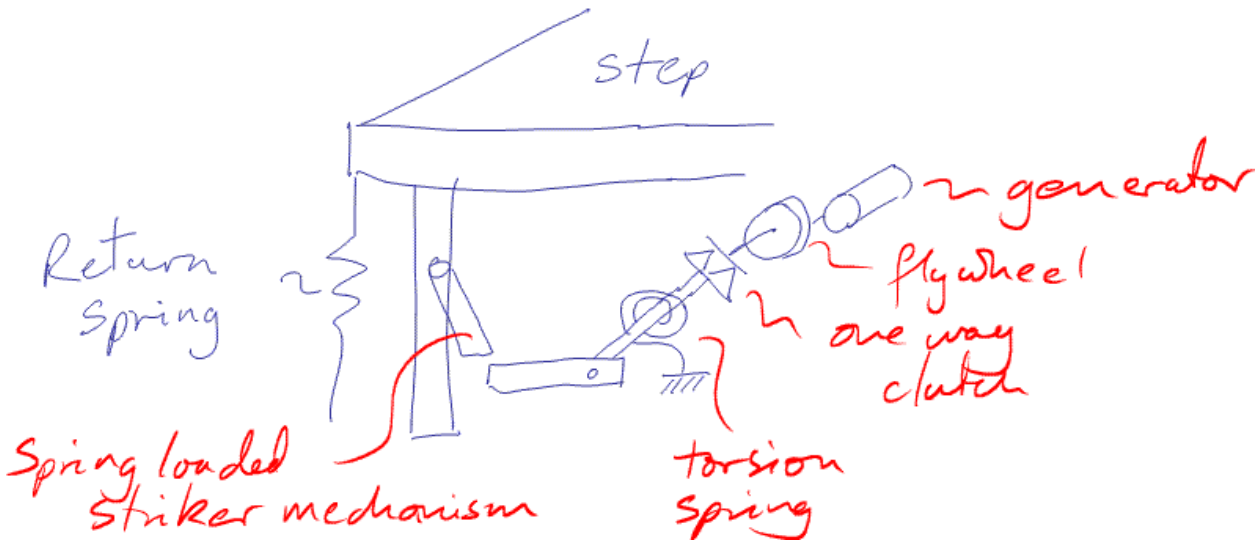

Figure 10-10 Flyback converter

Advantages

- Well developed theory
- Prototype mechanism available
- High output power

Disadvantages

- Complex mechanism
- Moderate reliability
- Large spec requirement

Vibrational Electromagnetic systems

Although rotational machines are well understood and give good performance, for this application a vibration based system has some attraction because it permits a relatively simple coupling mechanism.

Concept 12. Vibrating cantilever electromagnetic converter

This concept developed by UoH, based on vibration energy harvesting systems, makes use of a cantilever beam with a set of magnets at the free end which surround a coil. When the cantilever vibrates the changing magnetic field experienced by the coil causes a voltage to be induced. A number of mechanisms have been proposed for coupling the linear motion of the step/floor to initiate vibration in the cantilever. The system shown in Figure 10-11 is a simplified representation of a typical device. The system is relatively simple and, based on tests carried out previously by UoH, it appears to offer good efficiency.

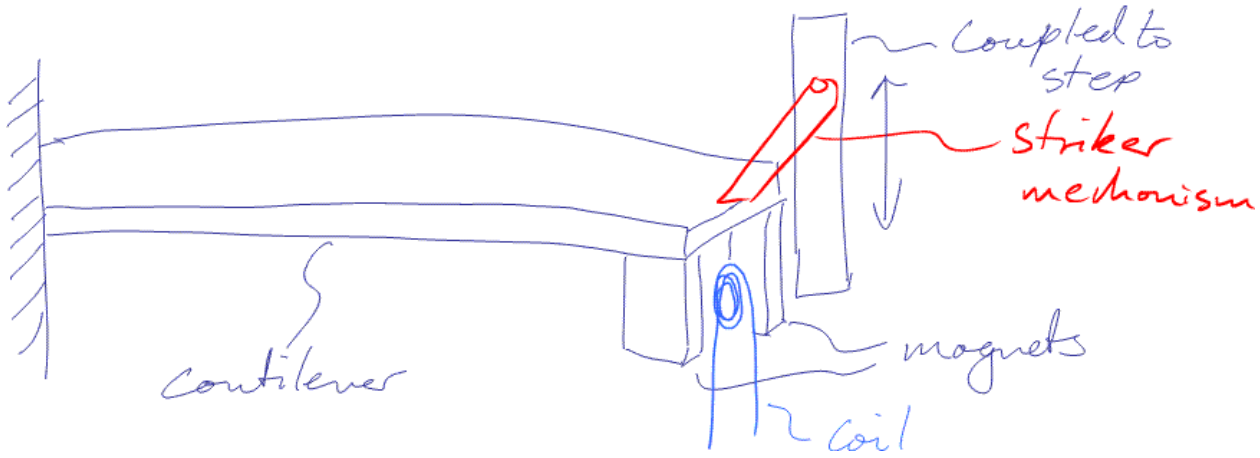

Figure 10-11 Vibrating cantilever electromagnetic converter

Advantages

- Fairly simple construction
- Moderate space requirement
- High output power

Disadvantages

- Moderate reliability
- Output independent of GRF
- May be noisy

10.1.3. Fluid based systems

Hydraulic and pneumatic systems for coupling step motion to a rotational electromagnetic generator provide flexibility in terms of speed conversion. They tend to give relatively poor efficiency when scaled to the sizes considered here. The concepts outlined below are applicable to either hydraulic or pneumatic media. Pneumatic systems are affected by the compressibility of air which results in poorer efficiency but they are advantageous in terms of the consequences of leakage. In addition, pneumatic systems do not require a fluid return line since air may be drawn from the atmosphere, thus reducing cost and simplifying some elements of the system. In most commercial hydraulic systems, hydraulic oil is used but this is potentially dangerous if leaks occur in public areas due to the resulting slip hazard. For the relatively low pressure system considered here, water would probably be a more suitable hydraulic medium. For a fluid system there are three essential components: a means to convert the step/floor motion to fluid flow, a turbine or similar device to convert fluid flow to rotation and a rotational generator. A cross flow turbine has been designed and manufactured using rapid prototyping techniques as shown in Figure 10-12 to allow initial evaluations to be carried out.

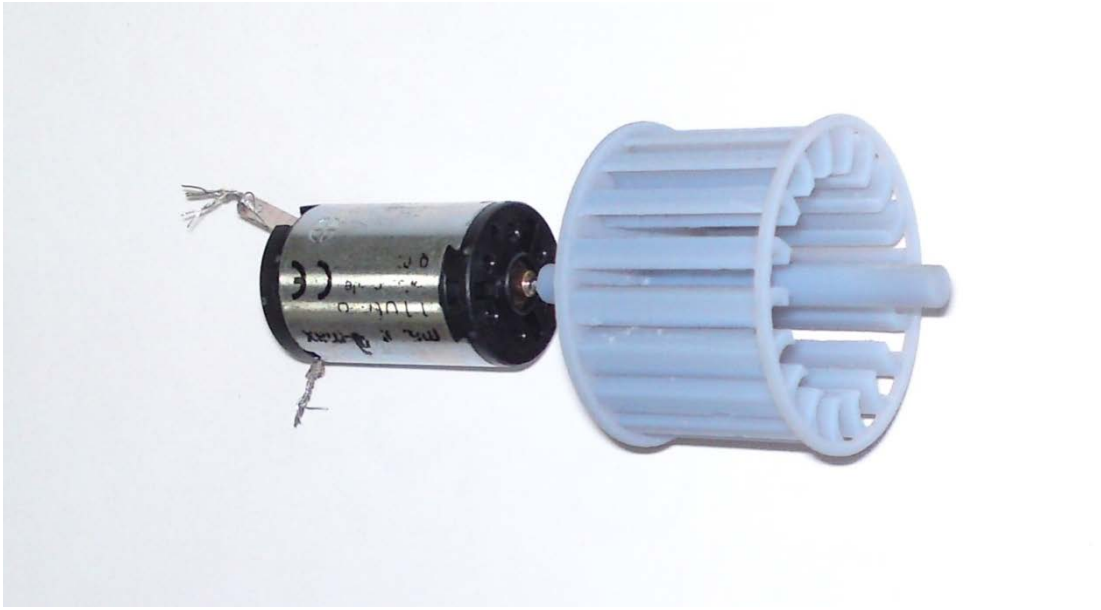

Figure 10-12 Cross flow turbine and generator

Concept 13. Fluid cylinder system

A conventional hydraulic or pneumatic cylinder may be used to convert linear motion of the piston into fluid flow. A non-return valve may be used to ensure the flow is in only one direction and this will cause the turbine to rotate, driving the generator. The outflow from the turbine can then be coupled back into the cylinder which sucks fluid back in when the step rises under the effect of a return spring (not shown). The fact that the turbine only rotates during the foot impact means that the turbine, which is designed for constant flow rate, may not be as efficient as would be possible.

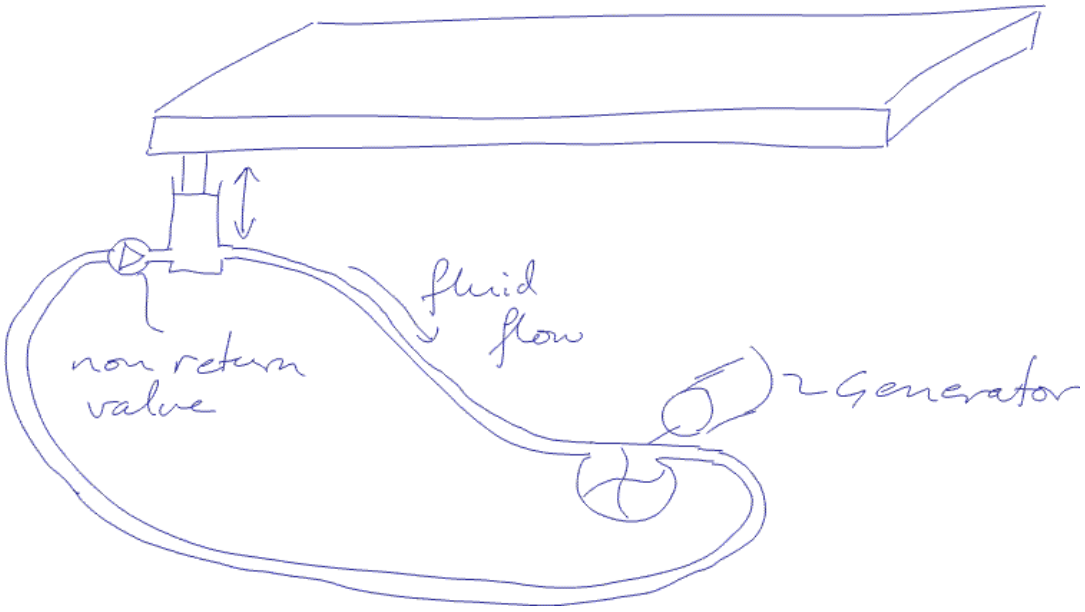

Figure 10-13 Cylinder based fluid system

Advantages

- Simple construction
- Moderate space requirement
- Good reliability

Disadvantages

- Uncertain output power
- Varying flow rate reduces efficiency
- Not readily scaled to multiple inputs

Concept 14. Fluid cylinder system with accumulator

By adding a pressure vessel accumulator to the above system, it is possible to smooth out the fluid flow, giving more efficient turbine performance. This would add to the cost of the system and the improvement in efficiency is not currently known. The presence of the accumulator would allow the inputs from several steps/floor panels to be combined to drive a single generator.

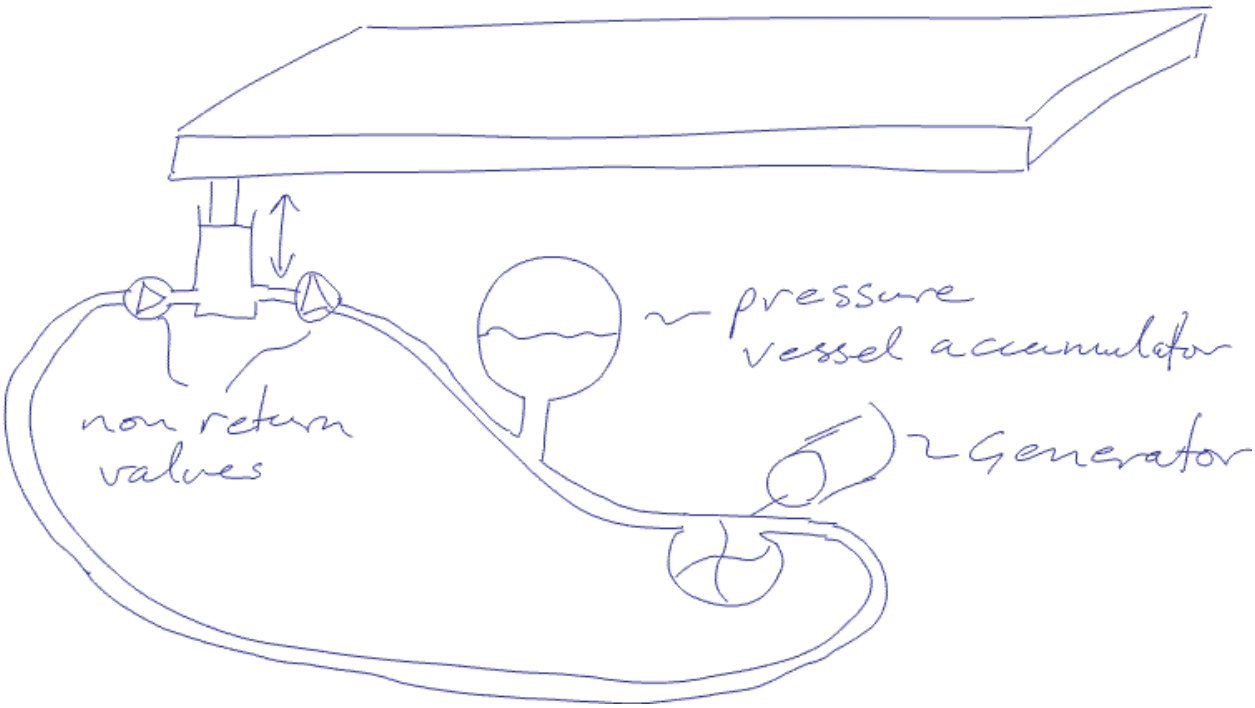

Figure 10-14 Cylinder based fluid system with accumulator

Advantages

- Simple construction
- Moderate space requirement
- Good reliability
- May be scaled to multiple inputs

Disadvantages

- Uncertain output power
- Higher cost than non-accumulator version for single input system

Concept 15. Fluid bladder system

A relatively expensive element of hydraulic and pneumatic systems is the cylinders since these require good quality seals. An alternative which could be combined with either of the preceding two concepts would be to replace the cylinder with a bladder placed under the floor panel/step. This also reduces the space requirement.

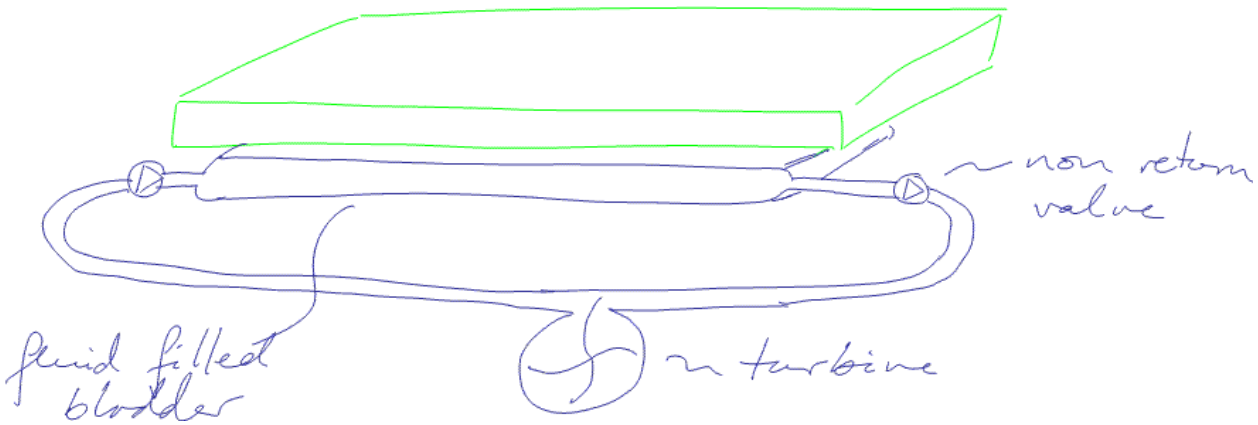

Figure 10-15 bladder based fluid system

Advantages

- Simple construction
- Low space requirement
- May be scaled to multiple inputs if accumulator used

Disadvantages

- Uncertain output power
- Uncertain reliability
-

Concept 16. Compressible tube system

The cylinder and bladder described in the preceding concepts are discrete components which must be replicated in order to harvest energy from multiple inputs. By using a series of connected tubes, it may be possible to produce a scalable ‘mat’ which could harvest energy over a large area and drive a single turbine/generator, as illustrated in Figure 10-16 and Figure 10-17. Figure 10-16 shows a cross section through the tubing mat. Under foot pressure, the tubing would be crushed, forcing fluid through the tube. Once the foot pressure is removed, the elasticity of the tubing would cause it to recover its original shape, sucking fluid back into the affected area. By using non return vales as illustrated in Figure 10-17, it would be possible to ensure that the fluid flow was unidirectional and capable of driving the turbine. These non return values would also allow multiple tubes to be connected to a single

turbine so that whichever part of the matt were compressed, the fluid would flow through the turbine and, indeed, if multiple pedestrians were present, the system would capture energy from them all simultaneously. What is not currently clear is how to optimize the tubing length, tubing material etc for given fluid characteristics (air or water) so that as much fluid flow as possible occurs without energy dissipation or pressure losses in the tubing. It is anticipated that it will not be possible to attain very high levels of efficiency with this type of device but it may be possible to produce a large area harvesting system at relatively low cost.

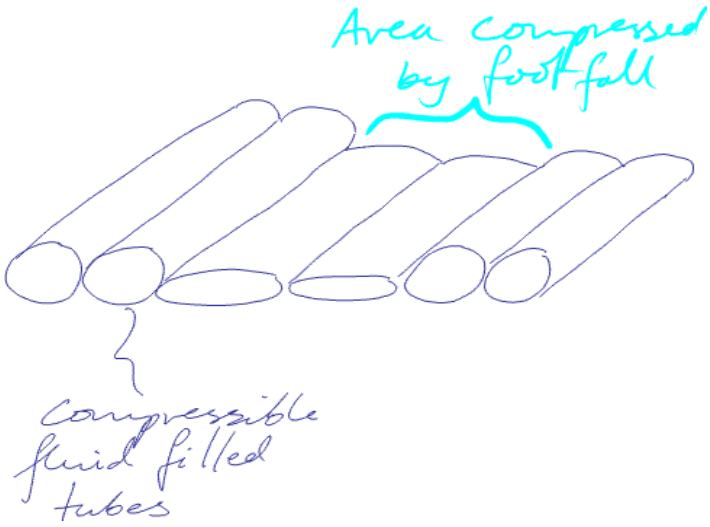

Figure 10-16 Tubing mat

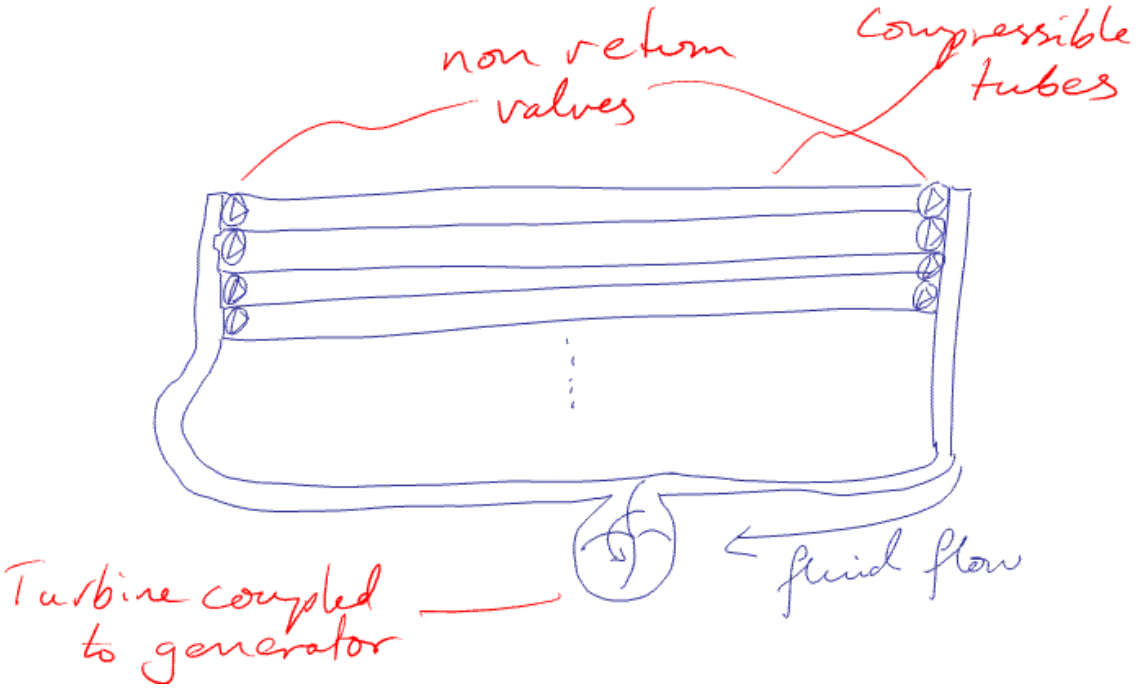

Figure 10-17 Connection of large area mat to single turbine

Advantages

- Simple construction
- Low space requirement
- Readily scaled to large areas
- Low cost

Disadvantages

- Uncertain efficiency
- Significant design work required

10.2. Concept Selection Process

The selection matrix for the two application scenarios are given in Table 10-1 and Table 10-2. It can be seen that three candidates (flyback converter, vibrating cantilever electromagnetic converter and compressible tube system) score most highly in both application scenarios with the compressible tube system scoring most highly in the shop entrance scenario because of its greater ease of expansion while the flyback converter and vibrating cantilever score more highly in the tube stair scenario because of greater expected output power. It may also be noted that the differences in scores are not great with, in particular, the flyback converter and the vibrating cantilever gaining very similar scores.

Number	Selection Criterion	Anticipated power output	Cost of implementation	Reliability	Voltage/current level generated	Range of pedestrian weight/gait	Ease of expansion to multiple pedestrians	Installation space requirement	Technical risk	IP ownership	Weighted Total	Ranking
	Weighting	**10**	**5**	**3**	**1**	**2**	**3**	**2**	**5**	**2**		
1	Direct compression of piezo material	1	2	8	5	8	1	10	7	5	**133**	**15**
2	Direct bending of a cantilever of piezo material	2	2	8	5	7	1	8	8	5	**142**	**13**
3	Conversion to vibration of piezo cantilever	2	2	6	5	5	1	6	6	5	**118**	**16**
4	Direct compression of EAP	5	1	6	3	8	5	10	2	1	**139**	**14**
5	Contour Stretching EAP	8	1	6	3	8	5	8	2	1	**165**	**10**
6	Rack and pinion coupling	5	6	7	8	6	3	5	7	5	**185**	**8**
7	Rack and pinion with additional gearing	6	5	7	8	6	3	4	7	5	**188**	**5**
8	Rack and pinion with freewheel	6	5	7	8	6	3	3	7	5	**186**	**7**
9	Spinning top mechanism	6	5	7	8	6	3	4	7	5	**188**	**5**
10	Spring-freewheel converter	7	4	6	8	5	4	3	8	5	**194**	**4**
11	Flyback Converter	8	4	6	8	6	5	3	8	8	**215**	**1**
12	Vibrating cantilever electromagnetic converter	8	6	7	7	5	1	5	7	8	**212**	**2**
13	Fluid cylinder system	3	4	7	8	6	1	5	6	5	**144**	**12**
14	Fluid cylinder system with accumulator	3	4	7	9	7	5	4	6	5	**157**	**11**
15	Fluid bladder system	3	6	6	8	7	5	8	6	5	**171**	**9**
16	Compressible tube system	3	8	6	8	7	9	10	6	10	**207**	**3**

Table 10-1 Selection matrix for tube station stairs application

Number	Selection Criterion	Anticipated power output	Cost of implementation	Reliability	Voltage/current level generated	Range of pedestrian weight/gait	Ease of expansion to multiple pedestrians	Installation space requirement	Technical risk	IP ownership	Weighted Total	Ranking
	Weighting	**10**	**5**	**3**	**1**	**1**	**5**	**4**	**5**	**2**		
1	Direct compression of piezo material	1	2	8	5	8	1	10	7	5	**147**	**15**
2	Direct bending of a cantilever of piezo material	2	2	8	5	7	1	8	8	5	**153**	**13**
3	Conversion to vibration of piezo cantilever	2	2	6	5	5	1	6	6	5	**127**	**16**
4	Direct compression of EAP	5	1	6	3	8	5	10	2	1	**161**	**12**
5	Contour Stretching EAP	8	1	6	3	8	5	8	2	1	**183**	**10**
6	Rack and pinion coupling	5	6	7	8	6	3	5	7	5	**195**	**7**
7	Rack and pinion with additional gearing	6	5	7	8	6	3	4	7	5	**196**	**5**
8	Rack and pinion with freewheel	6	5	7	8	6	3	3	7	5	**192**	**8**
9	Spinning top mechanism	6	5	7	8	6	3	4	7	5	**196**	**5**
10	Spring-freewheel converter	7	4	6	8	5	4	3	8	5	**203**	**4**
11	Flyback Converter	8	4	6	8	6	5	3	8	8	**225**	**2**
12	Vibrating cantilever electromagnetic converter	8	6	7	7	5	1	5	7	8	**219**	**3**
13	Fluid cylinder system	3	4	7	8	6	1	5	6	5	**150**	**14**
14	Fluid cylinder system with accumulator	3	4	7	9	7	5	4	6	5	**168**	**11**
15	Fluid bladder system	3	6	6	8	7	5	8	6	5	**190**	**9**
16	Compressible tube system	3	8	6	8	7	9	10	6	10	**238**	**1**

Table 10-2 Selection matrix for shop entrance application

10.3. Prototype Development

As discussed previously the concept generation suggested three concepts for prototyping. These concepts were developed in parallel to determine their suitability to the scenarios under consideration.

10.3.1. Flyback converter

This was the most highly desirable concept. Although not used for an energy harvesting application, it formed part of a separate study by the author's PhD supervisor [147] and together with its high compatibility with the specification described in Table 10-1 and Table 10-2, it was chosen as preferred mechanism for prototyping. The next stage of development for this mechanism was to prototype for energy harvesting, characterise and identify optimum system parameters to determine the design parameters for a full scale device. The prototype is presented with results and analysis in Chapter 5.

10.3.2. Vibrating cantilever electromagnetic converter

This was the second most desirable mechanism for prototyping for its compatibility to the specifications as discussed above. It is envisaged that the prototype will utilise a simplified striker mechanism since the construction of this element is complex but there is less uncertainty about its performance than the cantilever element. A small scale, proof of concept, model of the cantilever and striker mechanism were constructed followed by a detailed design which led to a near full scale version which will be presented in Chapter 6.

10.3.3. Compressible tube system

This was highly desirable concept and so was developed to a proof of concept stage. The design. Given the time and resource constraints, it was therefore intended to take this to a less sophisticated prototype stage than the other two candidates. The aim was therefore be to

obtain an initial estimate of the likely power levels achievable and assess the key design parameters. The important considerations to be assessed were the choice of fluid (air or water), the nature of the tubing and its dimensions and the turbine dimensions.

10.3.4. Conclusion

Based on the proposed application scenarios of a tube station staircase and a shop entrance, a number of footfall energy harvesting concepts have been generated and evaluated. These have been compared using a weighted scoring matrix and three leading candidate concepts selected. The three candidate concepts selected were the Flyback Converter, the Vibrating Cantilever Electromagnetic Converter and the Compressible Tube System. Due to time limitation the compressible Tube System was not developed to an advance prototype stage. Mathematical modelling and other calculation for the Tube system is provided in Appendix G, page 204.

11. Appendix B – Semi analytical solution to footfall generator equations

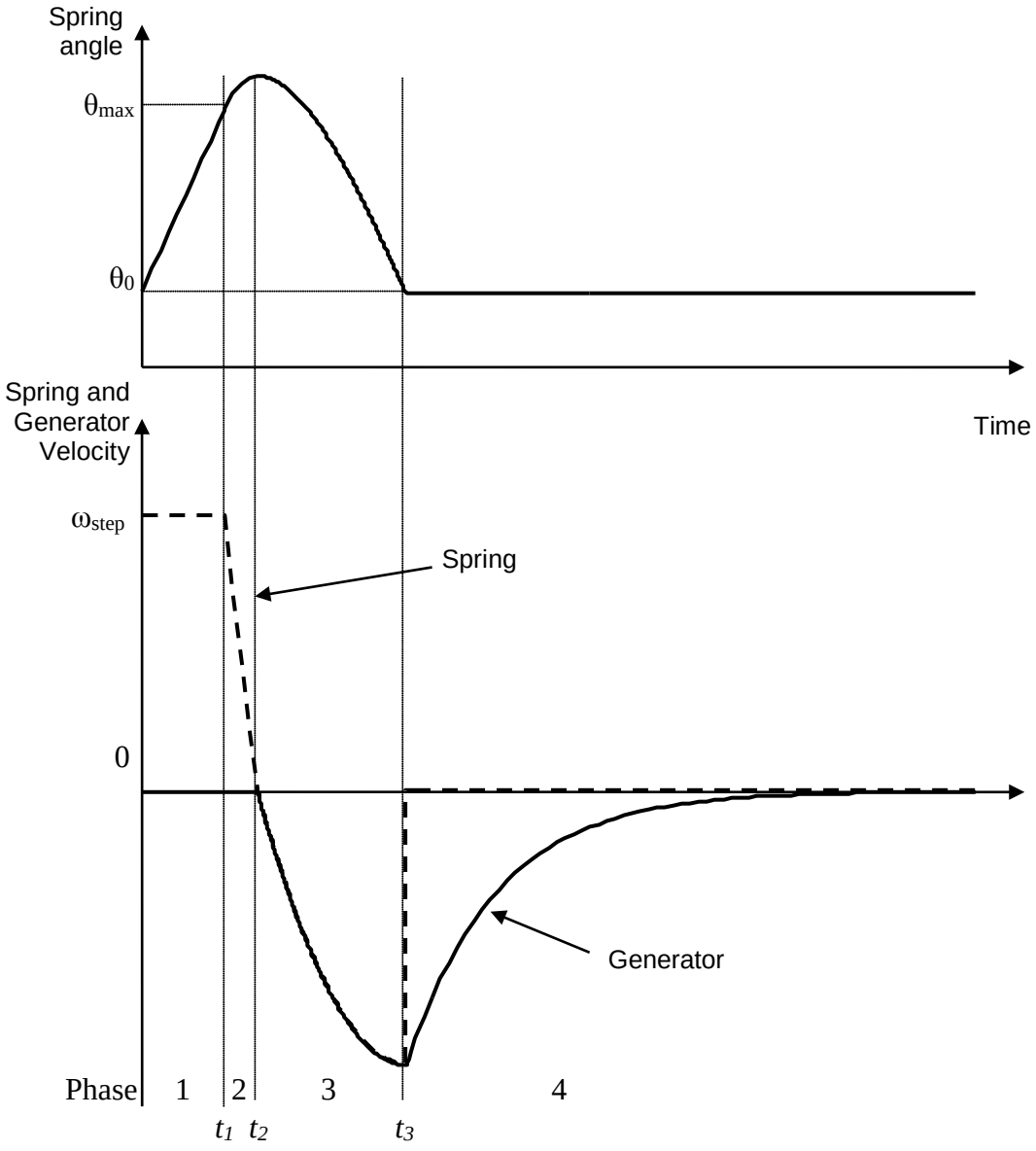

Phase 1 - Spring windup during footfall (*0*<*t*<).

The dynamics during phase 1 are determined by the pedestrian input and so we are only concerned with the conditions at the end of phase 1. At this point

$$\theta_s = \theta_{\max}$$

and

$$\dot{\theta}_s = \omega_{step}$$

The total energy at this point is:

$$E_1 = \frac{1}{2} k_s \theta_{\max}^2 + \frac{1}{2} J_s \omega_{step}^2$$

The energy extracted from the pedestrian is:

$$E_{in} = \frac{1}{2} k_s \left(\theta_{\max}^2 - \theta_0^2 \right) + \frac{1}{2} J_s \omega_{step}^2 \qquad (1)$$

Phase 2 - Spring unwind to zero velocity (<*t*<). During this phase the spring velocity is governed by the equation:

$$J_s \ddot{\theta}_s = -k_s \theta_s - B_s \dot{\theta}_s - D_s \operatorname{sgn}\left(\dot{\theta}_s\right) \qquad (2)$$

where is the angle of rotation of the spring

is the viscous friction coefficient associated with the spring

is the coulomb friction coefficient associated with the spring

with initial conditions $\theta_s(t_1) = \theta_{\max}$ and $\dot{\theta}_s(t_1) = \omega_{step}$.

since we are interested in the period for which $\dot{\theta}_s > 0$, $\text{sgn}(\dot{\theta}_s) = +1$.

Taking Laplace transforms we get:

$$J_s\left[s^2\Theta(s) - s\theta_{\max} - \omega_{step}\right] = -k_s\Theta_s(s) - B_s\left[\Theta_s(s) - \theta_{\max}\right] - \frac{D_s}{s}$$

so

$$\Theta_s(s) = \frac{s^2 J_s\theta_{\max} + s\left[J_s\omega_{step} + B_s\theta_{\max}\right] - D_s}{s\left[s^2 J_s + sB_s + k_s\right]} \qquad (3)$$

and

$$\Omega_s(s) = s\Theta_s(s) = \frac{s^2 J_s\theta_{\max} + s\left[J_s\omega_{step} + B_s\theta_{\max}\right] - D_s}{\left[s^2 J_s + sB_s + k_s\right]} \qquad (4)$$

splitting (4) as:

$$\Omega_s(s) = \frac{\left[s^2 J_s + sB_s + k_s\right]\theta_{\max} - k_s\theta_{\max} + sJ_s\omega_{step} - D_s}{\left[s^2 J_s + sB_s + k_s\right]} = \theta_{\max} + \frac{-k_s\theta_{\max} + sJ_s\omega_{step} - D_s}{\left[s^2 J_s + sB_s + k_s\right]} \qquad (5)$$

completing the square in the denominator:

$$s^2 + s\frac{B_s}{J_s} + \frac{k_s}{J_s} = (s+a)^2 + b^2$$

where $a = \frac{B_s}{2J_s}$ and $b = \sqrt{\frac{J_s k_s - \left(B_s/2\right)^2}{J_s^2}}$, (5) can be written as:

$$\Omega_s(s) = \theta_{\max} + \frac{\omega_{step}(s+a) - \omega_{step}a - \frac{k_s\theta_{\max} + D_s}{J_s}}{(s+a)^2 + b^2} \qquad (6)$$

and from tables, we can write:

$$\omega_s(t) = \theta_{\max}\delta + e^{-at}\left\{\omega_{step}\cos(bt) - \frac{1}{b}\left[\omega_{step}a + \frac{k_s\theta_{\max} + D_s}{J_s}\right]\sin(bt)\right\} \qquad (7)$$

Phase 2 ends at time when the spring velocity reaches zero: $\dot{\theta}_s(t_2) = 0$. This may be found from (7):

$$t_2 = \frac{1}{b}\tan^{-1}\left\{\frac{\omega_{step}J_s b}{\omega_{step}J_s a + k_s\theta_{\max} + D_s}\right\} \qquad (8)$$

The spring angle $\theta_s(t)$ can be determined by integrating (7) to give:

$$\theta_s(t) = e^{-at}\left\{\frac{\omega_{step}k_s\sin(bt) + (k_s\theta_{\max} + D_s)[b\cos(bt) + a\sin(bt)]}{k_s b}\right\} + \frac{D_s}{k_s} \qquad (9)$$

where we use the fact that $a^2 + b^2 = k_s / J_s$. The final term is the integration constant required to ensure that $\theta_s(0) = \theta_{\max}$. The spring angle at the end of Phase 2, $\theta_{s2} = \theta_s(t_2)$ can be found by substituting from 8 into 9.

Phase 3 - Spring drives generator (<*t*<).

The dynamics during Phase 3 are governed by:

$$(J_s + J_g)\ddot{\theta}_s = -k_s\theta_s - (B_s + B_g)\dot{\theta}_s - (D_s + D_g)\text{sgn}(\dot{\theta}_s) - k_t \frac{k_e\dot{\theta}_g}{R_g + R_l} \quad (10)$$

where is the moment of inertia of the generator, flywheel and associated parts

is the viscous friction coefficient associated with the generator/flywheel

is the coulomb friction coefficient associated with the generator/flywheel

is the torque constant of the generator

i is the current flowing through the generator and into the load

is the emf constant of the generator

is the winding resistance of the generator

is the load resistance

Equation 10 may be rewritten as:

$$J\ddot{\theta}_s = -k_s\theta_s - B\dot{\theta}_s - D\,\text{sgn}(\dot{\theta}_s) \quad (11)$$

where:

$$J = J_s + J_g$$

$$B = B_s + B_g + \frac{k_e k_t}{R_g + R_l}$$

$$D = D_s + D_g$$

The initial conditions at the beginning of phase 3 are $\dot{\theta}_s(t_2) = 0$ and $\theta_s(t_2) = \theta_{s2}$.

taking Laplace transforms of 11 with these initial conditions gives:

$$J\left(s^2\Theta(s) - s\theta_{s2}\right) = -k_s\Theta(s) - B\left(s\Theta(s) - \theta_{s2}\right) + \frac{D}{s}$$

and so

$$\Theta(s) = \frac{\left(Js^2 + Bs\right)\theta_{s2} + D}{s\left(Js^2 + Bs + k_s\right)} \qquad (12)$$

or

$$\Theta(s) = \frac{\theta_{s2}}{s} + \frac{-k_s\theta_{s2} + D}{s\left(Js^2 + Bs + k_s\right)}$$

and

$$\Omega(s) = \theta_{s2} + \frac{-k_s\theta_{s2} + D}{Js^2 + Bs + k_s} = \theta_{s2} + \frac{(-k_s\theta_{s2} + D)/J}{(s+\alpha)^2 + \beta^2} \qquad (13)$$

where $\alpha = \frac{B}{2J}$ and $\beta = \sqrt{\frac{Jk_s - (B/2)^2}{J^2}}$

so

$$\omega(t) = \theta_{s2}\delta + \frac{-k_s\theta_{s2} + D}{J\beta} e^{-\alpha t} \sin(\beta t) \qquad (14)$$

and

$$\theta(t) = \frac{k_s\theta_{s2} - D}{k_s\beta} e^{-\alpha t} \{\beta \cos(\beta t) + \alpha \sin(\beta t)\} + \frac{D}{k_s} \qquad (15)$$

Phase 3 ends when the spring angle returns to its initial value, $\theta_s(t_3) = \theta_0$. This appears to only be soluble analytically if $\theta_0 = 0$ and $D = 0$, in which case the solution becomes:

$$t_3 = \frac{1}{\beta} \tan^{-1}\left(\alpha/\beta\right)$$

In the more general case, 15 can be solved numerically and substituted into 14. At this point the spring and generator velocities are equal $\dot{\theta}_s(t_3) = \dot{\theta}_g(t_3) = \dot{\theta}_{g3}$.

The voltage applied to the load during phase 3 can be found from:

$$v(t) = \frac{k_e R_l}{R_g + R_l}\omega(t) = \frac{k_e R_l}{R_g + R_l}\left\{\theta_{s2}\delta + \frac{-k_s\theta_{s2} + D}{J\beta}e^{-\alpha t}\sin(\beta t)\right\} \qquad (16)$$

and so the instantaneous power delivered to the load is:

$$p(t) = \frac{v^2}{R_l} = R_l\left(\frac{k_e}{R_g + R_l}\right)^2\left\{\theta_{s2}\delta + \frac{-k_s\theta_{s2} + D}{J\beta}e^{-\alpha t}\sin(\beta t)\right\}^2$$

and the energy delivered during phase 3 is:

$$E_3 = \int_0^{t_3} p(t)dt \quad E_3 = \frac{k_e^2\left(D - k_s\theta s_2\right)^2\left[\left\{-k_s/J - ab\sin(2bt_3) + a^2\cos(2bt_3)\right\}e^{-2at_3} + b^2\right]}{4Jb^2\left(R_l + R_g\right)^2 R_l a k_s}$$

(17)

Phase 4 - Rundown of flywheel (<*t*<). When the spring reaches its end stop it is assumed that it stops rapidly and the flywheel continues to rotate. The precise behaviour of the spring during this phase is unimportant since it does not affect the output power. The dynamics of the flywheel and generator during this phase is described by:

$$J_g\ddot{\theta}_g = -B_g\dot{\theta}_g - D_g\,\mathrm{sgn}\left(\dot{\theta}_g\right) - \frac{k_t k_e\dot{\theta}_g}{R_g + R_l} \qquad (18)$$

or

$$J_g\ddot{\theta}_g = -B_1\dot{\theta}_g + D_g$$

where $B_1 = B_g + \dfrac{k_t k_e}{R_g + R_l}$ and $\text{sgn}\left(\dot{\theta}_g\right) = -1$

The initial conditions for phase 4 are $\theta_g\left(t_3\right) = \theta_0$ and $\dot{\theta}_g\left(t_3\right) = \dot{\theta}_{g3}$.

Thus

$$\Theta_g\left(s\right) = \frac{\theta_0}{s} + \frac{J_g s\dot{\theta}_{g3} + D_g}{s\left(J_g s^2 + B_1 s\right)}$$

and

$$\Omega_g\left(s\right) = \theta_0 + \frac{J_g s\dot{\theta}_{g3} + D_g}{J_g s^2 + B_1 s} = \theta_0 + \frac{D_g/B_1}{s} + \frac{\dot{\theta}_{g3} - D_g/B_1}{s + B_1/J_g}$$

which leads to:

$$\omega_g\left(t\right) = \theta_0\delta + \frac{J_g s\dot{\theta}_{g3} + D_g}{J_g s^2 + B_1 s} = \theta_0\delta + \frac{D_g}{B_1} + \left(\dot{\theta}_{g3} - \frac{D_g}{B_1}\right)e^{-\frac{B_1}{J_g}t}$$

Phase 4 ends at where $\omega_g\left(t_4\right) = 0$. This time may be found from:

$$t_4 = -\frac{J_g}{B_1}\log\left\{-\frac{D_g}{\dot{\theta}_{g3}B_1 - D_g}\right\}$$

Once again, the voltage and power delivered to the load are

$$v(t) = \frac{k_e R_l}{R_g + R_l}\omega_g(t) = \frac{k_e R_l}{R_g + R_l}\left\{\theta_0\delta + \frac{D_g}{B_1} + \left(\dot{\theta}_{g3} - \frac{D_g}{B_1}\right)e^{-\frac{B_1}{J_g}t}\right\}$$

$$p(t) = \frac{v^2}{R_l} = R_l\left(\frac{k_e}{R_g + R_l}\right)^2\left\{\theta_0\delta + \frac{D_g}{B_1} + \left(\dot{\theta}_{g3} - \frac{D_g}{B_1}\right)e^{-\frac{B_1}{J_g}t}\right\}^2$$

and the energy delivered during phase 4 is

$$E_4 = \int_0^{t_4} p(t)dt = \frac{J_g k_e^2\left\{-2D_g^2\log\left\{-\frac{D_g}{\dot{\theta}_{g3}B_1 - D_g}\right\} + \dot{\theta}_{g3}B_1\left(\dot{\theta}_{g3}B_1 + 2D_g\right)\right\}}{2g\left(R_l + R_g\right)^2 R_l B_1^3}$$

The total energy reaching the load is $E_{out} = E_3 + E_4$ and the efficiency of the overall conversion is $\eta = \frac{E_{out}}{E_{in}}$.

12. Appendix B – MATLAB Source Code for Stair Generator derived from analytical solutions

12.1. Heel_param.m

```
    Rg=5.95;
    Rl=8;
    Ke=21.4e-3;
    Kt=Ke;
    Bg=0.0000005;
    Dg=0.0054;
    Jg=(0.936e-3)/150; % 0.136e-3
% Phase 2
    Js=0.00001e-3;
    Ks=1.92;
    Bs=0.000002;
    wstep=0;
    thmax=0.8;
    Ds=0.0001;


% Phase 3
    Jp=Jg+Js;
    Ksp=Ks;
    Bp=Bs+Bg+Ke*Kt/(Rg+Rl);
    Dp=Ds+Dg;
    th0p=0;
% Phase 4
    B1=Bg+Ke*Kt/(Rg+Rl);
 %   th0=5;
 %   wg3=-4;
```

12.2. Phase2.m

```
num=1;
if num==1

    heel_param
    num=[Js*wstep -Ks*thmax-Ds];
    den=[Js Bs Ks];
    t=0:0.001:1;
    ws=impulse(num,den,t);
    ths=step(num,den,t)+thmax;
    a=Bs/(2*Js);
    b=sqrt((Ks/Js)-Bs^2/(4*Js));
    w=wstep*exp(-a*t).*cos(b*t)-(wstep*a+(Ks*thmax+Ds)/Js)*exp(-
a*t).*sin(b*t)/b;
    th=wstep*(-a/(a^2+b^2)*exp(-a*t).*cos(b*t)+b/(a^2+b^2)*exp(-
a*t).*sin(b*t))-(wstep*a+(Ks*thmax+Ds)/Js)/b*(-b/(a^2+b^2)*exp(-
a*t).*cos(b*t)-a/(a^2+b^2)*exp(-a*t).*sin(b*t))-Ds/Ks;

    t2=atan(wstep*Js*b/(wstep*a*Js+Ks*thmax+Ds))/b;
    th2=wstep*(-a/(a^2+b^2)*exp(-
a*atan(b*wstep*Js/(wstep*a*Js+Ks*thmax+Ds))/b)/(b^2*wstep^2*Js^2/(wstep*a*J
s+Ks*thmax+Ds)^2+1)^(1/2)+b^2/(a^2+b^2)*exp(-
a*atan(b*wstep*Js/(wstep*a*Js+Ks*thmax+Ds))/b)*wstep*Js/(wstep*a*Js+Ks*thma
x+Ds)/(b^2*wstep^2*Js^2/(wstep*a*Js+Ks*thmax+Ds)^2+1)^(1/2))-
(wstep*a+(Ks*thmax+Ds)/Js)/b*(-b/(a^2+b^2)*exp(-
a*atan(b*wstep*Js/(wstep*a*Js+Ks*thmax+Ds))/b)/(b^2*wstep^2*Js^2/(wstep*a*J
s+Ks*thmax+Ds)^2+1)^(1/2)-a/(a^2+b^2)*exp(-
a*atan(b*wstep*Js/(wstep*a*Js+Ks*thmax+Ds))/b)*b*wstep*Js/(wstep*a*Js+Ks*th
max+Ds)/(b^2*wstep^2*Js^2/(wstep*a*Js+Ks*thmax+Ds)^2+1)^(1/2))-Ds/Ks;
%     plot(t,ws,t,ths,t2,0,'+',t2,th2,'o')  %,t,th','*',t,w,'+'
```

```
else
    syms Js Ks Bs wstep thmax Ds t a b
    num=[Js*wstep -Ks*thmax-Ds];
    den=[Js Bs Ks];
%     a=Bs/(2*Js)
%     b=sqrt((Ks/Js)-Bs^2/(4*Js^2))
    pretty(simple(a^2+b^2))
    w=wstep*exp(-a*t).*cos(b*t)-(wstep*a+(Ks*thmax+Ds)/Js)*exp(-
a*t).*sin(b*t)/b;
    simple(w)
    pretty(simple(w))
    th=int(w,t)-Ds/Ks
     simple(th)
%     pretty(simple(th))
    th0=subs(th,t,0);
    th0=simple(th0)
    t2=solve(w,t)
    pretty(simple(t2))
    th2=subs(th,t,t2);
    th2=simple(th2)
    pretty(simple(th2))
end
```

12.3. Phase3.m

```
num=1;
if num==1
    J=Jp;
    Ks=Ksp;
    B=Bp;
    ths2=ths2p;
```

```
    D=Dp;
    th0=th0p;
    num=[J*ths2 B*ths2 D]
    den=[J B Ks]
    t=0:0.00001:0.2;
%     ws=impulse(num,den,t);
%     ths=step(num,den,t);
     a=B/(2*J);
     b=sqrt((Ks/J)-B^2/(4*J));
     w=(-Ks*ths2+D)/(J*b)*exp(-a*t).*sin(b*t);
     th=(Ks*ths2-D)*(b*cos(b*t)+a*sin(b*t)).*exp(-a*t)/(b*Ks)+D/Ks-th0;
     thf=[0 th(1:length(th)-1)];
     cross=min(find(th.*thf<0))
     thf=@(t)((Ks*ths2-D)*(b*cos(b*t)+a*sin(b*t)).*exp(-a*t)/(b*Ks)+D/Ks-
th0);

     t3=t(cross) %fzero(thf,[0 t(cross+10)]);
     wg3=(-Ks*ths2+D)/(J*b)*exp(-a*t3).*sin(b*t3);
     e3=-1/4*Ke^2*Rl*(Ks^2*ths2^2*exp(-a*t3)^2*a^2+Ks^2*ths2^2*exp(-
a*t3)^2*b^2-Ks^2*ths2^2*exp(-2*a*t3)*a^2*cos(2*b*t3)+Ks^2*ths2^2*exp(-
2*a*t3)*a*b*sin(2*b*t3)-2*Ks*ths2*D*exp(-a*t3)^2*a^2-2*Ks*ths2*D*exp(-
a*t3)^2*b^2+2*Ks*ths2*D*exp(-2*a*t3)*a^2*cos(2*b*t3)-2*Ks*ths2*D*exp(-
2*a*t3)*a*b*sin(2*b*t3)+D^2*exp(-a*t3)^2*a^2+D^2*exp(-a*t3)^2*b^2-D^2*exp(-
2*a*t3)*a^2*cos(2*b*t3)+D^2*exp(-2*a*t3)*a*b*sin(2*b*t3)-
Ks^2*ths2^2*b^2+2*Ks*ths2*D*b^2-
D^2*b^2)/J^2/b^2/(Rl^2+2*Rl*Rg+Rg^2)/a/(a^2+b^2)';

    plot(t,w,t,th,'+') %,t3,th0,'+r')  %t,w,'+',t,th,'o'
else
    syms J Ks B ths2 D t a b th0 Ke Rg Rl t3
```

```
%     a=B/(2*J)
%     b=sqrt((K/J)-B^2/(4*J^2))
    w=(-Ks*ths2+D)/(J*b)*exp(-a*t).*sin(b*t);
    th=int(w,t)+D/Ks
    th=(Ks*ths2-D)*(b*cos(b*t)+a*sin(b*t)).*exp(-a*t)/(b*Ks); %+D/Ks;
    th=(Ks*ths2-D)*(sqrt(a^2+b^2)*cos(b*t-atan(a/b))).*exp(-
a*t)/(b*Ks)+D/Ks;
     pretty(simple(th))
%      t3=solve(th,t);
%      pretty(simple(t3))
    v=Ke*w*Rl/(Rl+Rg);
    p=v^2/Rl;
    pretty(simple(p))
    e=int(p,t,0,t3)
    pretty(simple(e))
end
```

12.4. Phase4.m

```
num=1;
if num==1
    heel_param

    num=[Jg*th0 B1*th0+Jg*wg3 Dg];
    den=[Jg B1 0];
    t=0:0.001:100;
%     ws=impulse(num,den,t);
%     ths=step(num,den,t);
    w=Dg/B1+(wg3-(Dg/B1))*exp((-B1/Jg)*t);
    th=Dg/B1*t-(wg3-Dg/B1)/B1*Jg*exp(-B1/Jg*t)+(wg3-Dg/B1)/B1*Jg+th0;
```

```
    t4 =-log(-Dg/(wg3*B1-Dg))*Jg/B1;
    e4=1/2*Jg*Ke^2*Rl*(-2*Dg^2*log(-Dg/(wg3*B1-
Dg))+wg3^2*B1^2+2*Dg*wg3*B1)/B1^3/(Rl^2+2*Rl*Rg+Rg^2);
%    plot(t,w,t,th,t4,0,'*')
else
    syms Jg B1 th0 Dg t wg3 Ke Rg Rl t3 Bg I0
    % constant load resistance
    B1=Bg+Ke*Ke/(Rg+Rl);
    D1=Dg;
    w=D1/B1+(wg3-(D1/B1))*exp((-B1/Jg)*t);
    th=int(w,t)+th0;
    t4=solve(w,t);
%     pretty(simple(t4))
    v=Ke*w*Rl/(Rl+Rg);
    p=v^2/Rl;
%     pretty(simple(p));
    e=int(p,t,0,t4);
    disp('Constant Resistance')
    pretty(simple(e))
    disp('Constant Resistance with Dg=0')
    pretty(simple(subs(e,Dg,0)))
%     e=subs(e,Dg,0);
%     pretty(simple(e))

    % constant load current
    B1=Bg;
    D1=Dg+I0*Ke;
    w=D1/B1+(wg3-(D1/B1))*exp((-B1/Jg)*t);
    th=int(w,t)+th0;
%     pretty(simple(th));
    t4=solve(w,t);
```

```
%     pretty(simple(t4));
 %   v=Ke*w*Rl/(Rl+Rg);
    p=I0^2*Rl;
%     pretty(simple(p));
    e=int(p,t,0,t4);
%     disp('Constant current')
%     pretty(simple(e))
%     disp('Constant current Bg=0')
%     pretty(simple(subs(e,Bg,0)))
%     e=subs(e,Dg,0);
%     pretty(simple(e))


%     th0=subs(th,t,0)
end
```

12.5. Combine.m

```
%clear
clf
Rll=100;
E=[];
Ein=[];
plots=1;
for Rl=Rll
    phase2
%     if plots
%         t=0:0.001:t2;
%         i=1:length(t);
%         plot(t,ws(i),t,ths(i),t2,0,'+',t2,th2,'o')
%         hold on
```

```
%     end


%     ths2p=th2;
    t2=0;
    ths2p=thmax;
    phase3
    if plots
        t=t2:0.00001:t2+t3;
        i=1:length(t);
        plot(t,w(i),t,th(i),t3+t2,th0,'+r')
        hold on


    end
    phase4
    if plots
        t=t2+t3:0.001:t2+t3+t4;
        i=1:length(t);
        plot(t,w(i),t3+t2+t4,0,'+r')
%         pause
    end
    Ein=[Ein Ks*(thmax^2-th0^2)/2+Js*wstep^2/2];
    E=[E e3+e4];
end
E
Ein
% te=x+5.36;
% we=y*(Rl+Rg)/(Rl*Ke);
% p=cumsum(y.^2/Rl)*(x(2)-x(1));
% i=1:20:length(te);
% plot(te(i),we(i),'r',te,-p*1000,'g',te,-y)
```

```
%plot(t,-y)
hold off
%plot(Rll,E./Ein)
```

12.6. polynomial_current.m

```
a1m=[];
a0m=[];
mm=[];
VVV=0.01:0.01:0.2
for VV=VVV
    syms w V Bg a0 a1 a2 a3 Rg t Ke w0 J
    w=dsolve('Dw=(-Bg*w-V-Ke*(a0+a1*w))/J','w(0)=w0')
    i=a0+a1*w
    t4=solve(w,t)
    v=Ke*w-Rg*i
    pretty(simple(v))
    p=v*i;
    pretty(simple(p))
    e=int(p,t,0,t4);
    pretty(simple(e))
    e=subs(e,V,0.01);
    e=subs(e,Bg,VV);
    e=subs(e,Rg,20);
    e=subs(e,Ke,4);
    e=subs(e,w0,2);
    e=subs(e,J,6);
    a00=0:0.0002:0.01;
    e=subs(e,a0,a00);
    E=[];
    a111=0.005:0.001:0.1;
    for a11=a111
        E=[E; subs(e,a1,a11)];
    end
    %pretty(simple(E));
```

```
    figure(1)
%     meshc(a00,a111,E)
%     figure(2)
    contour(a00,a111,E,50)
    xlabel('a0')
    ylabel('a1')
    m=max(max(E))
    [i,j]=find(m==E);
    a0max=a00(j)
    a1max=a111(i)
    a0m=[a0m a0max];
    a1m=[a1m a1max];
    mm=[mm m];
end
plot(VVV,a0m,VVV,a1m,VVV,mm)
```

13. Appendix C – Spring constant from model and experimental values

The note aims to document the process of obtaining the spring constant form experimental values and validation of through mathematical modelling.

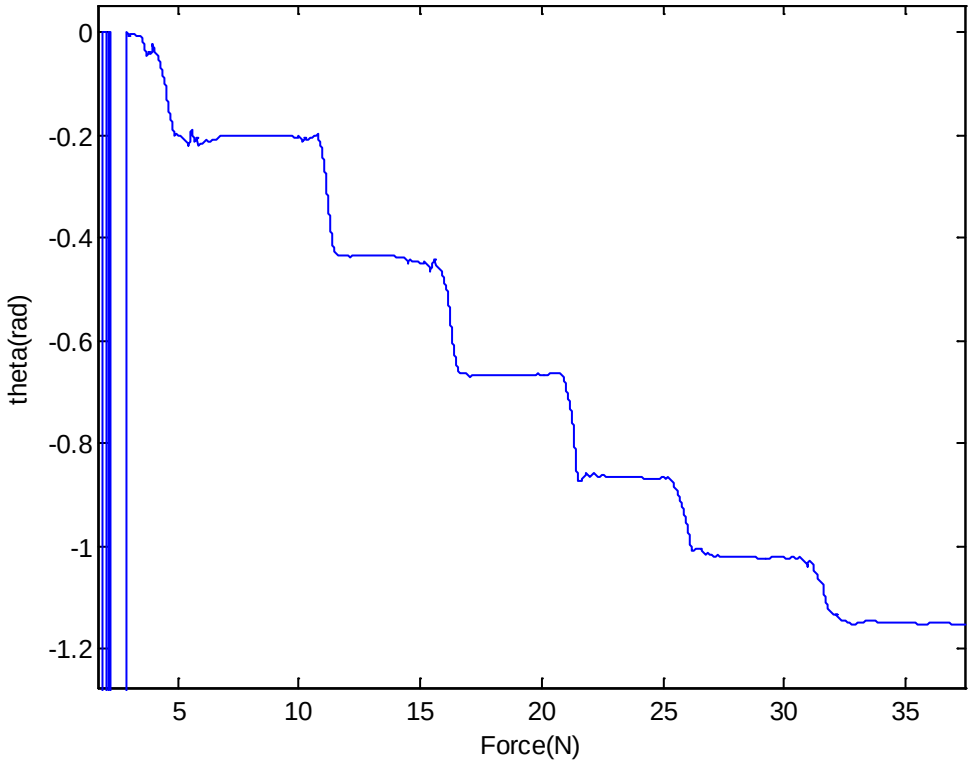


```
%%
%%Spring constant form Model and measured values
%%
plot(time,theta)
plot(time,theta(1,:)-theta(1,5000));axis([0 40 -10 10])
q=ginput
% q =
%     3.3214   -0.0027
%     8.7007   -0.2028
%    13.1834   -0.4374
%    18.3996   -0.6683
```

```
%    24.0234   -0.8683
%    29.6471   -1.0222
%    35.5154   -1.1492
q2=-q(:,2)
% q2 =
%     0.0027
%     0.2028
%     0.4374
%     0.6683
%     0.8683
%     1.0222
%     1.1492
% f=0:5:30
% f =
%      0     5    10    15    20    25    30
f=0:5:30
plot(q2,f)
th0=0.66;k=1.6;r=0.07;F=k*q2./(r*cos(q2-th0));plot(q2,f,'+-',q2,F)
%%
```

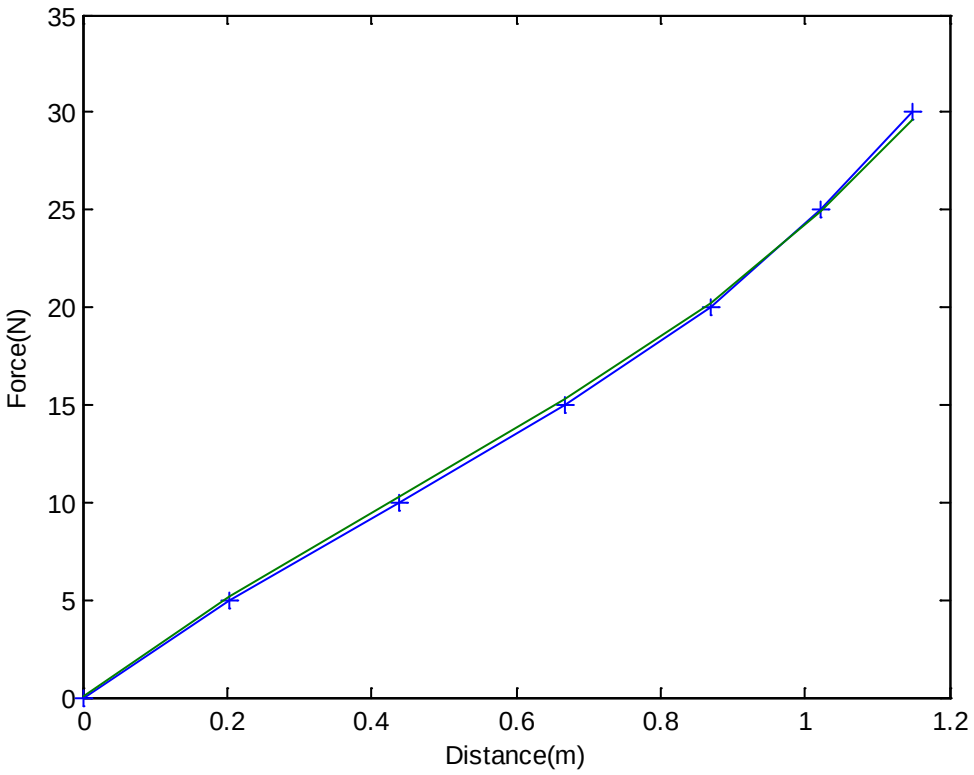
35
30
25
20
15
10
5
0
Force(N)
0
0.2
0.4
0.6
0.8
1
1.2
Distance(m)

14. Appendix D – Optical Encoder Drivers for Flyback

```
function varargout = EncPollAI(varargin)

% Last Modified by GUIDE v2.5 08-Feb-2008 11:51:26

% Begin initialization code - DO NOT EDIT
gui_Singleton = 1;
gui_State = struct('gui_Name',       mfilename, ...
                   'gui_Singleton',  gui_Singleton, ...
                   'gui_OpeningFcn', @EncPollAI_OpeningFcn, ...
                   'gui_OutputFcn',  @EncPollAI_OutputFcn, ...
                   'gui_LayoutFcn',  [] , ...
                   'gui_Callback',   []);
if nargin && ischar(varargin{1})
    gui_State.gui_Callback = str2func(varargin{1});
end

if nargout
    [varargout{1:nargout}] = gui_mainfcn(gui_State, varargin{:});
else
    gui_mainfcn(gui_State, varargin{:});
end
% End initialization code - DO NOT EDIT


% --- Executes just before EncPollAI is made visible.
function EncPollAI_OpeningFcn(hObject, eventdata, handles, varargin)
```

```
% Choose default command line output for EncPollAI
handles.output = hObject;
handles.fred = zeros(2,2);
handles.i(1) = 0;
handles.theta = zeros(2,2);
handles.time = 0;
handles.tm = 0;
handles.dx = 0;
% Update handles structure
guidata(hObject, handles);

% --- Outputs from this function are returned to the command line.
function varargout = EncPollAI_OutputFcn(hObject, eventdata, handles)

% Get default command line output from handles structure
varargout{1} = handles.output;

% --- Executes on button press in btnStart.
function btnStart_Callback(hObject, eventdata, handles)

set(handles.btnStop,'Value',1)

LoadTask(handles.activex1,'C:\ADLINK\DAQPilot\Task
Folder\ReadEncoder.tsk');
ai_device = analoginput('mwadlink',0);
ai0 = addchannel(ai_device, 0);
set(ai_device,'InputType','SingleEnded');
set(ai_device,'SampleRate',10000);
set(ai_device,'SamplesPerTrigger',1000);
Start(handles.activex1);
```

```
tic;
start(ai_device);
while (get(handles.btnStop,'Value')==1) %((toc<10) ||
(get(handles.btnStop,'Value')==1))%
    handles.i=handles.i+1;
    handles.time(handles.i) = toc;
    handles.fred(:,handles.i)=Read(handles.activex1)';
    handles.theta(:,handles.i)=2*pi/1000*handles.fred(:,handles.i);
    drawnow;
    guidata(hObject,handles);
end

[data,tm]=getdata(ai_device);
handles.dx=data;
handles.tm=tm;

assignin('base','time',handles.time);
assignin('base','theta',handles.theta);
assignin('base','tm',handles.tm);
assignin('base','dx',handles.dx);

% --- Executes on button press in btnStop.
function btnStop_Callback(hObject, eventdata, handles)

set(handles.btnStop,'Value',0);
guidata(hObject,handles);
Stop(handles.activex1);
% % --- Executes during object creation, after setting all properties.
% function editOutput_CreateFcn(hObject, eventdata, handles)
```

```
% % hObject    handle to editOutput (see GCBO)
% % eventdata  reserved - to be defined in a future version of MATLAB
% % handles    empty - handles not created until after all CreateFcns
called

function activex1_DAQPilotError(hObject, eventdata,handles)
set(handles.editOutput,'String', eventdata.ErrorString)
```

15. Appendix E – Matlab source code for the vibrating cantilever system

```
num=1;
if num==1

    vel=[];     % Velocity
    volt=[];    % Voltage
    ke = 0.14;     % Emf constant
    Rc = 11;    % Generator Coil resistance
    x0 = 0.0136; % Deflection
    k=(180.8-85.4)/(0.015-0.011);    % Beam spring Constant
    roe=7850;   % Material Density (spring steel)
    l=254e-3;   % Beam lenght
    b=20e-3;    % Beam width
    h=3e-3;     % Beam height
    m=roe*l*b*h;% Beam mass
    mtip=176.6e-3;   % tip mass
    meff=mtip+0.23*m;           %285.9e-3;    % mtip+0.23*m; % Effective
mass
    tt=0:0.0001:100;  % time
    w = sqrt(k/meff);
    q=0.8/w;          % Seta
    bm = q*2*w*meff;  % mecanical damping factor


    for Rl = 3000000000;    % load resistance
```

```
        eata = (bm+(ke^2/(Rc+Rl)))/(2*w*meff);
        beta = sqrt(1-eata^2);
        vel = x0*w/beta*exp(-w*eata*tt).*(eata*sin(w*beta*tt) +
beta*cos(w*beta*tt));
        volt = ke*vel*Rl/(Rc+Rl);
    end

else



% syms vel x seta beta w t x0
%
% x = x0/beta*exp(-w*seta*t)*sin(w*beta*t)
%
% V = diff(x)

syms bm ke Rc Rl w m eata

eata = bm+(ke^2/Rc+Rl)/2*w*m
solve(eata,Rl);

end
```

16. Appendix F – Beam sizing for the vibrating cantilever system

For a 60kg individual of 600N weight deflecting a beam 10mm requires 6J of energy. The spring rate for the beam can be calculated from;

$$k = \frac{F}{\delta} = \frac{600}{0.01} = 60kN/m$$

The deflection at the end of a beam is given by;

$$\delta = \frac{Fl^3}{3EI}$$

Where;

E = Young's Modulus of the Material

I = Second moment of area for a rectangular section of beam $I = \frac{bh^3}{12}$

Thus the spring constant at the end of the beam can be;

$$k = \frac{F}{\delta} = \frac{3EI}{l^3} = \frac{3Ebh^3}{12l^3}$$

Inserting the dimensions;

B = 20mm

H = 4mm

And transposing for l

$$l = \sqrt[3]{\frac{3EI}{k}} = \sqrt[3]{\frac{3Ebh^3}{12k}} = \sqrt[3]{\frac{3\times 207\times 10^9 \times 0.02\times 0.004^3}{12\times 60000}} = 103mm$$

The maximum stress on the beam is;

$$\sigma_{\max} = \frac{6Fl}{bh^2}$$

Rearranging

$$\frac{b^2h^4}{l^2} = \frac{36F^2}{\sigma^2_{\max}} \qquad (0.1)$$

And from the equation for the spring rate;

$$\frac{l^3}{bh^3} = \frac{\delta E}{4F} \qquad (0.2)$$

Equating (0.1) & (0.2) to give the volume of the beam;

$$bhl = \frac{9\delta EF}{\sigma^2_{\max}} = V$$

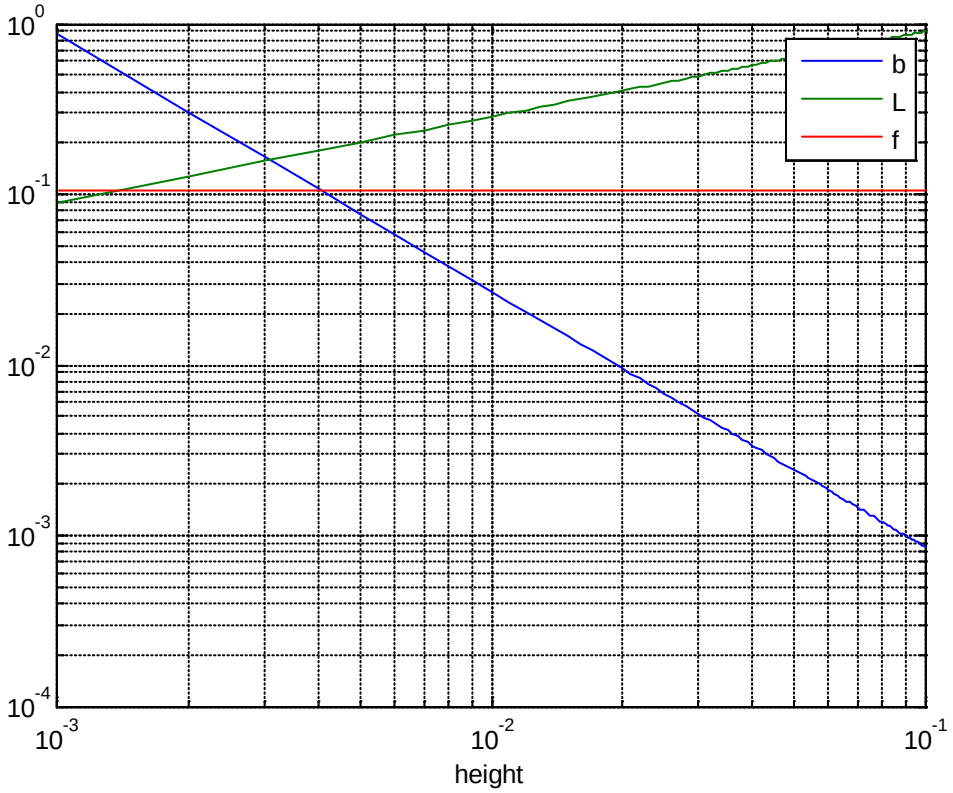
10^0
10^-1
10^-2
10^-3
10^-4
10^-3
10^-2
10^-1
height
b
L
f

17. Appendix G – Compressible Tubing System

The under-floor hydraulic system consists of fluid filled tubing formed into a mat which could harvest energy over a large area and drive a single turbine, as illustrated in Figure 17-1.

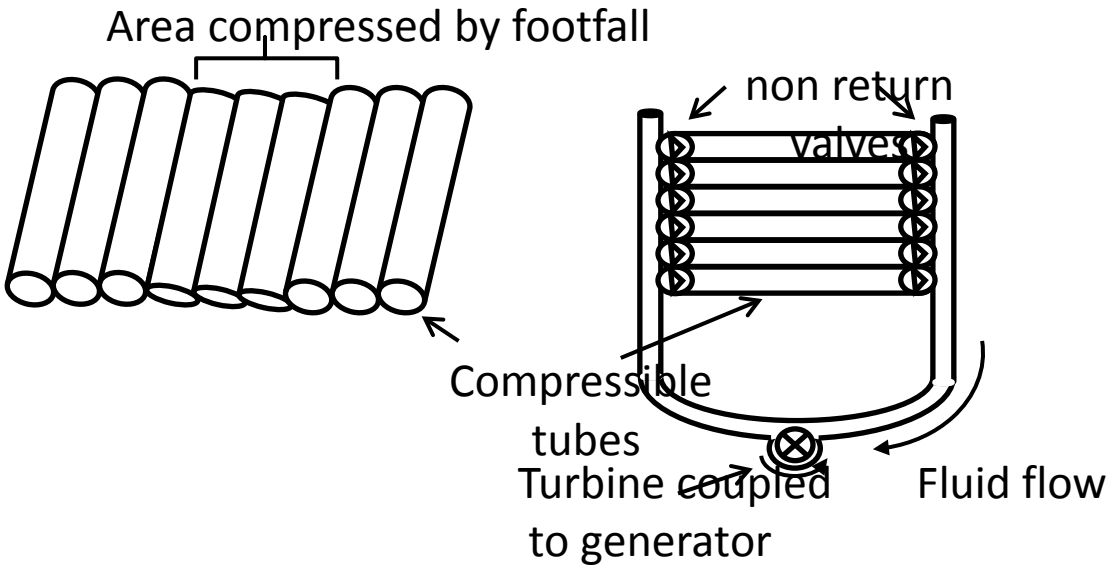

Figure 17-1 Hydraulic generator with fluid filled tubing

The left side of Figure 17-1 shows a cross section through the tubing mat. Under foot pressure, the tubing would be crushed, forcing fluid through the tube. Once the foot pressure is removed the elasticity of the tubing would cause it to recover its original shape, sucking fluid back into the affected area. By using non return valves as illustrated by the right side of the Figure 17-1, it is possible to ensure that the fluid flow is unidirectional and capable of driving the turbine. These non return valves would also allow multiple tubes to be connected to a single turbine so that whichever part of the mat were compressed, the fluid would flow through the turbine and, indeed, if multiple pedestrians were present, the system would capture energy from them all simultaneously.

17.1. Experimental Results

To evaluate the performance of the proposed system a turine/generator structure has been constructed using rapid prototyping techniques based on the CAD model shown in **Error! Reference source not found.**. The resulting structure and prototype tubing system, is shown in Figure 17-3.

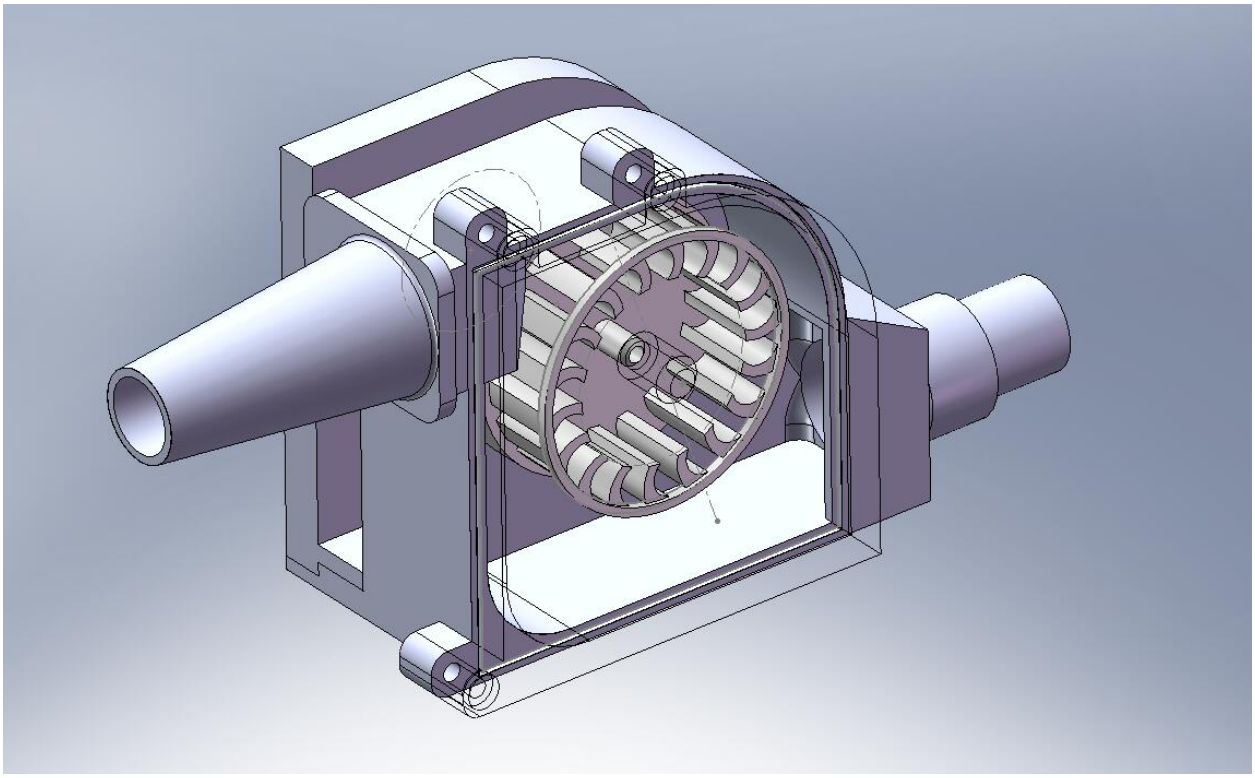

Figure 17-2 Experimental turbine/generator structure

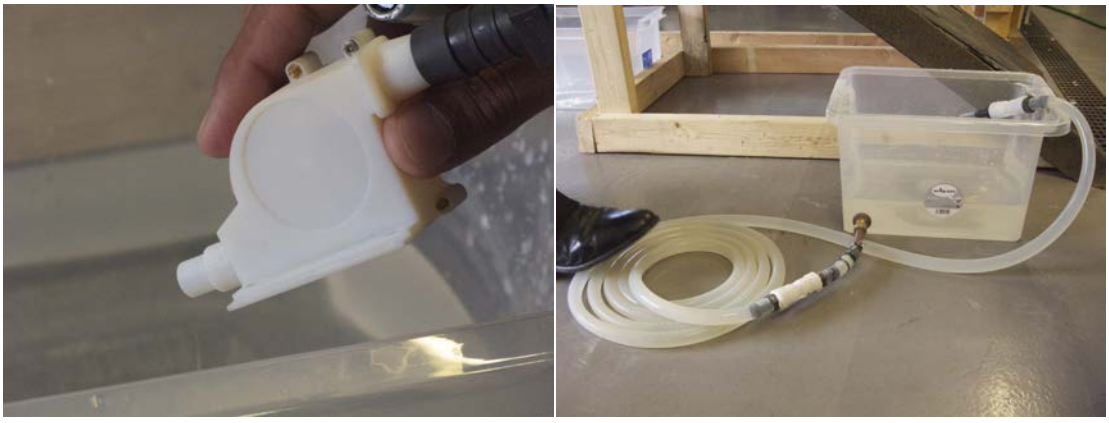

Figure 17-3 Photos of prototype turbine and pumping system

The prototype system has been tested using a single length of tubing of approximately 25mm inner diameter and 30mm outer diameter. This was tested with a single section under foot pressure, a double section or three sections, the latter two formed by coiling the tube into a spiral. It was found that a singe section gave the highest power output. It is believed that for multiple sections, the flow in one coil was impeded by the compression of the tube in the subsequent coil. The turbine was formed using 4 permanent magnets in the turbine and four pick up coils connected in series. A load resistance in the range 20-30Ω was found to give the maximum output power. Under repeated foot pressure applied at 1 second intervals, the turbine span freely and, owing to its inertia, continued to spin from one footfall to the next. The output voltage was AC, owing to the absence of any rectification or commutation. The output voltage is shown in

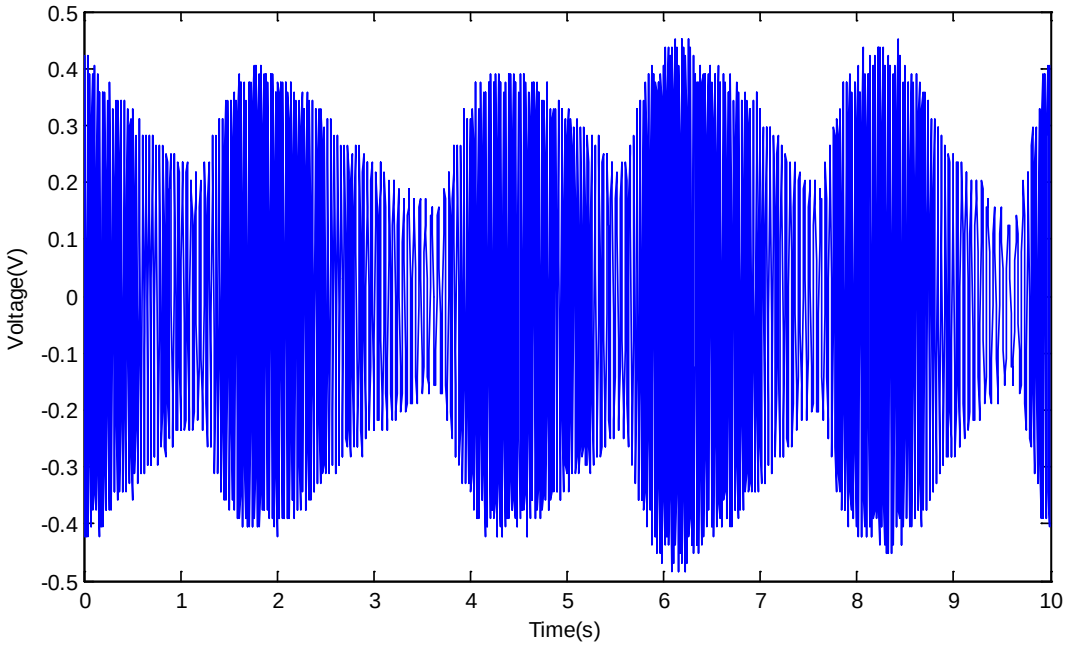

Figure 17-4 for a series of 5 steps for a 75kg pedestrian. It may be seen that the voltage builds up over the first 2 steps and gradually decays away once the footfall stops. The average voltage during footfall is 0.45V rms and the AC frequency is approximately 50Hz, corresponding to a turbine rotation speed of 1500rpm. This corresponds to an average power of 6.75mW.

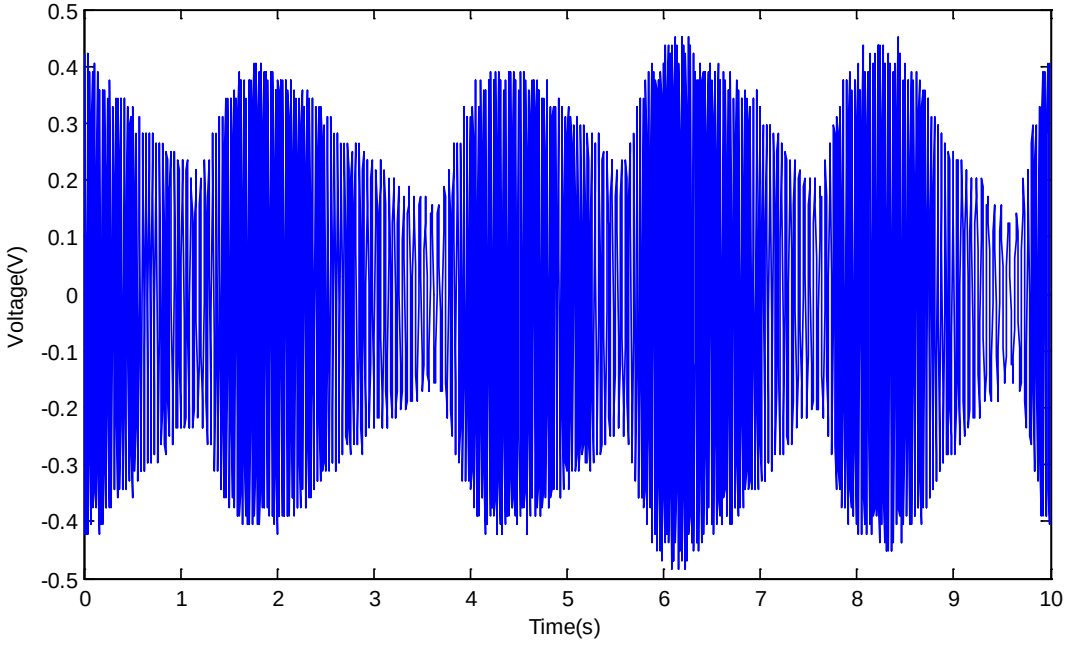

Figure 17-4 Turbine output voltage under repeated footfall

17.2. Estimation of expansion effects in hydraulic tubing

This note aims to determine the effect that internal pressure has on a tube and the consequent loss in transmitted volume.

Assume a tube with dimensions shown below:

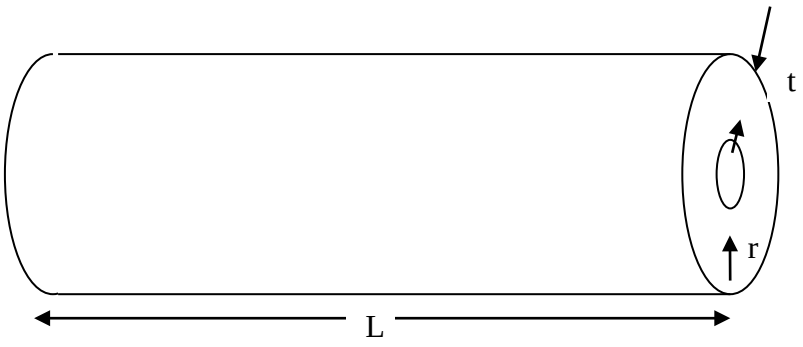

Where L is the length, t the wall thickness and r the internal radius.

Assuming a thin walled cylinder (typically valid for $\frac{r}{t} > 5$) and internal pressure, P, the hoop stress is 0:

$$\sigma_H = \frac{Pr}{t} \qquad (1)$$

And the hoop strain is

$$\varepsilon_H = \frac{1}{E}(\sigma_H - \upsilon\sigma_L)$$

Assuming the longitudinal stress, σ_L is negligible

$$\varepsilon_H = \frac{\sigma_H}{E} = \frac{\Delta r}{r}$$

Where Δr is the change in radius resulting from the pressure.

The change in internal volume is:

$$\Delta V = \pi(r + \Delta r)^2 L - \pi r^2 L$$

or

$$\Delta V = \pi r^2\{(1 +)^2 - 1\}L \approx 2\pi r^2 \varepsilon_{\mathrm{H}}{}^2 \mathrm{L}$$

Substituting from equation (1):

$$\Delta V = \frac{2\pi r^4 P^2 L}{E^2 t^2}$$

Single tube:

The volume displace by a step on a tube length is:

$$V_s = \pi r^2 L_s$$

The loss of volume is:

$$volume\ loss = \frac{\Delta V}{V_s} = \frac{2r^2 P^2 L}{E^2 t^2 L_s}$$

And assuming that the pressure balances the applied force, F, then:

$$P = \frac{F}{2rL_s}$$

So

$$volume\ loss = \frac{F^2 L}{2E^2 t^2 L_s^3}$$

For parameters: E=10MPa, F=1kN, =0.1m, L=1m, t=3mm

$$volume\ loss = 0.55$$

For r=0.01, = 3x10^{-}, P = 500kPa = 5 Bar = 70psi, ΔV=3x10^{-}

Multiple tube:

Assuming multiple tubes covering an area x with equal pressure:

$$P = \frac{F}{L_s^2}$$

So

$$volume\ loss = \frac{2r^2F^2L}{E^2t^2L_s^5}$$

And for the above parameters

$$volume\ loss = 0.022$$

For r=0.01, = 1.7x10^{-}, P = 100kPa, ΔV=7x10^{-}

[1] I Mech E data book

18. Appendix H – Mathematical Model of the Compressible Tubing System

The model of the fluid system is more limited than the other models in that it does not aim to predict the power output of the system but is rather used to give design guidelines. Prediction of power output would require extensive computational fluid dynamics analysis and experimental validation which are beyond the scope of the current work. In order to develop a model of the tubing system, consider the compressed section of tubing shown in Figure 18-1.

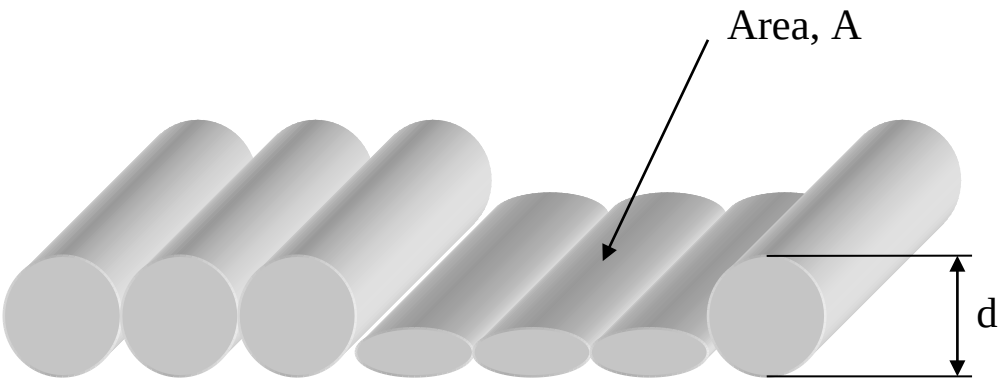

Figure 18-1 Section of compressed tubing

For an area compressed, A, compressed by a a distance d over a time period T, the fluid volume flow rate is:

$$Q = \frac{Ad}{T}$$

And for a fluid density, ρ the mass flow rate is $Q\rho$. If the compression is caused by a force, F, over the area of the fluid pressure is $P = \frac{F}{A}$

Treating the nozzle as an orifice plate, the flow rate can be written as [172]:

$$Q = C_d A_N \sqrt{\frac{2(P_1 - P_2)}{\rho}}$$

Where is the discharge coefficient, dependant on the shape of the nozzle

is the cross sectional area of the nozzle

and are the pressure in the nozzle and after the nozzle respectively and

ρ is the fluid density

Assuming = 1 and is atmospheric pressure and so taken as zero:

$$Q = A_N \sqrt{\frac{2P_1}{\rho}}$$

Or

$$A_N = \frac{Q}{\sqrt{2P_1/\rho}}$$

We wish to choose the nozzle area so that the back pressure matches that generated by the foot fall. Assuming a ground reaction force of 600N (a 60kg pedestrian) and a foot area of 0. (10cmx10cm) then the pressure $P_1 = 60000Nm^{-2}$. For a displacement of 10mm, the volume of water displaced is $V = 0.0001m^3$. If the resulting flow occurs over a period of 1s then the volume flow rate is $Q = 0.0001m^3s^{-1}$. The density of water is approximately 1000kg/ and so the optimum nozzle area is:

$$A_N = 9 \times 10^{-6}m^2$$

Corresponding to a circular nozzle with a radius of 3.4mm diameter.

The average velocity of water leaving the nozzle is

$$v = \frac{V}{A_N T} = 11ms^{-1}$$

For optimum energy transfer to the turbine wheel we wish the tangential speed, *u*, of the turbine to be half that of the incoming water jet [173], thus $u = 5.5ms^{-1}$.

The generator operates most efficiently at a speed of around 5000rpm (ω = 523rad/s) and so the radius of the turbine wheel

$$r = \frac{u}{\omega} = 10.5mm$$

19. List of Acronyms